Computers in Biology and Medicine 146 (2022) 105618

Contents lists available at ScienceDirect

Computers in Biology and Medicine

journal homepage: www.elsevier.com/locate/compbiomed

# Multilevel threshold image segmentation for COVID-19 chest radiography: A framework using horizontal and vertical multiverse optimization

Hang Su [a], Dong Zhao [a,*], Hela Elmannai [b], Ali Asghar Heidari [c,1], Sami Bourouis [d], Zongda Wu [e], Zhennao Cai [c,**], Wenyong Gui [c], Mayun Chen [f,***]

[a] *College of Computer Science and Technology, Changchun Normal University, Changchun, Jilin, 130032, China*
[b] *Department of Information Technology, College of Computer and Information Sciences, Princess Nourah bint Abdulrahman University, P.O. Box 84428, Riyadh, 11671, Saudi Arabia*
[c] *College of Computer Science and Artificial Intelligence, Wenzhou University, Wenzhou, Zhejiang, 325035, China*
[d] *Department of Information Technology, College of Computers and Information Technology, Taif University, P.O. Box 11099, Taif, 21944, Saudi Arabia*
[e] *Department of Computer Science and Engineering, Shaoxing University, Shaoxing, 312000, China*
[f] *Department of Pulmonary and Critical Care Medicine, The First Affiliated Hospital of Wenzhou Medical University, Wenzhou, 325000, China*

ARTICLE INFO

*Keywords:*
Novel coronavirus pneumonia
COVID-19
Multi-threshold image segmentation
Meta-heuristic
Optimization
Multi-verse optimization

ABSTRACT

COVID-19 is currently raging worldwide, with more patients being diagnosed every day. It usually is diagnosed by examining pathological photographs of the patient's lungs. There is a lot of detailed and essential information on chest radiographs, but manual processing is not as efficient or accurate. As a result, how efficiently analyzing and processing chest radiography of COVID-19 patients is an important research direction to promote COVID-19 diagnosis. To improve the processing efficiency of COVID-19 chest films, a multilevel thresholding image segmentation (MTIS) method based on an enhanced multiverse optimizer (CCMVO) is proposed. CCMVO is improved from the original Multi-Verse Optimizer by introducing horizontal and vertical search mechanisms. It has a more assertive global search ability and can jump out of the local optimum in optimization. The CCMVO-based MTIS method can obtain higher quality segmentation results than HHO, SCA, and other forms and is less prone to stagnation during the segmentation process. To verify the performance of the proposed CCMVO algorithm, CCMVO is first compared with DE, MVO, and other algorithms by 30 benchmark functions; then, the proposed CCMVO is applied to image segmentation of COVID-19 chest radiography; finally, this paper verifies that the combination of MTIS and CCMVO is very successful with good segmentation results by using the Feature Similarity Index (FSIM), the Peak Signal to Noise Ratio (PSNR), and the Structural Similarity Index (SSIM). Therefore, this research can provide an effective segmentation method for a medical organization to process COVID-19 chest radiography and then help doctors diagnose coronavirus pneumonia (COVID-19).

## 1. Introduction

The latest coronavirus pneumonia (COVID-19) outbreak, which occurred at the end of 2019, is a new acute respiratory disease. On March 11, 2020, the World Health Organization declared the COVID-19 outbreak a public health emergency of international significance and confirmed it as a pandemic, drawing widespread attention. COVID-19's possible pathogenicity and highly infectious nature have had a significant and far-reaching effect on the lives of billions of people worldwide and the global economy. The number of people infected worldwide has continued to rise exponentially since the outbreak until April 2021. More than 140 million cases have been diagnosed in more than 200 countries and regions worldwide, with more than three million cumulative deaths. In such a critical situation, it is essential to improve the method of COVID-19 diagnosis to improve the quality and accuracy of the diagnosis. Several studies using computer technology to assist in

* Corresponding author.
** Corresponding author.
*** Corresponding author.
*E-mail addresses:* suhang_v@163.com (H. Su), zd-hy@163.com (D. Zhao), hselmannai@pnu.edu.sa (H. Elmannai), aliasghar68@gmail.com (A.A. Heidari), s.bourouis@tu.edu.sa (S. Bourouis), zongda1983@163.com (Z. Wu), cznao@wzu.edu.cn (Z. Cai), 20180171@wzu.edu.cn (W. Gui), chenmayun@126.com (M. Chen).
[1] https://aliasgharheidari.com

https://doi.org/10.1016/j.compbiomed.2022.105618
Received 26 March 2022; Received in revised form 7 May 2022; Accepted 12 May 2022
Available online 18 May 2022

COVID-19 diagnosis have been suggested [1–6]. In addition, clinical imaging data are seen as one of the critical diagnostic bases in all COVID-19 diagnostic data. However, due to the complexity of chest radiography and computed tomography, manually drawing the target area of medical images is a time-consuming and laborious task, which adds a significant burden to the diagnosis work of clinicians. Therefore, computer technology can be used to segment chest radiography and computed tomography, which can quickly process the images to make them more intuitive and more transparent. Thus, it can effectively improve diagnostic efficiency.

There are many methods to process images efficiently in the computer field [7–9], among which image segmentation is an integral part of image processing and a hot topic of research nowadays [10–12]. In the past few years, more and more image segmentation techniques have been proposed, such as multilevel threshold image segmentation (MTIS) [13], deep learning-based image segmentation [14], hierarchical clustering-based image segmentation [15], wavelet transform-based image segmentation [16], and others. MTIS has become one of the most applied image segmentation methods because of its high stability, low complexity, and easy implementation. Yue et al. [17] proposed a novel multilevel thresholding method using between-class variance (Otsu) based on an improved invasive weed optimization algorithm to accurately and efficiently select the optimal threshold in MTIS.

Wu et al. [18] proposed multi-threshold image segmentation (MTIS) methods via an better-quality teaching-learning-based optimizer to tackle MTIS problems modeled by Otsu's between class variance and Kapur's entropy functions. Sun et al. [19] proposed to determine the iteration step size adaptively based on the fitness value of the current iteration for improving the cuckoo search algorithm to reduce the algorithmic complexity of MTIS to find the optimal threshold. Ewees et al. [20] presented a hybrid meta-heuristic approach for MTIS by integrating the artificial bee colony algorithm and the sine-cosine algorithm. Alwerfali et al. [21] proposed an alternative MTIS based on a new metaheuristic method, a modified spherical search optimizer. Yue et al. [22] proposed a hybrid bat algorithm incorporating a bat algorithm with invasive weed optimization to choose the optimal threshold. Tarkhaneh et al. [23] suggested a differential Evolution solution that achieves a good balance between exploration and exploitation through a new adaptive approach and new mutation strategies to reduce the amount of MTIS.

Hemei et al. [24] developed the electromagnetic optimization algorithm (EMO) based on the levy function to enhance the EMO performance for determining the optimal MTIS. Dhal et al. [25] presented a stochastic fractal search with a fuzzy entropy-based multilevel thresholding model for MTIS of color satellite images. Borjigin et al. [26] applied a particle swarm optimization algorithm to obtain the optimal threshold values for each component of an RGB image. Alwerfali et al. [27] developed an alternative MTIS method using a modified version of the salp swarm algorithm. Shen et al. [28] proposed a new and improved version of the flower pollination algorithm and combined it with MTIS to improve the accuracy of image segmentation. Satapathy et al. [29] proposed a 2D histogram-based image segmentation model by combining the improved chaotic bat algorithm with Otsu's interclass variance. Mittal et al. [30] improved the 2D histogram method to assist in finding thresholds for multilevel image segmentation, improving the processing efficiency of the original model.

Gao et al. [31] proposed an Otsu segmentation method based on a new Artificial Bee Colony algorithm for doing more fine-tuning searches and further enhancing the achievements of image segmentation. In the past few years, researchers have been thinking about improving the segmentation efficiency of traditional MTIS. The key to improving the performance of traditional methods is to improve the precision and efficiency of the segmentation threshold. As a result, more and more researchers have started introducing swarm intelligence algorithm (SIOA) into the traditional MTIS to improve the segmentation efficiency instead of the traditional exhaustive method. These SIOAs has offered greater efficiency in optimization tasks such as expensive optimization problems [32,33], medical diagnosis [34–37], PID optimization control [38–40], plant disease recognition [41], feature selection [42–45], object tracking [46,47], economic emission dispatch problem [48], engineering design [49–51], parameter tuning for machine learning models [52–54], constrained optimization problems [55,56], combination optimization problems [57], traveling salesman problem [58], multi-objective or many optimization problems [59–61], and scheduling problems [62–64].

The SIOA is a simple and efficient low-sequence optimization-seeking algorithm. It aims to find the optimal solution by modeling the collaborative behavior of animals, fish, insects, etc., using the collaborative behavior of populations in nature. The well-known SIOAs nowadays are different evolution (DE) [65], moth search algorithm (MSA) [66], monarch butterfly optimization (MBO) [67], Harris hawks optimization (HHO) [68], Slime mould algorithm (SMA) [69], whale optimizer (WOA) [70], hunger games search (HGS) [71], moth-flame optimization (MFO) [72], particle swarm optimization (PSO) [73], Harris hawks optimization (HHO) [74], sine cosine algorithm (SCA) [75], chaotic BA (CBA) [76], comprehensive learning PSO (CLPSO) [77], SCA with differential evolution(SCADE) [78], improved WOA (IWOA) [79], A-C parametric WOA (ACWOA) [80], biogeography-based learning PSO (BLPSO) [81], enhanced GWO with a new hierarchical structure (IGWO) [82], and so on. In 2016, Seyedali et al. proposed a novel nature-inspired algorithm called Multi-Verse Optimizer (MVO) [83], which has a strong merit-seeking performance. Furthermore, many improved versions of MVO have been developed by researchers and used in various fields. Shukri et al. [84] proposed an enhanced version of the MVO as a superior task scheduler in cloud computing.

Rezk et al. [85] presented a reliable approach based on MVO for designing load frequency control incorporated in multi-interconnected power systems comprising wind power and photovoltaic (PV) plants. Mohammadi et al. [86] proposed coupling the classical multi-layer perceptron with MVO to improve the performance of streamflow modeling. Ali et al. [87] presented a recent metaheuristic optimization approach of MVO to design load frequency control-based model predictive control incorporated in the large multi-interconnected system. Abdel-Basset et al. [88] introduced an enhanced metaheuristic algorithm called MVO with an overlapping detection phase to optimize wireless sensor networks' area coverage percentage. Abasi et al. [89] proposed a novel technique of adapting the MVO called the link-based Multiverse optimizer (LBMVO) to advance the exploitation stage in the basic MVO. Lai et al. [90] introduced an improved MVO used to optimize Density-based spatial clustering of applications with noise to find out its highest clustering accuracy quickly. Kandhway et al. [91] proposed an MVO algorithm based on the energy curve and the minimum cross-entropy to search the accurate and near-optimal thresholds for segmentation.

Wang et al. applied a self-adaptive MVO to optimize the parameters of the support vector machine (SVM). Fathy et al. applied an MVO to identify the optimal parameters of the proton exchange membrane fuel cell under certain operating conditions. Geng et al. [92] improved the original multi-objective MVO algorithm to improve the convergence accuracy of the algorithm and used the algorithm for the hybrid flow shop scheduling problem. Ewees et al. [93] provided a novel chaotic MVO algorithm to avoid drawbacks of MVO, where chaotic maps are used to improve the results of the MVO algorithm. Al-qaness et al. [94] introduced an adaptive mechanism into the MVO algorithm, proposed a fuzzy inference model, and applied it to the oil consumption prediction problem. Zhao et al. [95] combined the MVO algorithm with traditional machine learning techniques and proposed a hybrid scheduling prediction model, and MVO was used to determine the key parameters of the model. Wang et al. [96] used the MVO algorithm to determine the appropriate parameters for the problem of inaccurate key parameters during support vector machine (SVM) training. Fathy et al. [97] used the improved MVO algorithm to find the optimal parameters when

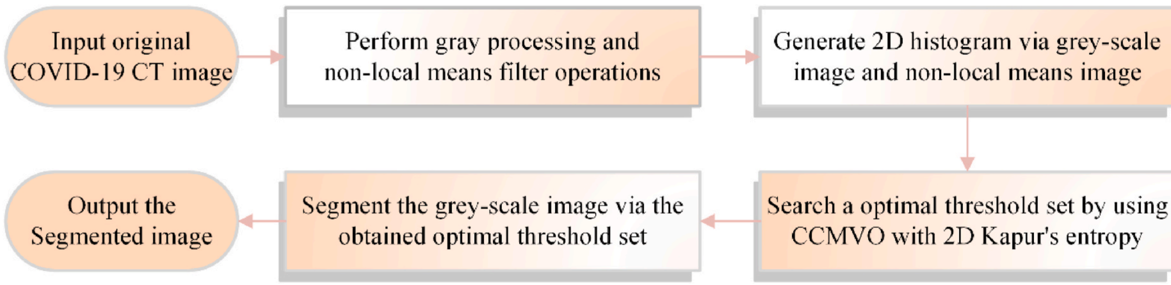


**Fig. 1.** Flowchart of MTIS

exchanging protons in a battery. Faris et al. [98] combined the MVO algorithm with SVM to propose a high-performance feature selection model. Peng et al. [99] artificially optimize the bias and weights of the artificial neural network and use the improved MVO algorithm for optimal parameter search. Jangir et al. [100] propose a hybrid algorithm combining the PSO algorithm and the MVO algorithm for the reactive power scheduling problem for power system optimization. Ali et al. [101] use the MVO algorithm for the parameter determination problem of photovoltaic cells for optimization search. It can be seen that MVO, as a new swarm intelligence algorithm proposed in recent years, has the characteristics of simplicity and strong optimization ability and has been applied to optimization problems in various fields by the majority of researchers.

However, when MVO is applied to MTIS, the search efficiency and ability to jump out of the local optimum are low, and the search for the optimum is often poor. Therefore, we propose a novel improved MVO (CCMVO) in this paper. The horizontal and vertical search mechanisms are introduced to improve the search capability of the algorithm through crossover updates between individuals of the population. To illustrate that CCMVO can jump out of local optimums and obtain higher-quality solutions more quickly, the article compares CCMVO to 30 test functions from CEC2014. The proposed CCMVO algorithm is compared with four well-known algorithms and four enhanced algorithms in the benchmark function experiment. Moreover, this paper also analyzes the comparison results by the non-parametric test of Wilcoxon [102] and Freidman [103] to demonstrate that the algorithm performance of CCMVO not only outperforms MVO but also significantly outperforms similar algorithms. Then in the image segmentation section, CCMVO is likewise compared in detail with related algorithms. Additionally, this article makes use of the Feature Similarity Index (FSIM) [104], the Peak Signal to Noise Ratio (PSNR) [105], and the Structural Similarity Index (SSIM) [69] to evaluate picture segmentation findings. The findings of the thorough examination reveal unequivocally that the CCMVO-based MTIS approach is not prone to optimization stalls, yielding better segmentation results that may give some technical support for the diagnosis of COVID-19. The following summarizes the study's major contributions:

- In this study, an improved multidimensional optimizer (CCMVO) based on the MVO algorithm is proposed, an important reference for the performance improvement of the optimization algorithm.
- CCMVO is used to segment COVID-19 images with multiple thresholds using nonlocal means, 2D histogram, and 2D Kapur's entropy.
- In this paper, benchmark function experiments demonstrate that CCMVO is a significant improvement in finding optimal solutions compared to other peer algorithms and is expected to become a new standard for high-performance optimization algorithms.
- In this paper, the proposed MTIS model is validated based on the real COVID-19 dataset, and the results demonstrate that the model has excellent segmentation ability and is expected to be a new medical aid diagnosis model.

The rest of this work is organized in the following manner. In Section 2, we discuss the CCMVO-based MTIS in detail. The original MVO is discussed in Section 3. Section 4 describes the CCMVO that is based on MVO. Section 5 compares CCMVO's performance to benchmark functions and image segmentation issues. Finally, Section 6 summarizes the whole article and suggests future research directions.

## 2. Related research on image segmentation

### 2.1. Image segmentation with multiple-level threshold

MTIS is a significant image segmentation technique that uses multiple thresholds to identify targets with distinct attributes in an image. Thus, the most critical part of MTIS is how the thresholds are chosen since this directly affects the impact of the segmented image. Histogram-based segmentation methods are one of the hot methods in the field of MTIS, which commonly include one-dimensional (1D) histogram and two-dimensional (2D) histogram segmentation methods. Since 1d histograms do not take advantage of the spatial features of the image, the results obtained are often inaccurate. Abutaleb et al. [106] suggested a 2D histogram-based segmentation approach that merged grayscale and local mean images while preserving the spatial characteristics of the image. The typical 2D histogram, which is constructed using a grayscale picture and a local mean image, overlooks the features of certain points and edges. The exhaustive technique is used to identify the ideal threshold, which is a highly computationally costly operation. Therefore, this paper first performs preprocessing to generate a 2D histogram (which is composed of grayscale images and nonlocal mean images), then models the problem as an optimal solution finding problem through the concept of Kapur's entropy, and finally performs efficient and accurate optimal solution finding through the CCMVO algorithm. The method is shown in detail in Fig. 1.

### 2.2. Nonlocal means

Nonlocal mean is a new image denoising technique proposed by Buades [107]. It denoises the image by using redundant information while preserving the image's detailed elements to the fullest degree possible. Moreover, the nonlocal mean of pixels is calculated by averaging pixels with comparable neighborhood structures in the image. Assume that the image containing noise is $g$, the original noise-free image is $s$ , and the random noise is $n$. The image model containing noise is as Eq. (1).

$$g(i) = s(i) + n(i) \tag{1}$$

where $(i) \in I$ , $I$ is the image domain; $g(i)$ is the noisy image; $s(i)$ is the original image; $n(i)$ is the Gaussian white noise with mean 0 and variance $\sigma^2$.

The nonlocal mean filtering algorithm calculates the similarity of all pixel points in the image to a pixel point $i$ in the image, and finds the weighting coefficients of each point in the image to pixel point $i$ based on the similarity, and then obtains the denoised estimate of pixel point $i$ by

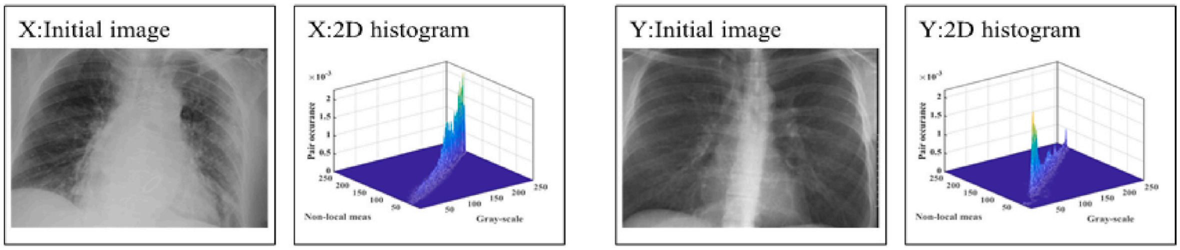


**Fig. 2.** Preview of the two-dimensional histogram on X and Y.

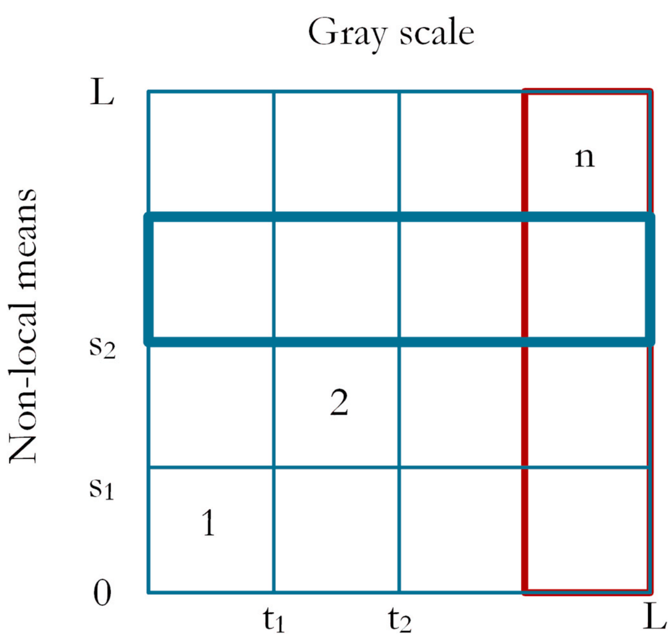


**Fig. 3.** Two-dimensional planar histogram.

averaging the weighted sum of all pixel points in the image with the obtained weighting coefficients. The nonlocal mean filtering algorithm is formulated as Eq. (2).

$$ng(i) = \frac{\sum_{j \in I} w(i,j) g(j)}{\sum_{j \in I} w(i,j)} \tag{2}$$

where $ng(i)$ is the filtering result; $w(i,j)$ is the weighting function, which is determined by the similarity between pixel $i$ and pixel $j$.

$N_i$ and $N_j$ are square domains centered at pixel $i$ and pixel $j$ . The similarity of pixel $i$ and pixel $j$ depends on the similarity between the neighborhood matrices $g(N_i)$ and $g(N_j)$, and the similarity between the neighborhood matrices is measured by the Gaussian-weighted distance $d(i,j)$. The Gaussian-weighted distance is formulated as Eq. (3).

$$d(i,j) = g(N_i) - g(N_j)^2_{2,\alpha} \tag{3}$$

where $\alpha > 0$ is the standard deviation of Gaussian weighting; $\cdot_2$ is the L2 parametrization, and the smaller $d(i,j)$ is the greater the similarity between the neighborhood matrices and the corresponding weight coefficient $w(i,j)$ is larger. The weighting function $w(i,j)$ is formulated as Eq. (4).

$$w\left(i,j\right) = exp\left(-\frac{d(i,j)}{h^2}\right) \tag{4}$$

where $h$ is the smoothing parameter that determines the attenuation of the weighting coefficients based on the similarity of pixel $i$ to pixel $j$.

### 2.3. 2D histogram

The grayscale images based on the aforementioned approach are combined to generate the nonlocal mean image, resulting in a two-dimensional histogram. As a result, the grayscale image $G(x,y)$ and range of values $[0,L]$ must be the same as the nonlocal mean image $D(x,y)$ size and range of values $[0,L]$. Then, the correlation values are normalized by Eq. (5) to construct a 2D histogram based on grayscale images and nonlocal mean images. The effect is shown in Fig. 2, where images X and Y are from the COVID-19 dataset [108].

$$P_{ij} = \frac{h(i,j)}{M \times N} \tag{5}$$

where $i$ is the $G(x,y)$ pixel value, $j$ denotes the $D(x,y)$ pixel value, and $h(i,j)$ signifies the number of times the point $(i,j)$ occurs on the gray value vector $(s,t)$.

### 2.4. Kapur's entropy for 2D histogram

Fig. 3 shows a 2D planar histogram based on the aforementioned 2D histogram, where $\{t_1, t_2 \ldots, L\}$ represents the grayscale image value and $\{s_1 s_2 \ldots, L\}$ signifies the nonlocal average image value. Since the major diagonal of the 2D histogram provides enough image information, and to make the computation easier, the Kapur entropy of the subregion on the main diagonal is computed using Eq. (6). The optimum solution produced by CCMVO in $(t_1, t_2, \ldots, t_d)$ is the ideal threshold since CCMVO uses Kapur's entropy as the objective function.

$$H(t_1, t_2, \ldots, t_d) = H_0 + H_1 + \cdots + H_d \tag{6}$$

where $H_0$, $H_1$ and $H_d$ parameters are set as follows.

$$H_0 = -\sum_{i=0}^{t_1-1}\left(\frac{P_{ij}}{\omega_0}\right)\ln\left(\frac{P_{ij}}{\omega_0}\right), \omega_0 = \sum_{i=0}^{S_1-1}\sum_{j=0}^{t_1-1} P_{ij}$$

$$H_1 = -\sum_{i=t_1}^{t_2-1}\left(\frac{P_{ij}}{\omega_1}\right) ln\left(\frac{P_{ij}}{\omega_1}\right), \omega_1 = \sum_{i=t_1}^{S_2-1}\sum_{j=t_1}^{t_2-1} P_{ij}$$

$$H_d = -\sum_{i=t_d}^{L-1}\left(\frac{P_{ij}}{\omega_d}\right)\ln\left(\frac{P_{ij}}{\omega_d}\right), \omega_d = \sum_{i=t_d}^{S_L-1}\sum_{j=t_d}^{t_L-1} P_{ij}$$

The optimal thresholds $(t_1^*, t_2^*, \cdots, t_d^*)$ should obey Eq. (7).

$$(t_1^*, t_2^*, \cdots, t_d^*) = \underset{0<t_1<t_2<\cdots<t_d<L-1}{\mathrm{argmax}} \{H(t_1, t_2, \cdots, t_d)\} \tag{7}$$

Larger Kapur's entropy values indicate more accurate corresponding segmentation thresholds and better segmentation results. In order to reduce the time required for the whole computational effort, the CCMVO algorithm is proposed to find the optimal threshold vector in the MTIS method to improve its efficiency of this segmentation method.

## 3. An overview of MVO

Recently, many SIOAs have been developed, such as Runge Kutta

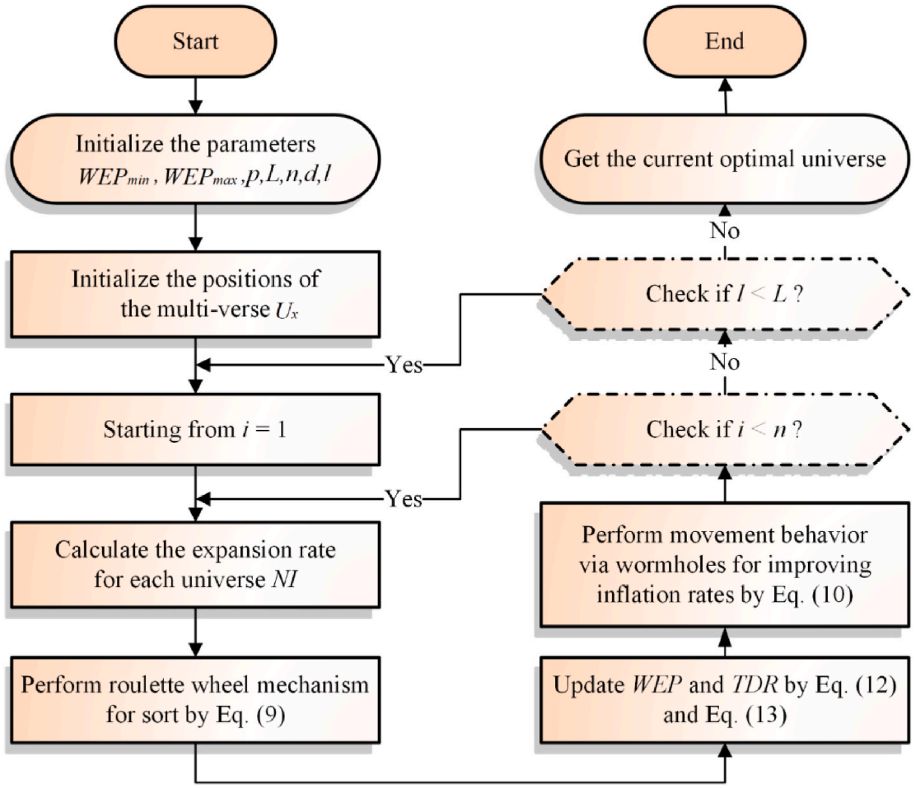


**Fig. 4.** Flowchart of MVO

optimizer (RUN)[2] [109], colony predation algorithm (CPA) [110], HHO[3] [68], the weighted mean of vectors (INFO)[4] [111], HGS,[5] [112], and slime mould algorithm (SMA)[6] [69]. These SIOAs have shown great potential in solving many problems in various fields such as education [82,113], energy [114,115], engineering [51,116], medicine [117–119], and finance [120,121]. Multiverse optimization (MVO) can effectively balance the relationship between global and local search, with fewer adjustment parameters, strong global search ability, good convergence, etc., and is gradually applied to solve various optimization problems.

The MVO builds a mathematical model as follows:

$$\boldsymbol{U}_x = \begin{bmatrix} x_{11} & x_{12} & \cdots & x_{1d} \\ x_{21} & x_{22} & \cdots & x_{2d} \\ \vdots & \vdots & \ddots & \vdots \\ x_{n1} & x_{n2} & \cdots & x_{nd} \end{bmatrix} \tag{8}$$

$$x_{ij} = \begin{cases} x_{kj} r_1 < NI(U_i) \\ x_{ij} r_1 \geqslant NI(U_i) \end{cases} \tag{9}$$

First, the entire universe space $U_x$ is initialized, where $n$ denotes the number of universes (candidate solutions) and $d$ denotes the number of matters in a universe (dimension of the solution). $x_{ij}$ represents the $j$ th matter in the $i$ th universe, and accordingly, $x_{kj}$ represents the $j$ th matter in the $k$ th universe. $U_i$ represents the $i$ th universe, and $NI(U_i)$ is the standard expansion rate of the $i$ th universe. The $j$ th matter of the $k$ th universe is selected as $x_{kj}$ by the roulette wheel mechanism in the MVO algorithm. In addition, $r_1$ is a random number between [0, 1].

Before developing a mathematical model of the wormhole mechanism, two important parameters in the multiverse algorithm are defined: the wormhole existence probability (WEP) and the travel distance rate (TDR), which are the probabilities of the existence of wormholes in the universe; the WEP increases with the number of iterations, and the probability of the existence of wormholes increases with the number of iterations. The TDR, on the other hand, decreases over generations to allow for more accurate exploration of the optimal universe. The mechanism is expressed as Eq. (10)- Eq. (11).

When $r_2 < WEP$,

$$x_{ij} = \begin{cases} X_j + TDR \cdot \left( \left( b_{u,j} - b_{l,j} \right) \cdot r_4 + b_{l,j} \right) r_3 < 0.5 \\ X_j - TDR \cdot \left( \left( b_{u,j} - b_{l,j} \right) \cdot r_4 + b_{l,j} \right) r_3 \geqslant 0.5 \end{cases} \tag{10}$$

when $r_2 \geqslant WEP$,

$$x_{ij} = x_{ij} \tag{11}$$

where $X_j$ is the $j$ th matter in the current optimal universe, and the upper bound of the $j$ th matter is $b_{u,j}$ and the lower bound is $b_{l,j}$. $r_2, r_3, r_4$ are random numbers in the interval [0, 1], respectively. The $WEP$ and $TDR$ formulas are defined as Eq. (12)- Eq. (13).

$$WEP = WEP_{min} + l \cdot \left( \frac{WEP_{max} - WEP_{min}}{L} \right) \tag{12}$$

$$TDR = 1 - \frac{l^{1/p}}{L^{1/p}} \tag{13}$$

where $WEP_{max}$ and $WEP_{min}$ are the upper and lower limits of $WEP$ values, respectively, $WEP_{min} = 0.2$ and $WEP_{max} = 1$; $l$ is the current iteration number; $L$ is the maximum iteration number; $p$ is the accuracy of iterative exploitation, and the value is 6.

The flowchart based on the description of the MVO mathematical model in subsection 3.1 is shown in Fig. 4.

2 https://aliasgharheidari.com/RUN.html.
3 https://aliasgharheidari.com/HHO.html.
4 https://aliasgharheidari.com/INFO.html.
5 https://aliasgharheidari.com/HGS.html.
6 https://aliasgharheidari.com/SMA.html.

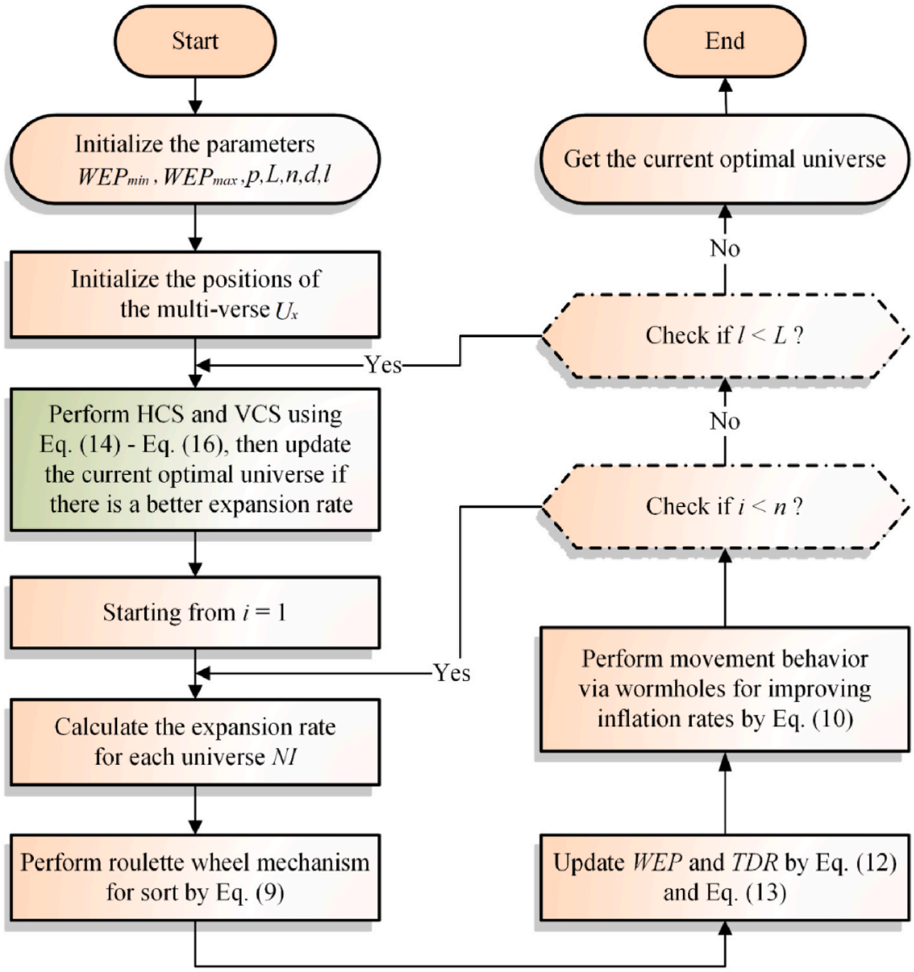


**Fig. 5.** Flowchart of CCMVO

## 4. Proposed CCMVO

This section describes the two search strategies, horizontal crossover search and vertical crossover search, and the CCMVO based on them. At the same time, this research employs horizontal crossover search (HCS) and vertical crossover search (VCS) [122], which are primarily utilized to increase the search efficiency and the ability of the MVO algorithm to jump out of the local optimum early on.

### 4.1. Optimization strategies

Meng et al. introduced CSO in 2014 [122] to demonstrate the possibility of using the HCS and VCS strategies to improve the algorithm. Experiments have similarly shown that the strategies improve the efficiency and accuracy of the algorithm in finding the optimal. Not only that, Zhao et al. [123] similarly used the HCS and VCS strategies to optimize the ACOR algorithm in the swarm intelligence algorithm to enhance the overall performance of the algorithm. As a result, this article incorporates HCS and VCS into MVO to enhance the algorithm's search capability during iteration.

#### 4.1.1. Horizontal crossover search

The HCS mainly acts on two different universes individually by crossing all the corresponding dimensions arithmetically. As a result, introducing HCS to the MVO algorithm enhances the possibility of exchanging useful objects (i.e., dimensions of universes) between different universes through wormholes, which enables rapid optimization and improves the convergence efficiency of the algorithm. Assuming that the $n$ th column dimension of the parent universes $x_i$ and $x_j$ performs HCS, then the lateral crossover update formula can be expressed as Eq. (14) and Eq. (15).

$$MS_i^n = \varepsilon_1 \times x_{in} + (1 - \varepsilon_1) \times x_{jn} + c_1 \times (x_{in} - x_{jn}) \tag{14}$$

$$MS_j^n = \varepsilon_2 \times x_{jn} + (1 - \varepsilon_2) \times x_{in} + c_2 \times (x_{jn} - x_{in}) \tag{15}$$

where $\varepsilon_1$ and $\varepsilon_2$ are random numbers between $(0, 1)$, $c_1$ and $c_2$ are random numbers between $(-1, 1)$, $x_{in}$ is the $n$ th dimension of the $i$ th universe, $x_{jn}$ is the $n$ th dimension of the $j$ th universe, and $MS_i^n$ and $MS_j^n$ are the new universes generated by the parent universes $x_i$ and based on HCS.

#### 4.1.2. Vertical crossover search

The VCS is mostly used to cross the individuals of the associated universes across two distinct dimensions arithmetically. This enables some individuals who search stagnation to continue participating in the search, while the ones who do the search generally stay unaffected. VCS is represented in the MVO algorithm by exchanging objects inside the same universe (i.e., universe dimensions), which prevents the MVO algorithm from readily searching stagnation. Assuming that the dimension of the $n$ th universe implements VCS, the vertical cross update formula is Eq (16).

$$MS_i^m = \varepsilon \times x_{im} + (1 - \varepsilon) \times x_{in} \tag{16}$$

where $\varepsilon$ is a random number between $(0, 1)$, $x_{im}$ and $x_{in}$ are the $m$ th and $n$ th dimensions of the $i$ th universe, and $MS_i^m$ is the new universe

**Algorithm 1** Pseudo-code of CCMVO

Initialize important parameters $WEP_{min}$, $WEP_{max}$, $p$, $L$ and relevant variables $n$, $d$, $l$
Initialize the multiverse population $\boldsymbol{U}_x$
Get the current optimal universe
**While** $l \leq L$
  **While** $l \leq (L/2)$
   Perform HCS and VCS using Eq. (14) - Eq. (16) after population initialization
    **If** calculating fitness is better
      Update the current optimal universe
    **End If**
    continue
  **End While**
  **For** $i = 1 : n$
   Update $WEP$ and $TDR$ by Eq. (12) and Eq. (13)
    **For** $j = 1 : d$
     $r_1 = rand$
     **If** $r_1 < Normalize\ inflation\ rate\ of\ U_i$
      Perform roulette wheel mechanism for sort by Eq. (9)
     **End If**
     $r_2 = rand$
     **If** $r_2 < WEP$
      $r_3 = rand;$
       $r_4 = rand$
      Perform movement behavior via wormholes for improving inflation rates by Eq. (10)
     **End If**
    **End For**
   **End For**
   **If** calculate fitness is better
     Update the current optimal universe
   **End If**
   $l = l + 1$
   **End While**
   Get the current optimal universe

generated by the universe $x_i$ based on VCS.

### 4.2. The proposed CCMVO

In response to the problem that the original MVO is prone to fall into local optimum and low efficiency at the pre-optimal search stage, this paper proposes the CCMVO algorithm with stronger overall performance. The specific improvement idea is: when the algorithm enters the preliminary search phase, the HCS and VCS strategies are first used for population preprocessing to find the optimal solution more comprehensively using the stronger randomness of the strategies; in the middle process of the iteration, the HCS and VCS strategies cooperate with the MVO to find the optimal, to realize jumping out of the local optimal trap; in the later stage of the iteration, the optimal solution is determined by making full use of the exploitation performance of the MVO. To illustrate the improvement idea more conveniently, the flow chart of CCMVO is shown in Fig. 5. The pseudocode of CCMVO is shown in Algorithm 1.

**Algorithm 1.**
Pseudo-code of CCMVO

The complexity of CCMVO consists of the introduced HCS and VCS, roulette selection mechanism, fast sorting algorithm, and the fitness value calculation. First, the complexity level of HCS and VCS is $O(l*n*d + l*n^2)$. Then, the complexity level of the roulette selection mechanism in the two extreme cases is $O(n)$ and $O(logn)$. The complexity of the quick sort algorithm in the best and worst cases is $O(n*logn)$ and $O(n^2)$, respectively. Finally, the complexity level of the fitness value calculation is $O(n*logn)$. As a result, the overall complexity level of the CCMVO algorithm is $O(CCMVO) = O((d + n + d*logn)*l*n)$.

**Table 1**
Parameter setting for the optimization process.

| Parameter name | Value |
|---|---|
| Population size | 30 |
| Maximum number of evaluations | 300,000 |
| Number of tests per algorithm | 30 |

## 5. Experiments and results

To demonstrate that CCMVO outperforms 4 well-known optimization algorithms and 5 enhanced algorithms in terms of jumping out of local optimums and upfront search capability, this section compares CCMVO to 30 benchmark functions and nine algorithms. This research compares CCMVO to eight comparable algorithms and examines the segmentation results using FSIM, PSNR, and SSIM to indicate that CCMVO performs better in multilevel image segmentation.

### 5.1. Experiment setup

This study employs 30 benchmark functions from CEC 2014 to illustrate the algorithmic performance of CCMVO in the experimental section of benchmark functions, and Table A1 in Appendix A contains the specifics of benchmark functions F1–F30. The default value is used as the test value for the benchmark function. Additionally, to ensure the studies are as objective as feasible, all algorithm comparison tests in this study are conducted under identical circumstances as described below, using the parameters in Table 1.

The segmented images A, B, C, D, E, F, G, H, I, and J are from the COVID-19 dataset [108]. Their original images and the nonlocal average 2D histogram are shown in Fig. 6. A fair comparison is a well-accepted

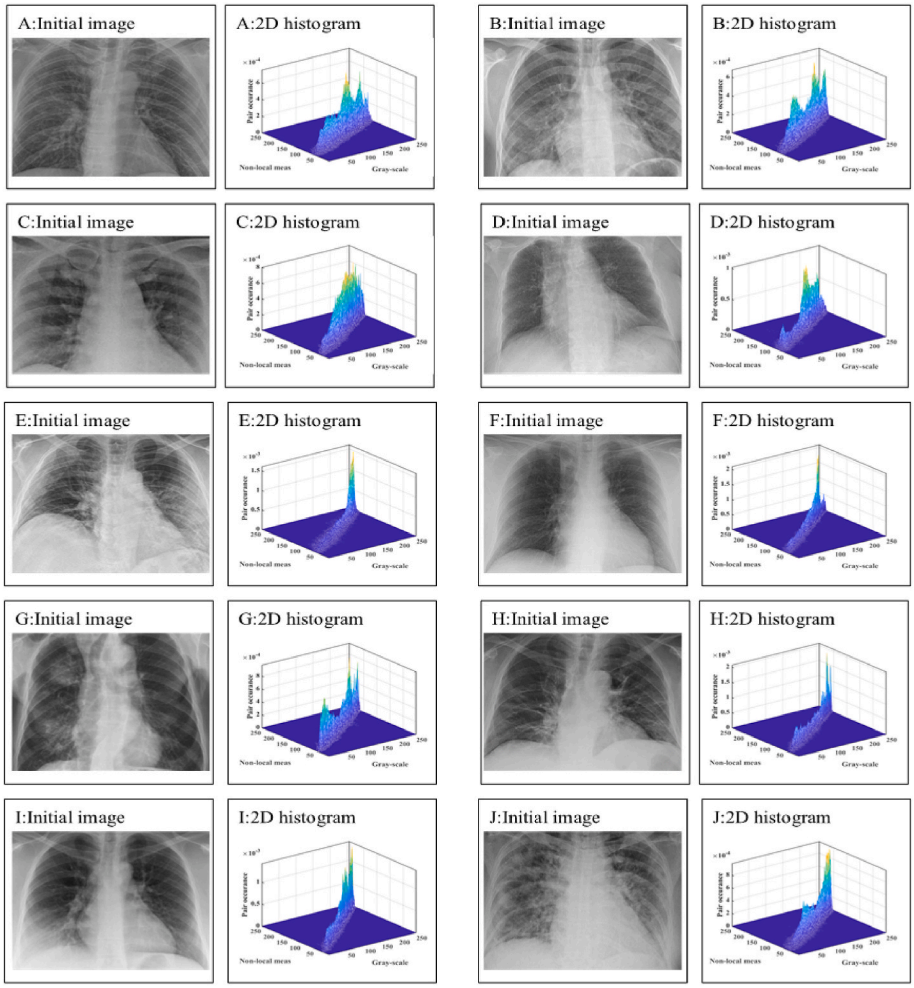


**Fig. 6.** Samples of the segmented images.

**Table 2**
Parameter setting of MTIS experiments.

| Parameter name | Value |
|---|---|
| Image size | 512 × 400 |
| Number of iterations | 100 |
| Number of tests per algorithm | 30 |
| Threshold levels | 2, 4, 6, 10, 15, 20 |

rule in the optimization and machine learning community, which we also followed in these experiments [124–127]. These fair rules can guarantee that the experiments are done under the same settings, and there is no bias towards a specific method in competition [128–130]. All algorithms were evaluated under identical circumstances to ensure the experiment was fair, using the parameters provided in Table 2. To more accurately describe the performance of each algorithm at different threshold levels, 2, 4, 6, 10, 15, and 20 were chosen as the threshold levels for the image segmentation experiments, where 2, 4, and 6 denote low threshold levels and 10, 15 and 20 denote high threshold levels.

Additionally, all studies were done on the Windows Server 2008R2 operating system to guarantee that all trials took place in the same environment. The device is powered by an Intel(R) Xeon(R) CPUE5-2660v3 (2.60 GHz) processor and 16 GB of RAM, with Matlab2017b serving as the code execution software.

**Table 3**
CCMVO and peer's algorithms comparison results.

| Algorithm | +/−/ = | Mean | Rank |
|---|---|---|---|
| CCMVO | ~ | 2.07 | 1 |
| MVO | 24/0/6 | 3.53 | 2 |
| DE | 19/7/4 | 3.63 | 3 |
| SCA | 29/1/0 | 8.33 | 9 |
| HHO | 22/5/3 | 4.6 | 4 |
| CBA | 29/0/1 | 5.96 | 6 |
| SCADE | 27/2/1 | 8.37 | 10 |
| IGWO | 28/2/0 | 4.74 | 5 |
| ACWOA | 26/2/2 | 7.21 | 8 |
| ASCA_PSO | 29/1/0 | 6.54 | 7 |

### *5.2. Experimenting with CCMVO's benchmark functions*

#### *5.2.1. Comparison of CCMVO and peer algorithms*

CCMVO is compared in this section to four fundamental algorithms and five enhanced algorithms using 30 benchmark functions. The fundamental algorithms are MVO, DE, SCA, and HHO, while the improved algorithms are CBA, SCADE, IGWO, ACWOA, and ASCA_PSO [131]. The comparison of CCMVO to other comparable algorithms is summarized in Table A2, where AVG and STD reflect the mean and variance of the methods after 30 separate runs, respectively. By comparing and observing the mean values, we can initially see that for most of the benchmark functions, CCMVO has the smallest mean value. This indicates that CCMVO obtains relatively higher quality solutions

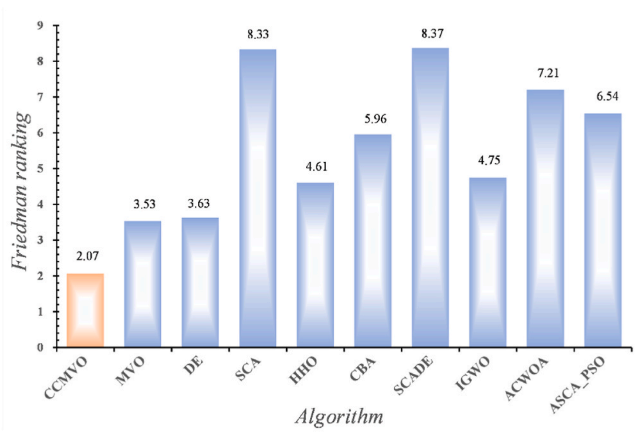


**Fig. 7.** Friedman ranking results of CCMVO and peer algorithms.

when the benchmark functions are optimized using CCMVO and similar algorithms. Also, the variance of the optimal solution is smaller, which indicates the high stability of CCMVO in optimizing the benchmark functions.

Wilcoxon signed-rank test and Freidman test were used to test and rank the experimental results in this paper to verify the intuitiveness and reliability of the comparison experiments. Table 3 shows the comparison results between CCMVO and other well-known algorithms. The experimental results are carefully analyzed using the Wilcoxon signed-rank test, where "$+/-/=$" indicates that the optimization performance of CCMVO is better than, worse than, and equal to other similar algorithms respectively. "Mean" represents the average performance ranking of cross-validation, and "Rank" represents the final ranking after cross-validation. In addition, the experimental results were verified by the Freidman test to show the advantages of CCMVO more accurately, as shown in Fig. 7. In Table 3, CCMVO is superior to the original MVO by 24 benchmark functions and superior to the very classical DE algorithm by 19. In addition, CCMVO ranks first in both the Wilcoxon signed-rank and Freidman test and outperforms the second place by a large margin. Therefore, it can be concluded that CCMVO is a flawless variant algorithm compared to other similar algorithms.

The convergence curves for CCMVO and other comparable algorithms on various functions are shown in Fig. 8. The convergence curves demonstrate that CCMVO has found better solutions when optimizing the benchmark functions F1, F5, and F17, even though CCMVO converges somewhat slower in the initial stage. Not only are high-quality solutions found by optimizing F9, F11, and F16, but the method also exhibits a clear jump out of the locally optimum inflection point. When F18, F21, and F30 are optimized, it is clear that CCMVO produces high-quality solutions and converges more quickly than the other algorithms. According to the benchmark function analysis findings above, CCMVO has a strong capacity to escape local optimal solutions, a strong ability to generate high-quality solutions, and a quicker convergence time. As a result, CCMVO is a better strategy for optimizing the benchmark function and produces an excellent SIOA.

### 5.2.2. *Comparative analysis of CCMVO and MVO*

The HCS and VCS mechanisms are primarily incorporated into MVO by the proposed CCMVO algorithm. As a result, this section will concentrate on the performance of CCMVO and MVO while optimizing benchmark functions.

The findings of CCMVO and MVO's qualitative assessment of 23 benchmark functions are shown in Fig. 9. The graphic in the first column (a) depicts the CCMVO search history's three-dimensional spatial

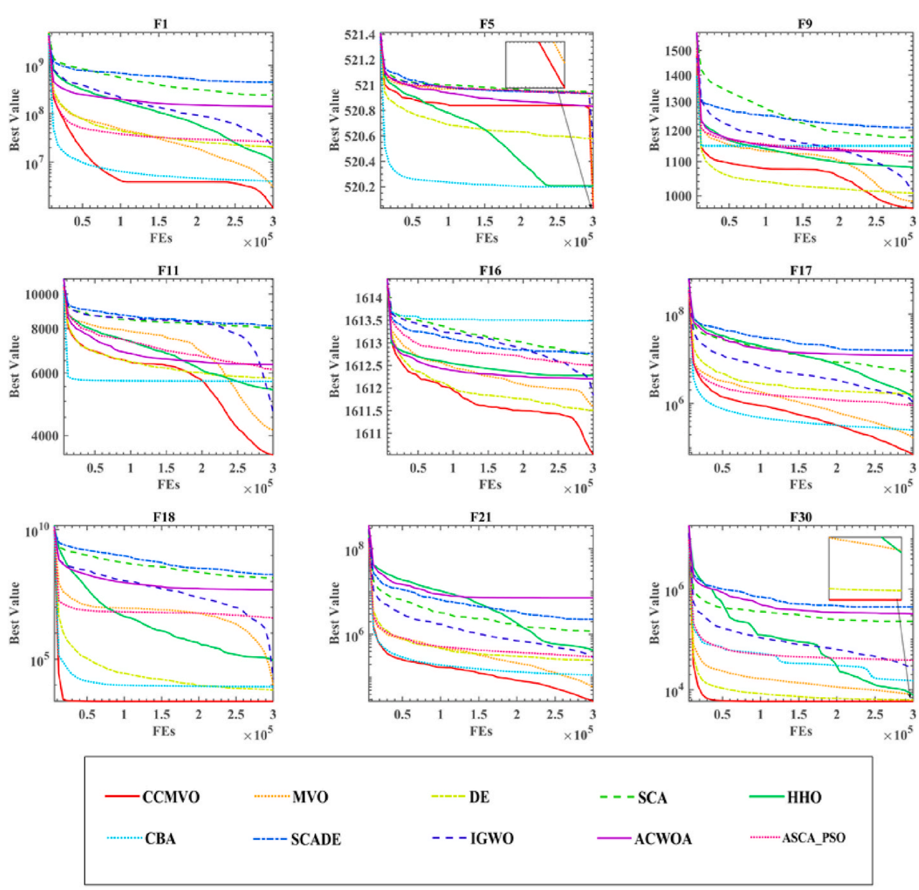


**Fig. 8.** Convergence curves of CCMVO and peer algorithms.

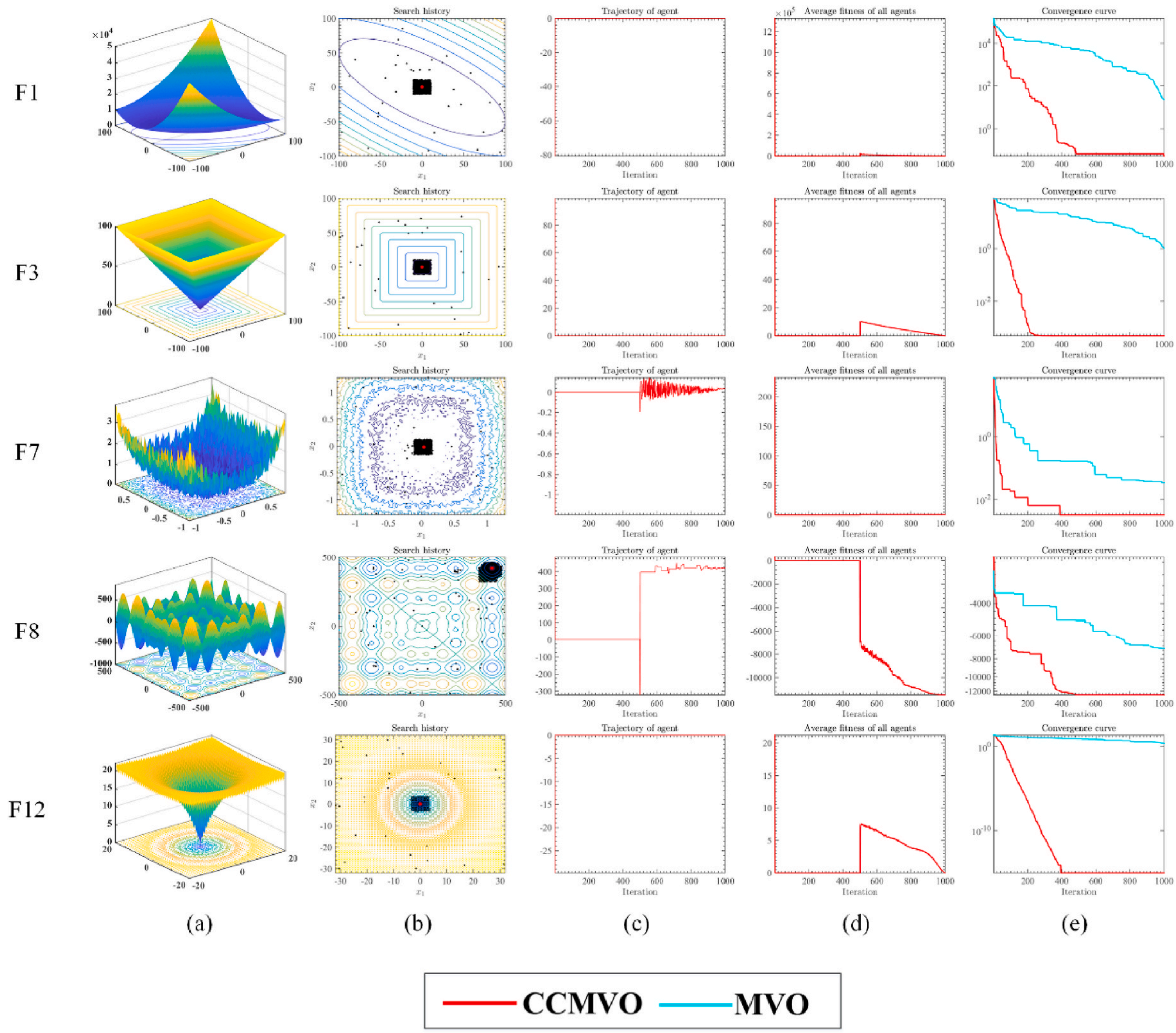


**Fig. 9.** CCMVO and MVO's optimization search process.

dispersion. The 2nd column (b) graphic depicts the CCMVO search history's 2D spatial distribution. The graphic in the 3rd column (c) depicts the iteration's trajectory for the first dimension of CCMVO individuals. The plots in the 4th column (d) depict CCMVO's average fitness, while the plots in the 5th column (e) depict CCMVO and MVO's convergence curves. The locations and distributions of the sought or created people are shown in Fig. 9(a) and (b), where it can be seen that most of the solutions generated during the iterations are close to the optimal solution. A few are more widely scattered due to the search. Moreover, this indicates that the individuals can quickly target the optimal solution that needs to be focused on exploitation during the search phase, allowing CCMVO to develop a better solution deeper in the convergence process. In Fig. 9(c), the first dimension of individuals in CCMVO is mainly unchanged in the middle and later stages of the iteration when facing single-peaked problems like F1, F3, and F12. This indicates that CCMVO can quickly confirm the approximate location of the optimal solution in the exploitation phase. In the case of complex problems such as F7 and F8, the first dimension of the individuals in CCMVO shows a significant and random fluctuation in general. This shows that CCMVO can jump out of the local optimum dilemma in time and has good algorithmic performance when facing multi-peaked problems. The average fitness curve is shown in Fig. 9(d), and it can be seen that the overall trend of the fitness values during the iterations is getting better. In terms of details, the search performance of the algorithm is powerful in the early part of the iteration, and it is more random in the middle of the iteration. It is easier to jump out of the local optimum trap. For example, F8 has a significant improvement in the final result. The convergence curves in Fig. 9(e) demonstrate that CCMVO can find solutions of more outstanding quality quicker than MVO.

On 30 CEC 2014 functions, the balance and variety of CCMVO and MVO were assessed, and the performance of CCMVO was further studied. The balance analysis of CCMVO and MVO is shown in Fig. 10(a) and (b), while the diversity analysis of CCMVO and MVO is shown in Fig. 10 (c). Fig. 10(a) introduces increment-decrement curves (b). If the solution obtained by the algorithm during the iteration is better than (including equal to) the previous solution, the curve will show an upward trend. If not, it diminishes. It is set to zero when it has a negative value. Thus, a high number indicates substantial search activity, whereas a low value indicates vigorous exploitation activity.

Additionally, the length of the graph's high or low value indicates the persistent influence of search or exploitation in the iterative process. The increment-decrement curve is maximized when the search effect is equal to the exploitation effect. The x-axis in Fig. 10(c) depicts the number of iterations, whereas the y-axis reflects variety. As a result of random initialization, the population diversity is initially high and subsequently diminishes with the number of repeats. It is worth mentioning that SIOA is not a high sequential method, so there are very large fluctuations in the optimization process, especially in the first and middle of the algorithm, and it stabilizes later, such as F2, F24, and F30 in Fig. 10 (c).

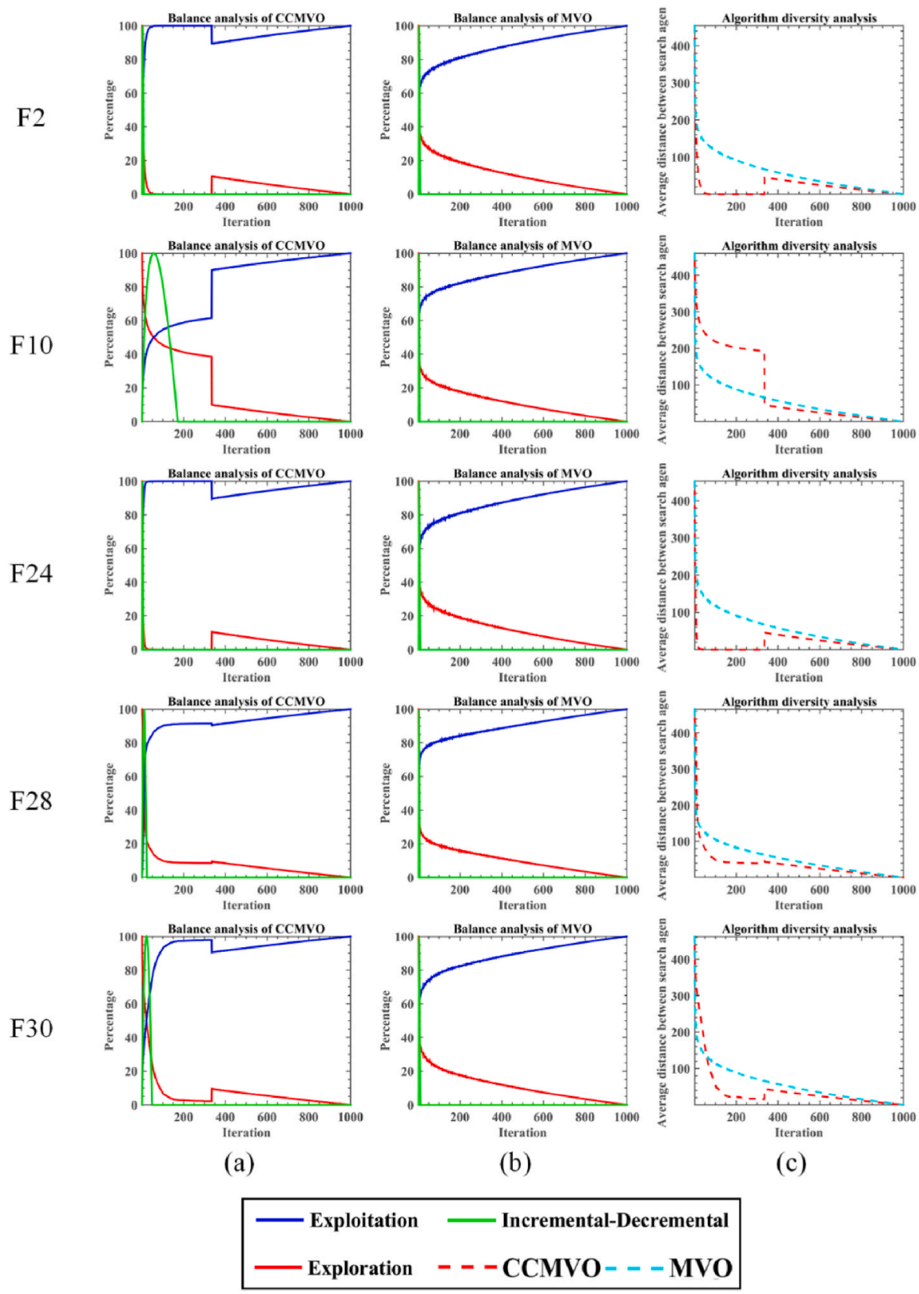


**Fig. 10.** Diversity and balance analysis of CCMVO and MVO.

Since the search and exploitation processes interact and might impact the ultimate outcome of the optimum search in a metaheuristic algorithm, it is vital to evaluate the balance between the two. As seen in Fig. 10(a) and (b), the search and exploitation results of CCMVO achieve superiority substantially sooner than those of MVO, indicating that CCMVO can locate a high-quality solution quicker in the search phase enter the exploitation phase more rapidly. Additionally, the distinct search and exploitation curves demonstrate that the search and exploitation effects of CCMVO are substantially greater than those of MVO. Owing to the strong optimization capability, the CCMVO can also be integrated with the machine learning techniques to tackle the real-world problems such as disease module identification [132,133], drug-disease associations prediction [134], drug discovery [135,136], pharmacoinformatic data mining [137,138], information retrieval services [139–141], text clustering [142], and recommender system [143,144].

**Table 4**
Indicators of performance for multilevel image segmentation algorithms.

| Formulation | Remark |
|---|---|
| $PSNR = 20\cdot\log_{10}\left(\frac{255}{RMSE}\right)$ | The ratio of the maximum power of the image signal and the destructive noise power. |
| $SSIM = \frac{(2\mu_I\mu_{Seg}+c_1)(2\sigma_{I,Seg}+c_2)}{(\mu_I^2+\mu_{Seg}^2+c_1)(\sigma_I^2+\sigma_{Seg}^2+c_2)}$ | Judging the degree of distortion by the brightness, contrast and structure of the image. |
| $FSIM = \frac{\sum_{I\in\Omega}S_L(X)PC_m(X)}{\sum_{I\in\Omega}PC_m(X)}$ | It is a variant of SSIM that weights the image information to determine the degree of distortion. |

### 5.3. CCMVO for multilevel image segmentation

This section performs MTIS experiments comparing CCMVO, MVO, WOA, SCA, HHO, BLPSO, IGWO, IWOA, and SCADE in this paper using

**Table 5**
The FSIM comparison results of CCMVO and other methods.

| Thresholds | | CCMVO | MVO | WOA | SCA | HHO | BLPSO | IGWO | IWOA | SCADE |
|---|---|---|---|---|---|---|---|---|---|---|
| 2 | +/−/ = | ~ | 7/1/2 | 7/0/3 | 3/0/7 | 10/0/0 | 9/1/0 | 5/4/1 | 6/1/3 | 5/3/2 |
| | Mean | 2.4 | 4.7 | 5.9 | 4.2 | 7.8 | 7.1 | 3.5 | 6.2 | 3.2 |
| | Rank | 1 | 5 | 6 | 4 | 9 | 8 | 3 | 7 | 2 |
| 4 | +/−/ = | ~ | 6/0/4 | 8/0/2 | 10/0/0 | 9/0/1 | 9/0/1 | 7/1/2 | 9/0/1 | 8/0/2 |
| | Mean | 1.5 | 2.5 | 5.3 | 6.5 | 6.6 | 6.7 | 4.1 | 6.2 | 5.6 |
| | Rank | 1 | 2 | 4 | 7 | 8 | 9 | 3 | 6 | 5 |
| 6 | +/−/ = | ~ | 3/0/7 | 8/0/2 | 10/0/0 | 9/0/1 | 9/0/1 | 7/0/3 | 6/0/4 | 10/0/0 |
| | Mean | 1.2 | 2.6 | 4.6 | 8.1 | 5.4 | 6.1 | 3.9 | 5.2 | 7.9 |
| | Rank | 1 | 2 | 4 | 9 | 6 | 7 | 3 | 5 | 8 |
| 10 | +/−/ = | ~ | 7/0/3 | 5/0/5 | 10/0/0 | 8/0/2 | 10/0/0 | 9/0/1 | 10/0/0 | 10/0/0 |
| | Mean | 1 | 2.4 | 3.1 | 8.3 | 5.1 | 5.8 | 4.7 | 6 | 8.6 |
| | Rank | 1 | 2 | 3 | 8 | 5 | 6 | 4 | 7 | 9 |
| 15 | +/−/ = | ~ | 6/0/4 | 6/0/4 | 10/0/0 | 10/0/0 | 10/0/0 | 10/0/0 | 10/0/0 | 10/0/0 |
| | Mean | 1 | 2.7 | 2.3 | 8.2 | 4.6 | 5.9 | 5.6 | 5.9 | 8.8 |
| | Rank | 1 | 3 | 2 | 8 | 4 | 6 | 5 | 6 | 9 |
| 20 | +/−/ = | ~ | 8/0/2 | 2/0/8 | 10/0/0 | 9/0/1 | 10/0/0 | 10/0/0 | 10/0/0 | 10/0/0 |
| | Mean | 1.2 | 3.1 | 1.8 | 8.7 | 5 | 6 | 6.1 | 4.8 | 8.3 |
| | Rank | 1 | 3 | 2 | 9 | 5 | 6 | 7 | 4 | 8 |

**Table 6**
The PSNR comparison results of CCMVO and other methods.

| Thresholds | | CCMVO | MVO | WOA | SCA | HHO | BLPSO | IGWO | IWOA | SCADE |
|---|---|---|---|---|---|---|---|---|---|---|
| 2 | +/−/ = | ~ | 3/1/6 | 6/0/4 | 8/0/2 | 7/1/2 | 2/3/5 | 7/2/1 | 5/1/4 | 6/1/3 |
| | Mean | 2.3 | 4.8 | 6.3 | 5.6 | 5.8 | 4.1 | 4.7 | 5.2 | 6.2 |
| | Rank | 1 | 4 | 9 | 6 | 7 | 2 | 3 | 5 | 8 |
| 4 | +/−/ = | ~ | 5/0/5 | 9/0/1 | 10/0/0 | 9/0/1 | 9/0/1 | 8/1/1 | 9/0/1 | 9/0/1 |
| | Mean | 1.4 | 2.4 | 5.7 | 8.3 | 6.2 | 5 | 3.4 | 4.8 | 7.8 |
| | Rank | 1 | 2 | 6 | 9 | 7 | 5 | 3 | 4 | 8 |
| 6 | +/−/ = | ~ | 4/0/6 | 10/0/0 | 10/0/0 | 10/0/0 | 10/0/0 | 9/0/1 | 10/0/0 | 10/0/0 |
| | Mean | 1 | 2.1 | 4.2 | 8.6 | 6.1 | 5.5 | 3.7 | 5.5 | 8.3 |
| | Rank | 1 | 2 | 4 | 9 | 7 | 5 | 3 | 5 | 8 |
| 10 | +/−/ = | ~ | 7/0/3 | 7/0/3 | 10/0/0 | 10/0/0 | 10/0/0 | 9/0/1 | 10/0/0 | 10/0/0 |
| | Mean | 1 | 2.2 | 3.3 | 8.3 | 5.5 | 5.1 | 5.1 | 5.9 | 8.6 |
| | Rank | 1 | 2 | 3 | 8 | 6 | 4 | 4 | 7 | 9 |
| 15 | +/−/ = | ~ | 5/0/5 | 5/0/5 | 10/0/0 | 10/0/0 | 10/0/0 | 10/0/0 | 10/0/0 | 10/0/0 |
| | Mean | 1.1 | 2.5 | 2.5 | 8.4 | 4.9 | 5.6 | 5.8 | 5.6 | 8.6 |
| | Rank | 1 | 2 | 2 | 8 | 4 | 5 | 7 | 5 | 9 |
| 20 | +/−/ = | ~ | 8/0/2 | 3/0/7 | 10/0/0 | 8/0/2 | 9/0/1 | 10/0/0 | 10/0/0 | 10/0/0 |
| | Mean | 1.1 | 3.3 | 1.9 | 8.6 | 4.7 | 5.6 | 6.1 | 5.3 | 8.4 |
| | Rank | 1 | 3 | 2 | 9 | 4 | 6 | 7 | 5 | 8 |

images A B, C, D, E, F, G, H, I, and J.

*5.3.1. Methodology evaluation indicators*

To correctly assess the quality of each algorithm's segmentation outputs in this part, we employ PSNR, SSIM, and FSIM as assessment criteria. Table 4 contains the definitions and explanations of the three assessment measures.

When PSNR is used to assess the outcomes of image segmentation, RMSE is the root mean square error of each pixel, defined as Eq. (17), where $M \times N$ represents the image's size, $I_{ij}$ denotes the original image's

**Table 7**
The SSIM comparison results of CCMVO and other methods.

| Thresholds | | CCMVO | MVO | WOA | SCA | HHO | BLPSO | IGWO | IWOA | SCADE |
|---|---|---|---|---|---|---|---|---|---|---|
| 2 | +/−/ = | ~ | 5/0/5 | 4/0/6 | 3/0/7 | 10/0/0 | 7/0/3 | 5/3/2 | 7/1/2 | 5/3/2 |
| | Mean | 2.1 | 5.4 | 5.6 | 3.4 | 8.3 | 7.3 | 3.2 | 6.1 | 3.6 |
| | Rank | 1 | 5 | 6 | 3 | 9 | 8 | 2 | 7 | 4 |
| 4 | +/−/ = | ~ | 3/0/7 | 9/0/1 | 8/0/2 | 9/0/1 | 7/1/2 | 5/3/2 | 7/0/3 | 5/2/3 |
| | Mean | 1.9 | 3.3 | 7 | 5.2 | 7.2 | 6.3 | 3.7 | 6.5 | 3.9 |
| | Rank | 1 | 2 | 8 | 5 | 9 | 6 | 3 | 7 | 4 |
| 6 | +/−/ = | ~ | 2/0/8 | 6/0/4 | 9/0/1 | 7/0/3 | 6/2/2 | 3/3/4 | 6/1/3 | 7/1/2 |
| | Mean | 2.1 | 3.1 | 5.6 | 6.4 | 6.2 | 5.1 | 4 | 5.8 | 6.7 |
| | Rank | 1 | 2 | 5 | 8 | 7 | 4 | 3 | 6 | 9 |
| 10 | +/−/ = | ~ | 5/0/5 | 4/0/6 | 10/0/0 | 6/0/4 | 10/0/0 | 8/0/2 | 10/0/0 | 10/0/0 |
| | Mean | 1.1 | 2.6 | 3.7 | 8.4 | 4.4 | 5.9 | 4.6 | 6 | 8.3 |
| | Rank | 1 | 2 | 3 | 9 | 4 | 6 | 5 | 7 | 8 |
| 15 | +/−/ = | ~ | 7/0/3 | 6/0/4 | 10/0/0 | 10/0/0 | 10/0/0 | 10/0/0 | 10/0/0 | 10/0/0 |
| | Mean | 1 | 2.6 | 2.8 | 8.5 | 4.3 | 5.8 | 5.8 | 5.7 | 8.5 |
| | Rank | 1 | 2 | 3 | 8 | 4 | 6 | 6 | 5 | 8 |
| 20 | +/−/ = | ~ | 7/0/3 | 3/1/6 | 10/0/0 | 8/0/2 | 10/0/0 | 10/0/0 | 10/0/0 | 10/0/0 |
| | Mean | 1.1 | 3.2 | 1.9 | 8.7 | 4.5 | 6.3 | 5.8 | 5.2 | 8.3 |
| | Rank | 1 | 3 | 2 | 9 | 4 | 7 | 6 | 5 | 8 |

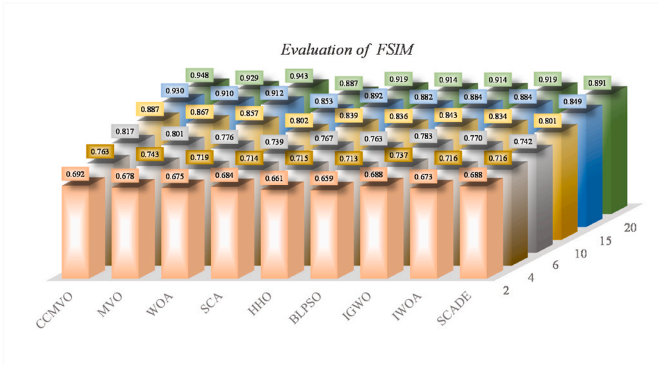


**Fig. 11.** The average of FSIM at each threshold level.

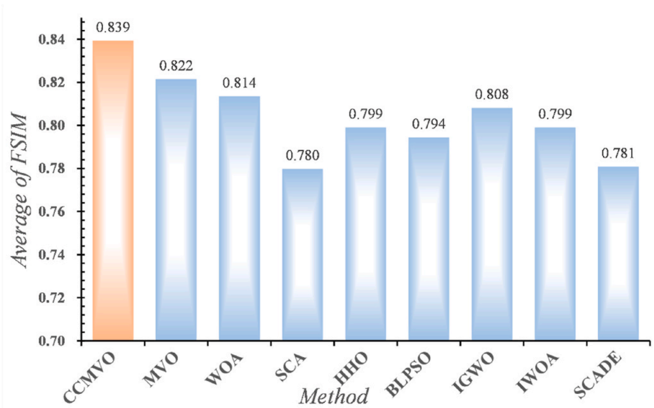


**Fig. 12.** The average of FSIM for all threshold levels.

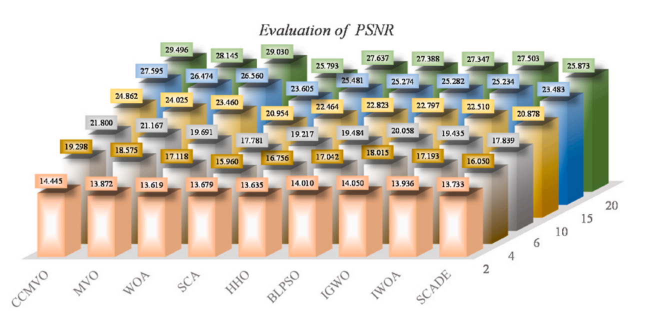


**Fig. 13.** The average of PSNR at each threshold level.

pixel gray value, and $Seg_{ij}$ means the segmented image's pixel gray value.

$$RMSE = \sqrt{\frac{\sum_{i=0}^{M-1}\sum_{j=0}^{N-1}\left(I_{ij} - Seg_{ij}\right)^2}{M \times N}} \tag{17}$$

Simultaneously, mean, variance, and Wilcoxon signed-rank tests were utilized to further examine the outcomes of the FSIM, PSNR, and SSIM evaluations.

### 5.3.2. Segmentation result analyses

Tables A3 - A5 in Appendix A represent the mean and variance of the segmentation results after evaluation using FSIM, PSNR, and SSIM, and Tables 5–7 illustrate the Wilcoxon signed-rank test analysis of the FSIM, PSNR, and SSIM data, where Mean denotes the overall mean and Rank denotes the ranking based on the overall mean. It can be seen that the

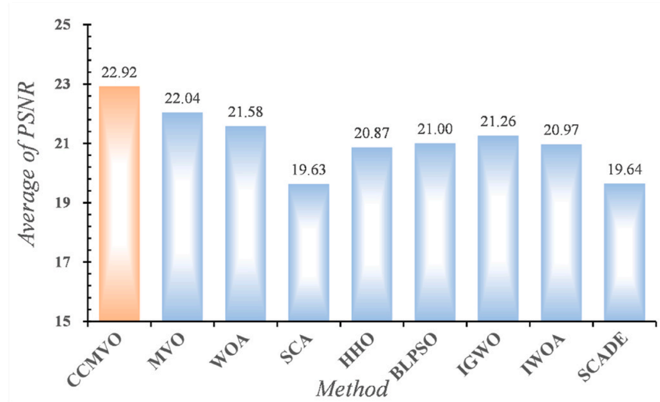


**Fig. 14.** PSNR averaged across all levels of threshold.

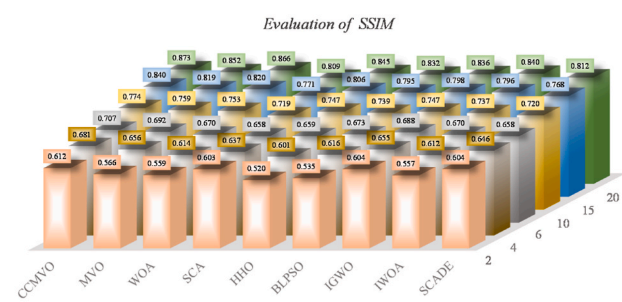


**Fig. 15.** The average of SSIM at each threshold level.

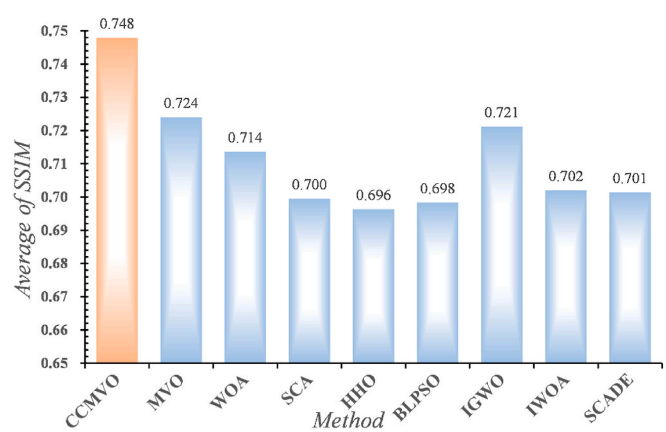


**Fig. 16.** SSIM averaged across all levels of threshold.

MTIS model based on CCMVO is quite superior compared to other peer models. In particular, CCMVO is a stable performance compared to MVO when there is no worse segmentation result than MVO in 10 images.

Figs. 11–12 represent the average evaluation of FSIM for each algorithm at the same threshold level, and the average evaluation of FSIM at all threshold levels. It can be seen that CCMVO performs more effectively under the FSIM evaluation method relative to the other algorithms, which indicates that the image features segmented by the CCMVO-based MTIS model are more distinct.

Figs. 13–14 represent the average PSNR evaluation for each algorithm at the same threshold level and the average PSNR evaluation at all threshold levels. It can be seen that the CCMVO-based MTIS model is excellent in the evaluation of PSNR both at a single threshold level and

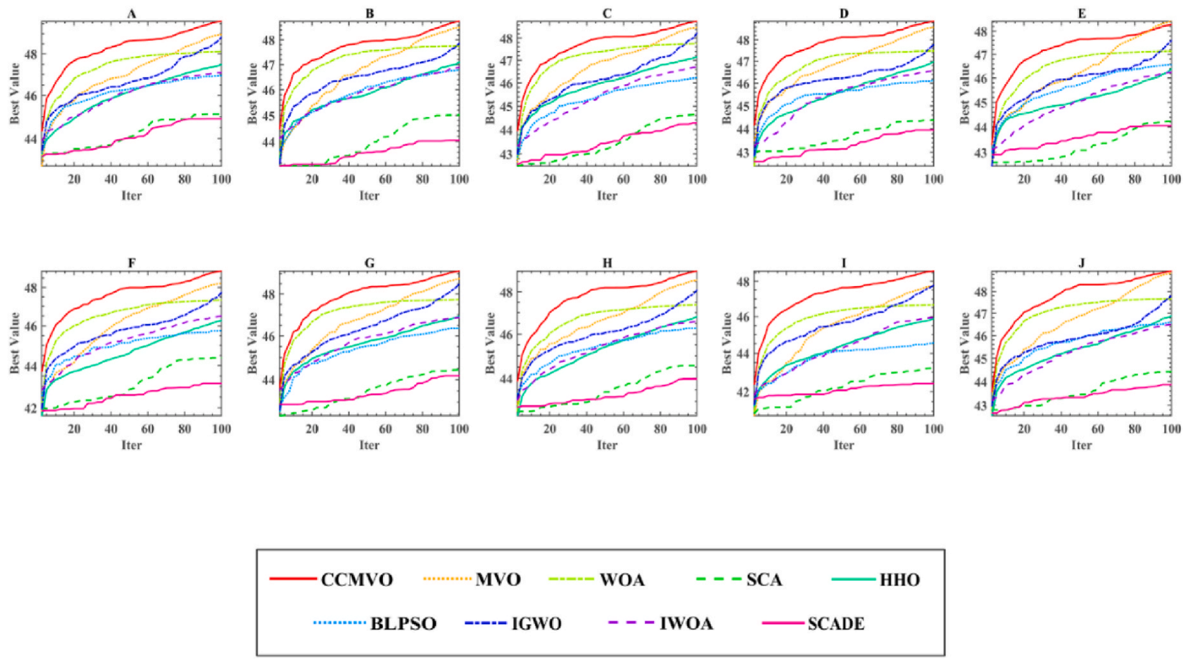


**Fig. 17.** Iteration curves for a threshold level of 6.

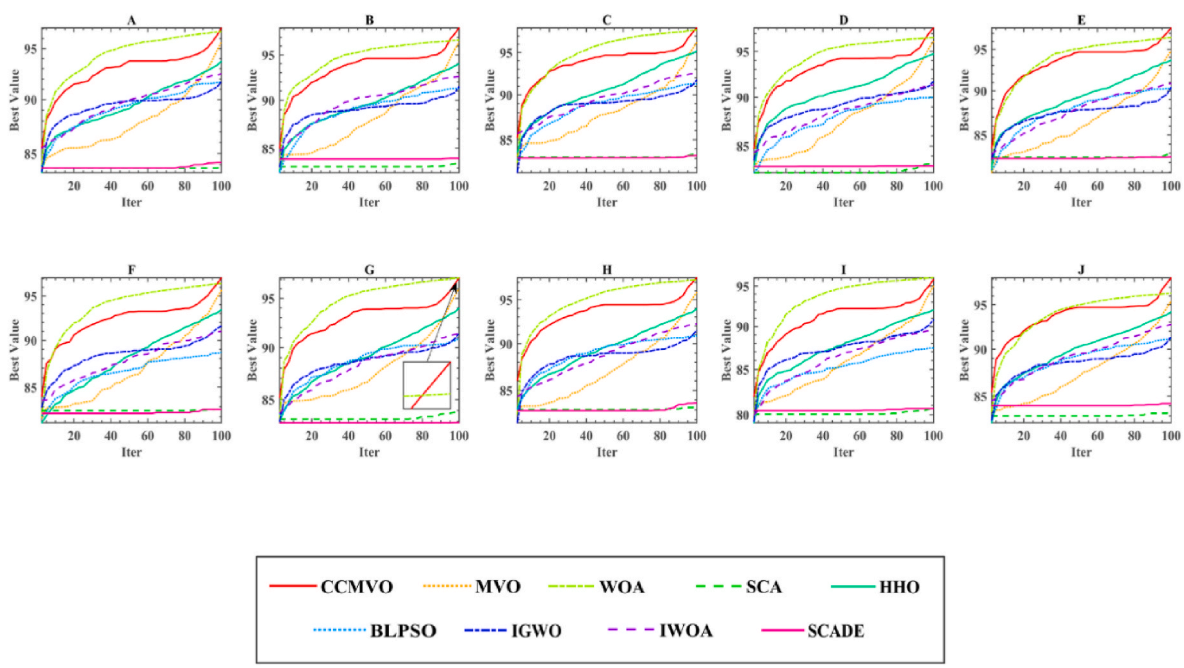


**Fig. 18.** Iteration curves for a threshold level of 20.

at the average of all threshold levels. This indicates that the proposed model produces images with very small distortion during segmentation, preserving the image quality as much as possible.

Figs. 15–16 show the average evaluation of SSIM for each algorithm at the same threshold level and the average evaluation of SSIM at each threshold level. It can be seen that the same CCMVO-based MTIS algorithm is much ahead of the other algorithms under the classical SSIM evaluation metrics. This indicates that CCMVO can compare the change of image structure information and consider the distortion of the image, which is better for obtaining objective and high-quality segmented images.

Looking at the mean and variance of FSIM, PSNR, and SSIM evaluations, for most images and thresholds, the mean of CCMVO is larger than the mean of the other methods, and its variance is smaller than the variance of the other methods. Wilcoxon signed-rank test examination of the assessment data for FSIM, PSNR, and SSIM revealed that the overall average rating for FSIM, PSNR, and SSIM at all threshold levels was first. Additionally, as seen in Figs. 11–16, CCMVO has the highest average assessment results for FSIM, PSNR, and SSIM at the same threshold levels and the same average assessment outcomes at all threshold levels. Thus, experiment results demonstrate the CCMVO-MTIS method's great superiority.

Table A6 represents the optimal Kapur's entropy (KE) found by all algorithms. Figures B1-B10 in Appendix B represent the specific

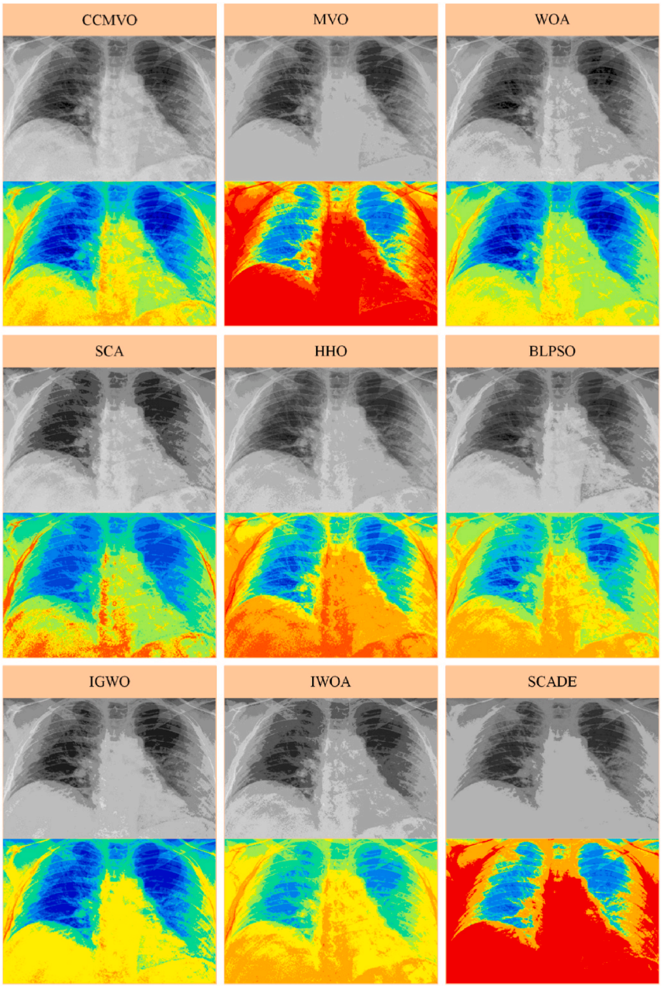


**Fig. 19.** Segmented images and Jet colormap images obtained by each algorithm.

segmentation thresholds for each algorithm to find images A-J when the threshold level is 6. Figs. 17–18 represent the convergence curves of CCMVO with similar algorithms when the threshold levels are 6 and 20. Fig. 19 represents image segmentation results for image I for all algorithms when the threshold level is 10.

As shown, most of the values discovered using CCMVO surpass the values obtained using other algorithms in terms of optimum KE. CCMVO is also the best in terms of keeping image information and overall segmentation outcomes for specialized segmentation findings. Thus, based on the appropriate KE, particular thresholds, and analysis of three metrics evaluation findings, the CCMVO-MTIS may achieve superior segmentation outcomes, making it an extremely effective segmentation method.

The image segmentation case is not enough to prove the effectiveness of the established CCMVO approach. In future work, the CCMVO can also be applied to more image processing and medical scenarios, such as multimode medical image registration [145], obtaining the optimal facade texture images [146], improving endoscopic imaging [147], optimizing medical-aided diagnosis systems [148], and optimizing E-healthcare systems [149].

Also, it can be applied to a wider area of applications that finding feasible solutions is a requirement including active surveillance [150], essay recommendation [151], location-based services [152,153], bionic electronic skin sensing [154,155], crystal structures optimization [156], kayak cycle phase segmentation [157], human motion capture [158], tomato pests diagnosis [159] and video deblurring [160].

## 6. Conclusions and future works

This paper offers the CCMVO meta-heuristic method and an upgraded MTIS system based on CCMVO for high-quality COVID-19 chest radiography segmentation. CCMVO is a modified MVO algorithm. We combine HCS and VCS into MVO in this study to increase CCMVO's search capacity and ability to jump out of local optimums, enabling CCMVO to get high-quality solutions. We begin with comparison testing against 30 benchmark functions. CCMVO surpasses MVO in terms of search efficiency and capacity to find high-quality solutions, as shown in the preceding comparative trials. Additionally, it can be demonstrated through the study and comparison of CCMVO and related SIOAs that CCMVO has a greater overall capacity to avoid search stagnation and achieve better solutions. As a result, CCMVO is an outstanding SIOA that has been thoroughly validated. We ran MTIS tests with CCMVO and other related algorithms, evaluating the segmentation results with FSIM, PSNR, and SSIM. Further analysis of the assessment data using the Wilcoxon signed-rank test revealed that CCMVO was ranked top overall in the comparative studies.

Additionally, we can observe that when the threshold level rises, the benefit of CCMVO-based MTIS segmentation becomes more apparent. Finally, this paper shows the overall segmentation performance of CCMVO-MTIS through experiments such as high and low threshold comparisons, histogram segmentation results, and adaptation curves, proving that CCMVO can find more reasonable optimal thresholds to peer algorithms. As a result, the enhanced MTIS approach based on CCMVO is rather good. Nevertheless, the CPU calculation for CCMVO in MTIS will take longer since HCS and VCS make CCMVO more complex than MVO. However, this issue will be resolved soon with parallel computing and high-performance computing methods fast exploitation.

In future work, to address the shortcomings of the current CCMVO application method, which is relatively simple, we will build a complete diagnostic system from image segmentation to feature selection to classification and prediction by starting from the direction of a complete system for medical diagnosis. On the other hand, we will address the efficiency problem of the CCMVO method and compensate for the shortcomings of the algorithm in the direction of parallel computing and hardware performance. In addition, CCMVO can be applied to medical diagnoses such as pneumonia, lung cancer et al., and other optimization problems. We will consider further improving the performance of CCMVO in different fields.

## Acknowledgments

We acknowledge Taif University for Supporting this study through Taif University Researchers Supporting Project number (TURSP-2020/26), Taif University, Taif, Saudi Arabia.

## Appendix A

**Table A.1**
CEC 2014 Benchmark Functions

| Class | No. | Functions | $F_i^* = F_i(x^*)$ |
|---|---|---|---|
| Unimodal Functions | 1 | Rotated High Conditioned Elliptic Function | 100 |
| | 2 | Rotated Bent Cigar Function | 200 |
| | 3 | Rotated Discus Function | 300 |
| Simple Multimodal Functions | 4 | Shifted and Rotated Rosenbrock's Function | 400 |
| | 5 | Shifted and Rotated Ackley's Function | 500 |
| | 6 | Shifted and Rotated Weierstrass Function | 600 |
| | 7 | Shifted and Rotated Griewank's Function | 700 |
| | 8 | Shifted Rastrigin's Function | 800 |
| | 9 | Shifted and Rotated Rastrigin's Function | 900 |
| | 10 | Shifted Schwefel's Function | 1000 |
| | 11 | Shifted and Rotated Schwefel's Function | 1100 |
| | 12 | Shifted and Rotated Katsuura Function | 1200 |
| | 13 | Shifted and Rotated HappyCat Function | 1300 |
| | 14 | Shifted and Rotated HGBat Function | 1400 |
| | 15 | Shifted and Rotated Expanded Griewank's plus Rosenbrock's Function | 1500 |
| | 16 | Shifted and Rotated Expanded Scaffer's F6 Function | 1600 |
| Hybrid Functions | 17 | Hybrid Function 1 ($N = 3$) | 1700 |
| | 18 | Hybrid Function 2 ($N = 3$) | 1800 |
| | 19 | Hybrid Function 3 ($N = 4$) | 1900 |
| | 20 | Hybrid Function 4 ($N = 4$) | 2000 |
| | 21 | Hybrid Function 5 ($N = 5$) | 2100 |
| | 22 | Hybrid Function 6 ($N = 5$) | 2200 |
| Composition Functions | 23 | Composition Function 1 ($N = 5$) | 2300 |
| | 24 | Composition Function 2 ($N = 3$) | 2400 |
| | 25 | Composition Function 3 ($N = 3$) | 2500 |
| | 26 | Composition Function 4 ($N = 5$) | 2600 |
| | 27 | Composition Function 5 ($N = 5$) | 2700 |
| | 28 | Composition Function 6 ($N = 5$) | 2800 |
| | 29 | Composition Function 7 ($N = 3$) | 2900 |
| | 30 | Composition Function 8 ($N = 3$) | 3000 |

**Table A.2**
Comparison results of CCMVO with other peer algorithms

| Fun | Item | CCMVO | MVO | DE | SCA | HHO | CBA | SCADE | IGWO | ACWOA | ASCA_PSO |
|---|---|---|---|---|---|---|---|---|---|---|---|
| F1 | AVG | **1.1146E+06** | 3.0903E+06 | 2.0663E+07 | 2.4397E+08 | 1.0746E+07 | 4.0100E+06 | 4.4884E+08 | 1.9063E+07 | 1.4195E+08 | 2.6134E+07 |
| | STD | **4.1713E+05** | 8.2442E+05 | 7.6353E+06 | 5.4570E+07 | 4.9999E+06 | 1.2454E+06 | 7.4696E+07 | 6.9309E+06 | 5.2824E+07 | 4.3503E+07 |
| F2 | AVG | 1.0438E+04 | 1.5150E+04 | **1.6716E+03** | 1.5706E+10 | 1.2265E+07 | 9.5298E+03 | 3.1279E+10 | 2.4278E+06 | 6.4054E+09 | 7.0247E+08 |
| | STD | 5.9941E+03 | 1.1039E+04 | **3.5554E+03** | 2.9404E+09 | 2.6830E+06 | 8.9048E+03 | 3.2927E+09 | 1.0902E+06 | 2.8006E+09 | 1.6683E+09 |
| F3 | AVG | 4.2878E+02 | 4.1738E+02 | **3.8121E+02** | 3.8045E+04 | 5.3642E+03 | 3.7768E+03 | 5.2681E+04 | 6.8487E+03 | 5.1795E+04 | 1.9509E+04 |
| | STD | **4.3812E+01** | 4.7276E+01 | 7.0592E+01 | 6.9218E+03 | 1.6852E+03 | 4.7197E+03 | 6.5942E+03 | 3.3437E+03 | 1.0565E+04 | 6.2139E+03 |
| F4 | AVG | 4.7932E+02 | **4.7697E+02** | 4.9315E+02 | 1.3375E+03 | 5.4688E+02 | 5.0230E+02 | 2.3377E+03 | 5.2487E+02 | 1.2874E+03 | 6.3235E+02 |
| | STD | 3.2225E+01 | 3.1732E+01 | **2.2515E+01** | 2.3590E+02 | 4.9393E+01 | 3.6932E+01 | 5.8362E+02 | 3.0048E+01 | 4.8704E+02 | 2.4222E+02 |
| F5 | AVG | **5.2003E+02** | 5.2008E+02 | 5.2058E+02 | 5.2095E+02 | 5.2021E+02 | 5.2020E+02 | 5.2093E+02 | 5.2054E+02 | 5.2083E+02 | 5.2094E+02 |
| | STD | **3.5196E-02** | 7.4381E-02 | 5.5247E-02 | 4.5268E-02 | 1.5950E-01 | 2.2855E-01 | 4.4471E-02 | 1.3466E-01 | 9.4729E-02 | 4.8905E-02 |
| F6 | AVG | 6.1060E+02 | **6.0943E+02** | 6.1919E+02 | 6.3380E+02 | 6.3038E+02 | 6.4095E+02 | 6.3371E+02 | 6.1931E+02 | 6.3407E+02 | 6.2388E+02 |
| | STD | 3.9609E+00 | 2.7394E+00 | **1.7090E+00** | 2.7540E+00 | 3.8784E+00 | 1.9213E+00 | 2.9493E+00 | 2.9433E+00 | 2.3707E+00 | 3.6019E+00 |
| F7 | AVG | **7.0000E+02** | 7.0004E+02 | 7.0000E+02 | 8.3162E+02 | 7.0111E+02 | 7.0007E+02 | 9.0454E+02 | 7.0097E+02 | 7.4526E+02 | 7.1281E+02 |
| | STD | **2.1111E-14** | 1.4401E-02 | 5.5143E-10 | 2.5597E+01 | 1.9919E-02 | 2.2278E-01 | 3.9740E+01 | 7.1644E-02 | 2.2224E+01 | 1.6104E+01 |
| F8 | AVG | 8.6908E+02 | 8.6615E+02 | **8.0112E+02** | 1.0400E+03 | 8.9682E+02 | 1.0228E+03 | 1.0673E+03 | 8.8713E+02 | 9.9899E+02 | 9.5155E+02 |
| | STD | 1.4024E+01 | 1.8074E+01 | **1.3843E+00** | 1.2657E+01 | 1.3630E+01 | 5.1509E+01 | 1.3130E+01 | 1.5470E+01 | 1.8197E+01 | 2.4840E+01 |
| F9 | AVG | **9.6587E+02** | 9.8469E+02 | 1.0072E+03 | 1.1774E+03 | 1.0822E+03 | 1.1495E+03 | 1.2099E+03 | 1.0131E+03 | 1.1318E+03 | 1.1167E+03 |
| | STD | 1.2641E+01 | 2.5753E+01 | **8.3008E+00** | 1.6570E+01 | 2.1053E+01 | 5.6257E+01 | 1.2614E+01 | 2.2365E+01 | 2.5847E+01 | 4.1061E+01 |
| F10 | AVG | 2.3195E+03 | 3.6613E+03 | **1.0245E+03** | 7.0068E+03 | 2.8557E+03 | 5.8040E+03 | 7.2866E+03 | 3.2856E+03 | 4.6402E+03 | 5.2262E+03 |

(*continued on next page*)

**Table A.2** (*continued*)

| Fun | Item | CCMVO | MVO | DE | SCA | HHO | CBA | SCADE | IGWO | ACWOA | ASCA_PSO |
|---|---|---|---|---|---|---|---|---|---|---|---|
| | STD | 3.5003E+02 | 6.3105E+02 | **2.3209E+01** | 4.2932E+02 | 7.7890E+02 | 8.2274E+02 | 4.1854E+02 | 5.9901E+02 | 1.0377E+03 | 6.7757E+02 |
| F11 | AVG | **3.5306E+03** | 4.1499E+03 | 5.8044E+03 | 8.0326E+03 | 5.3774E+03 | 5.6828E+03 | 8.1358E+03 | 4.6359E+03 | 6.3411E+03 | 6.1248E+03 |
| | STD | 4.9194E+02 | 6.4568E+02 | **1.8258E+02** | 2.6579E+02 | 6.2941E+02 | 5.7262E+02 | 3.0582E+02 | 7.6000E+02 | 8.3550E+02 | 7.3973E+02 |
| F12 | AVG | **1.2002E+03** | 1.2002E+03 | 1.2009E+03 | 1.2024E+03 | 1.2017E+03 | 1.2012E+03 | 1.2025E+03 | 1.2007E+03 | 1.2019E+03 | 1.2025E+03 |
| | STD | 1.2266E-01 | 1.1379E-01 | **1.0954E-01** | 3.1188E-01 | 4.8187E-01 | 7.0233E-01 | 3.5090E-01 | 2.8734E-01 | 5.5821E-01 | 3.5308E-01 |
| F13 | AVG | **1.3003E+03** | 1.3004E+03 | 1.3003E+03 | 1.3030E+03 | 1.3005E+03 | 1.3005E+03 | 1.3040E+03 | 1.3006E+03 | 1.3019E+03 | 1.3006E+03 |
| | STD | 4.3550E-02 | 9.9670E-02 | **3.9593E-02** | 2.1135E-01 | 1.4535E-01 | 1.4139E-01 | 2.6559E-01 | 1.1720E-01 | 9.3337E-01 | 2.7927E-01 |
| F14 | AVG | **1.4003E+03** | 1.4005E+03 | 1.4003E+03 | 1.4463E+03 | 1.4003E+03 | 1.4003E+03 | 1.4860E+03 | 1.4005E+03 | 1.4213E+03 | 1.4030E+03 |
| | STD | **3.8270E-02** | 2.7978E-01 | 5.9660E-02 | 9.9944E+00 | 4.7910E-02 | 1.4962E-01 | 1.2296E+01 | 3.2396E-01 | 1.8864E+01 | 5.5915E+00 |
| F15 | AVG | **1.5047E+03** | 1.5071E+03 | 1.5117E+03 | 4.4163E+03 | 1.5396E+03 | 1.5604E+03 | 1.9958E+04 | 1.5188E+03 | 2.0045E+03 | 1.5325E+03 |
| | STD | 1.1930E+00 | 1.9864E+00 | **9.7358E-01** | 2.5505E+03 | 8.5660E+00 | 1.5470E+01 | 6.9729E+03 | 5.2723E+00 | 5.8007E+02 | 3.9467E+01 |
| F16 | AVG | **1.6105E+03** | 1.6116E+03 | 1.6115E+03 | 1.6127E+03 | 1.6123E+03 | 1.6135E+03 | 1.6128E+03 | 1.6118E+03 | 1.6122E+03 | 1.6125E+03 |
| | STD | 6.2537E-01 | 5.6725E-01 | 2.9649E-01 | 2.5553E-01 | 3.2198E-01 | 3.0200E-01 | **2.2247E-01** | 5.6437E-01 | 5.0134E-01 | 3.0664E-01 |
| F17 | AVG | **7.0121E+04** | 1.6836E+05 | 1.6182E+06 | 5.2958E+06 | 1.3669E+06 | 2.5261E+05 | 1.5464E+07 | 1.0766E+06 | 1.2033E+07 | 9.1099E+05 |
| | STD | **4.4070E+04** | 1.1832E+05 | 7.3195E+05 | 2.4545E+06 | 9.0138E+05 | 1.9137E+05 | 5.8199E+06 | 7.8214E+05 | 1.0092E+07 | 8.3490E+05 |
| F18 | AVG | **2.3450E+03** | 1.0092E+04 | 6.4704E+03 | 1.3811E+08 | 8.9787E+04 | 8.6039E+03 | 1.8537E+08 | 1.7362E+04 | 4.7714E+07 | 3.8419E+06 |
| | STD | **7.2920E+02** | 8.3761E+03 | 3.5392E+03 | 8.2627E+07 | 4.4055E+04 | 9.0621E+03 | 1.0999E+08 | 1.7663E+04 | 5.3120E+07 | 1.1333E+06 |
| F19 | AVG | **1.9061E+03** | 1.9132E+03 | 1.9080E+03 | 1.9884E+03 | 1.9268E+03 | 1.9435E+03 | 2.0108E+03 | 1.9181E+03 | 2.0243E+03 | 1.9330E+03 |
| | STD | 1.0044E+00 | 1.3828E+01 | **7.5209E-01** | 2.2564E+01 | 2.4886E+01 | 3.8760E+01 | 1.1280E+01 | 1.3022E+01 | 4.6545E+01 | 3.0525E+01 |
| F20 | AVG | **2.2106E+03** | 2.2852E+03 | 4.6806E+03 | 1.6774E+04 | 1.1256E+04 | 3.2676E+03 | 2.7700E+04 | 3.2328E+03 | 3.7326E+04 | 6.3858E+03 |
| | STD | **5.2783E+01** | 8.1294E+01 | 1.2707E+03 | 6.4622E+03 | 5.7056E+03 | 1.3041E+03 | 9.6169E+03 | 1.1086E+03 | 1.6092E+04 | 2.8270E+03 |
| F21 | AVG | **2.7403E+04** | 5.8833E+04 | 2.4661E+05 | 1.2027E+06 | 4.2996E+05 | 1.1221E+05 | 2.2548E+06 | 2.9073E+05 | 7.1074E+06 | 3.0247E+05 |
| | STD | **1.2868E+04** | 3.6773E+04 | 1.0341E+05 | 6.2496E+05 | 3.2841E+05 | 6.2202E+04 | 1.1095E+06 | 2.3715E+05 | 6.8762E+06 | 2.2472E+05 |
| F22 | AVG | 2.3538E+03 | 2.5932E+03 | **2.3474E+03** | 2.9771E+03 | 3.0381E+03 | 3.4047E+03 | 3.1114E+03 | 2.5599E+03 | 3.0356E+03 | 2.7820E+03 |
| | STD | **8.0038E+01** | 2.0252E+02 | 8.1930E+01 | 1.7908E+02 | 2.7596E+02 | 3.5162E+02 | 1.7142E+02 | 1.4859E+02 | 2.2328E+02 | 2.0604E+02 |
| F23 | AVG | 2.6152E+03 | 2.6155E+03 | 2.6152E+03 | 2.6711E+03 | **2.5000E+03** | 2.6158E+03 | 2.5000E+03 | 2.6202E+03 | 2.5135E+03 | 2.6234E+03 |
| | STD | 6.7475E-05 | 1.9717E-01 | 1.3876E-12 | 1.3974E+01 | **0.0000E+00** | 3.1346E-01 | 0.0000E+00 | 2.5130E+00 | 5.1650E+01 | 5.0762E+00 |
| F24 | AVG | 2.6000E+03 | 2.6236E+03 | 2.6262E+03 | 2.6001E+03 | 2.6000E+03 | 2.6653E+03 | **2.6000E+03** | 2.6000E+03 | 2.6000E+03 | 2.6346E+03 |
| | STD | 6.9466E-03 | 1.2481E+01 | 1.8025E+00 | 3.6427E-02 | 6.6952E-05 | 2.2386E+01 | **2.0324E-06** | 4.5395E-03 | 1.3457E-05 | 6.1785E+00 |
| F25 | AVG | **2.7000E+03** | 2.7051E+03 | 2.7075E+03 | 2.7230E+03 | 2.7000E+03 | 2.7346E+03 | 2.7000E+03 | 2.7096E+03 | 2.7000E+03 | 2.7150E+03 |
| | STD | **0.0000E+00** | 1.1012E+00 | 1.1449E+00 | 8.3453E+00 | 0.0000E+00 | 1.2440E+01 | 0.0000E+00 | 3.2480E+00 | 0.0000E+00 | 8.6132E+00 |
| F26 | AVG | 2.7036E+03 | 2.7418E+03 | **2.7003E+03** | 2.7026E+03 | 2.7735E+03 | 2.7109E+03 | 2.7038E+03 | 2.7007E+03 | 2.7570E+03 | 2.7007E+03 |
| | STD | 1.8211E+01 | 6.5814E+01 | **3.8524E-02** | 5.8146E-01 | 4.4754E+01 | 5.6824E+01 | 4.5378E-01 | 1.4699E-01 | 5.0060E+01 | 1.4941E-01 |
| F27 | AVG | 3.0654E+03 | 3.2851E+03 | 3.1864E+03 | 3.4661E+03 | **2.9000E+03** | 3.9125E+03 | 3.2041E+03 | 3.1109E+03 | 3.7071E+03 | 3.5770E+03 |
| | STD | 4.6729E+01 | 1.0749E+02 | 8.0200E+01 | 3.2086E+02 | **0.0000E+00** | 4.6198E+02 | 2.3231E+02 | 3.8402E+00 | 3.3104E+02 | 2.4864E+02 |
| F28 | AVG | 3.6767E+03 | 3.8573E+03 | 3.6381E+03 | 4.7992E+03 | **3.0000E+03** | 5.4513E+03 | 5.1897E+03 | 3.8998E+03 | 4.0185E+03 | 4.3968E+03 |
| | STD | 3.6185E+01 | 2.6371E+02 | 2.1023E+01 | 2.9273E+02 | **0.0000E+00** | 7.2210E+02 | 7.7983E+02 | 2.7636E+02 | 1.1978E+03 | 3.9245E+02 |
| F29 | AVG | 4.3645E+03 | 1.4839E+06 | 3.3399E+05 | 1.3456E+07 | **3.1000E+03** | 4.6827E+07 | 1.6368E+07 | 1.1791E+06 | 1.9126E+07 | 6.4854E+06 |
| | STD | 4.4270E+02 | 3.8367E+06 | 1.2784E+06 | 8.2623E+06 | **0.0000E+00** | 3.8367E+07 | 8.7071E+06 | 3.5609E+06 | 1.7387E+07 | 7.7298E+06 |
| F30 | AVG | **5.8819E+03** | 7.9631E+03 | 6.2298E+03 | 2.2974E+05 | 7.8376E+03 | 1.5105E+04 | 4.4488E+05 | 2.4899E+04 | 3.2456E+05 | 3.8755E+04 |
| | STD | **8.6829E+02** | 1.2129E+03 | 1.0174E+03 | 1.0016E+05 | 1.3777E+04 | 8.0940E+03 | 1.2527E+05 | 9.8423E+03 | 2.0609E+05 | 2.9435E+04 |

**Table A.3**
FSIM's evaluation results

| Image | Thresholds | 2 | | 4 | | 6 | | 10 | | 15 | | 20 | |
|---|---|---|---|---|---|---|---|---|---|---|---|---|---|
| A | Item | AVE | STD | AVE | STD | AVE | STD | AVE | STD | AVE | STD | AVE | STD |
| | CCMVO | 6.7574E-01 | **2.8645E-03** | **7.6782E-01** | **3.6341E-02** | **8.4740E-01** | **2.6491E-02** | **8.8153E-01** | 5.6467E-02 | **9.3234E-01** | 3.4568E-02 | **9.4366E-01** | 3.9941E-02 |
| | MVO | 6.5356E-01 | 3.1622E-02 | 7.5228E-01 | 4.4125E-02 | 8.2106E-01 | 3.4577E-02 | 8.5024E-01 | 5.9990E-02 | 9.0908E-01 | 5.0700E-02 | 9.2790E-01 | 4.3593E-02 |
| | WOA | 6.6663E-01 | 2.0851E-02 | 7.1718E-01 | 5.0309E-02 | 7.9246E-01 | 6.2474E-02 | 8.4467E-01 | 7.3851E-02 | 9.1266E-01 | 3.5371E-02 | 9.4108E-01 | 3.5660E-02 |
| | SCA | 6.4560E-01 | 3.0690E-02 | 7.0108E-01 | 4.9605E-02 | 7.3734E-01 | 6.3408E-02 | 8.1712E-01 | 5.4318E-02 | 8.3808E-01 | 7.9513E-02 | 8.9998E-01 | 4.5554E-02 |
| | HHO | 6.4351E-01 | 5.3745E-02 | 7.2727E-01 | 6.2293E-02 | 7.7242E-01 | 4.8995E-02 | 8.3868E-01 | 5.8072E-02 | 8.9205E-01 | **3.3404E-02** | 9.2137E-01 | 5.3013E-02 |
| | BLPSO | 6.5731E-01 | 1.9906E-02 | 7.0770E-01 | 4.1906E-02 | 7.5632E-01 | 5.9868E-02 | 8.3218E-01 | 6.7180E-02 | 8.7854E-01 | 3.6050E-02 | 9.2124E-01 | 4.0685E-02 |
| | IGWO | 6.8333E-01 | 8.1370E-03 | 7.5187E-01 | 5.7288E-02 | 7.9156E-01 | 6.9928E-02 | 8.5639E-01 | **5.3532E-02** | 8.7290E-01 | 4.3607E-02 | 9.1431E-01 | 3.8417E-02 |

(*continued on next page*)

**Table A.3** (*continued*)

| Image | Thresholds | 2 | | 4 | | 6 | | 10 | | 15 | | 20 | |
|---|---|---|---|---|---|---|---|---|---|---|---|---|---|
| A | Item | AVE | STD | AVE | STD | AVE | STD | AVE | STD | AVE | STD | AVE | STD |
| | IWOA | 6.6192E-01 | 3.3756E-02 | 7.2911E-01 | 6.0149E-02 | 7.6030E-01 | 6.4801E-02 | 8.1598E-01 | 6.4743E-02 | 8.8041E-01 | 5.8714E-02 | 9.2512E-01 | **3.4560E-02** |
| | SCADE | **6.9095E-01** | 2.0998E-02 | 7.1794E-01 | 4.8632E-02 | 7.5090E-01 | 4.9154E-02 | 8.1311E-01 | 5.7350E-02 | 8.5507E-01 | 4.5185E-02 | 8.9351E-01 | 5.5275E-02 |
| Image | Thresholds | 2 | | 4 | | 6 | | 10 | | 15 | | 20 | |
| B | Item | AVE | STD | AVE | STD | AVE | STD | AVE | STD | AVE | STD | AVE | STD |
| | CCMVO | 6.3122E-01 | **5.7282E-04** | **7.5780E-01** | **3.8825E-02** | **8.0731E-01** | 4.5486E-02 | **8.9203E-01** | 3.3787E-02 | **9.3632E-01** | **2.8456E-02** | 9.5792E-01 | **1.6787E-02** |
| | MVO | 6.1400E-01 | 1.8543E-02 | 7.1288E-01 | 4.7695E-02 | 8.0364E-01 | 4.6970E-02 | 8.7097E-01 | 4.8156E-02 | 9.2373E-01 | 3.3749E-02 | 9.4554E-01 | 2.7038E-02 |
| | WOA | 6.0971E-01 | 3.0484E-02 | 6.7627E-01 | 6.0322E-02 | 7.8214E-01 | **3.8883E-02** | 8.7981E-01 | 4.4880E-02 | 9.2471E-01 | 3.0443E-02 | **9.5846E-01** | 2.5304E-02 |
| | SCA | 6.2553E-01 | 2.1697E-02 | 6.8015E-01 | 6.0334E-02 | 7.2623E-01 | 5.3200E-02 | 8.0956E-01 | 6.4623E-02 | 8.6573E-01 | 6.8945E-02 | 8.8975E-01 | 4.6624E-02 |
| | HHO | 6.0817E-01 | 2.4602E-02 | 6.8449E-01 | 5.2009E-02 | 7.7027E-01 | 5.3485E-02 | 8.2502E-01 | 5.1295E-02 | 8.8232E-01 | 6.1384E-02 | 9.4035E-01 | 3.7413E-02 |
| | BLPSO | 6.1746E-01 | 2.1588E-02 | 7.0063E-01 | 4.3711E-02 | 7.6285E-01 | 4.4884E-02 | 8.5370E-01 | **2.7601E-02** | 8.9936E-01 | 4.0308E-02 | 9.2391E-01 | 3.7855E-02 |
| | IGWO | 6.2049E-01 | 2.8171E-02 | 6.8454E-01 | 7.2105E-02 | 7.7446E-01 | 4.1178E-02 | 8.4053E-01 | 4.9562E-02 | 8.9670E-01 | 4.2586E-02 | 9.3140E-01 | 2.1997E-02 |
| | IWOA | 6.0739E-01 | 3.1423E-02 | 6.9717E-01 | 4.6747E-02 | 7.6782E-01 | 5.9587E-02 | 8.4565E-01 | 5.9370E-02 | 9.0383E-01 | 3.8814E-02 | 9.3528E-01 | 2.6023E-02 |
| | SCADE | **6.3258E-01** | 1.7322E-02 | 6.8776E-01 | 4.7126E-02 | 7.3358E-01 | 5.8828E-02 | 8.0420E-01 | 4.9446E-02 | 8.6067E-01 | 5.0460E-02 | 9.0110E-01 | 3.2973E-02 |
| Image | Thresholds | 2 | | 4 | | 6 | | 10 | | 15 | | 20 | |
| C | Item | AVE | STD | AVE | STD | AVE | STD | AVE | STD | AVE | STD | AVE | STD |
| | CCMVO | 6.8181E-01 | 5.7490E-03 | **7.6481E-01** | 2.6991E-02 | **8.2383E-01** | 4.6658E-02 | **8.6803E-01** | **2.7447E-02** | **9.2286E-01** | **2.3067E-02** | **9.4764E-01** | **1.8237E-02** |
| | MVO | 6.5784E-01 | 3.9719E-02 | 7.5040E-01 | 4.3609E-02 | 7.9540E-01 | 5.4081E-02 | 8.4811E-01 | 4.2599E-02 | 9.0127E-01 | 3.4247E-02 | 9.2305E-01 | 4.5098E-02 |
| | WOA | 6.5730E-01 | 4.2005E-02 | 7.1922E-01 | 7.1416E-02 | 7.5750E-01 | 5.9510E-02 | 8.5634E-01 | 5.0792E-02 | 9.0245E-01 | 4.2734E-02 | 9.4200E-01 | 2.6505E-02 |
| | SCA | 6.7421E-01 | 2.5936E-02 | 7.1030E-01 | 5.2179E-02 | 7.1054E-01 | 5.5955E-02 | 7.8766E-01 | 4.3997E-02 | 8.2913E-01 | 5.7177E-02 | 8.6879E-01 | 5.5272E-02 |
| | HHO | 6.6116E-01 | 2.7989E-02 | 7.1751E-01 | 6.5611E-02 | 7.7447E-01 | 6.6223E-02 | 8.4130E-01 | 5.4138E-02 | 8.8986E-01 | 4.3585E-02 | 9.0937E-01 | 3.6207E-02 |
| | BLPSO | 6.6152E-01 | 3.4170E-02 | 7.1250E-01 | 2.8663E-02 | 7.4847E-01 | 5.6014E-02 | 8.1885E-01 | 3.3862E-02 | 8.6418E-01 | 3.6029E-02 | 8.9544E-01 | 3.2565E-02 |
| | IGWO | 7.0038E-01 | **3.8523E-03** | 7.4379E-01 | **1.8177E-02** | 7.9009E-01 | **4.3947E-02** | 8.3521E-01 | 3.8667E-02 | 8.7282E-01 | 4.1916E-02 | 9.0684E-01 | 2.7121E-02 |
| | IWOA | 6.9146E-01 | 2.6580E-02 | 7.1124E-01 | 3.9378E-02 | 7.4493E-01 | 5.0933E-02 | 8.1344E-01 | 5.5479E-02 | 8.7887E-01 | 4.0731E-02 | 9.0879E-01 | 4.2722E-02 |
| | SCADE | **7.0302E-01** | 2.5605E-02 | 7.2222E-01 | 3.6281E-02 | 7.4588E-01 | 5.6238E-02 | 7.9389E-01 | 4.5816E-02 | 8.2550E-01 | 5.6561E-02 | 8.7744E-01 | 4.1798E-02 |
| Image | Thresholds | 2 | | 4 | | 6 | | 10 | | 15 | | 20 | |
| D | Item | AVE | STD | AVE | STD | AVE | STD | AVE | STD | AVE | STD | AVE | STD |
| | CCMVO | **7.1900E-01** | **2.5807E-03** | **7.5574E-01** | **1.4257E-02** | **8.0265E-01** | 2.9653E-02 | **9.1374E-01** | 2.6208E-02 | **9.4810E-01** | **2.1736E-02** | **9.5993E-01** | 2.3027E-02 |
| | MVO | 7.0592E-01 | 2.2671E-02 | 7.3550E-01 | 3.3377E-02 | 7.8835E-01 | **2.9249E-02** | 8.9262E-01 | **2.6118E-02** | 9.2586E-01 | 3.9928E-02 | 9.3864E-01 | 2.5111E-02 |
| | WOA | 6.9828E-01 | 3.2997E-02 | 7.4490E-01 | 3.1028E-02 | 7.6259E-01 | 4.5660E-02 | 8.5961E-01 | 4.9553E-02 | 9.2664E-01 | 2.8249E-02 | 9.5005E-01 | **2.1591E-02** |
| | SCA | 7.1704E-01 | 6.0937E-03 | 7.3290E-01 | 3.0649E-02 | 7.4420E-01 | 4.2009E-02 | 8.1147E-01 | 4.0735E-02 | 8.7488E-01 | 3.9493E-02 | 8.9742E-01 | 4.9340E-02 |
| | HHO | 6.7888E-01 | 2.8112E-02 | 7.2167E-01 | 3.5481E-02 | 7.5270E-01 | 4.3417E-02 | 8.2694E-01 | 7.0808E-02 | 9.1247E-01 | 4.0112E-02 | 9.2957E-01 | 3.5151E-02 |
| | BLPSO | 6.8764E-01 | 3.4211E-02 | 7.1929E-01 | 4.2990E-02 | 7.8059E-01 | 3.0725E-02 | 8.4980E-01 | 4.5655E-02 | 8.9007E-01 | 3.2166E-02 | 9.2507E-01 | 3.3232E-02 |
| | IGWO | 7.0373E-01 | 2.8072E-02 | 7.3502E-01 | 4.1618E-02 | 7.8108E-01 | 5.0813E-02 | 8.5429E-01 | 3.8932E-02 | 9.0036E-01 | 3.4811E-02 | 9.2683E-01 | 3.0278E-02 |
| | IWOA | 6.8693E-01 | 2.8156E-02 | 7.2569E-01 | 4.4261E-02 | 7.9469E-01 | 4.5159E-02 | 8.5844E-01 | 3.5336E-02 | 8.8561E-01 | 4.6162E-02 | 9.2701E-01 | 4.0742E-02 |

(*continued on next page*)

**Table A.3** (*continued*)

| Image | Thresholds | 2 | | 4 | | 6 | | 10 | | 15 | | 20 | |
|---|---|---|---|---|---|---|---|---|---|---|---|---|---|
| A | Item | AVE | STD | AVE | STD | AVE | STD | AVE | STD | AVE | STD | AVE | STD |
| | SCADE | 7.0857E-01 | 1.2665E-02 | 7.2267E-01 | 8.4406E-02 | 7.5592E-01 | 5.0356E-02 | 8.2411E-01 | 5.0599E-02 | 8.5702E-01 | 5.9410E-02 | 9.0803E-01 | 3.2390E-02 |
| Image E | Thresholds | 2 | | 4 | | 6 | | 10 | | 15 | | 20 | |
| | Item | AVE | STD | AVE | STD | AVE | STD | AVE | STD | AVE | STD | AVE | STD |
| | CCMVO | **6.9472E-01** | **1.6093E-03** | **7.3687E-01** | **9.1394E-03** | 7.8636E-01 | **1.8231E-02** | **9.0665E-01** | **2.5082E-02** | **9.3910E-01** | **2.1349E-02** | 9.5888E-01 | **1.2709E-02** |
| | MVO | 6.8488E-01 | 1.9411E-02 | 7.2243E-01 | 2.5778E-02 | 7.7667E-01 | 2.7186E-02 | 8.9977E-01 | 4.0658E-02 | 9.2289E-01 | 3.4631E-02 | 9.4202E-01 | 3.5819E-02 |
| | WOA | 6.8296E-01 | 1.9567E-02 | 7.1918E-01 | 3.3816E-02 | 7.3524E-01 | 3.4306E-02 | 8.8857E-01 | 3.3424E-02 | 9.3627E-01 | 3.0581E-02 | **9.6084E-01** | 2.0889E-02 |
| | SCA | 6.9304E-01 | 1.0770E-02 | 7.0898E-01 | 2.6364E-02 | 7.2301E-01 | 2.3803E-02 | 7.9364E-01 | 5.9128E-02 | 8.6517E-01 | 5.2430E-02 | 9.0500E-01 | 3.0307E-02 |
| | HHO | 6.6789E-01 | 1.6081E-02 | 6.9965E-01 | 3.0359E-02 | 7.3804E-01 | 3.9456E-02 | 8.4576E-01 | 6.0409E-02 | 9.0498E-01 | 3.8950E-02 | 9.3902E-01 | 3.1774E-02 |
| | BLPSO | 6.2691E-01 | 5.0238E-02 | 7.0406E-01 | 4.0272E-02 | **7.8865E-01** | 3.0922E-02 | 8.5826E-01 | 3.6895E-02 | 9.0452E-01 | 3.6368E-02 | 9.4598E-01 | 2.1037E-02 |
| | IGWO | 6.6199E-01 | 2.6004E-02 | 7.0250E-01 | 5.2337E-02 | 7.8700E-01 | 4.5673E-02 | 8.5748E-01 | 5.2063E-02 | 9.0771E-01 | 2.8768E-02 | 9.3307E-01 | 2.4042E-02 |
| | IWOA | 6.5137E-01 | 4.3252E-02 | 7.1543E-01 | 4.6551E-02 | 7.7919E-01 | 5.2659E-02 | 8.6649E-01 | 4.1003E-02 | 9.0333E-01 | 3.7484E-02 | 9.3936E-01 | 2.4483E-02 |
| | SCADE | 6.5174E-01 | 2.9248E-02 | 6.9838E-01 | 5.1552E-02 | 7.3433E-01 | 5.7222E-02 | 8.1294E-01 | 4.9405E-02 | 8.6300E-01 | 5.9016E-02 | 8.9158E-01 | 5.4027E-02 |
| Image F | Thresholds | 2 | | 4 | | 6 | | 10 | | 15 | | 20 | |
| | Item | AVE | STD | AVE | STD | AVE | STD | AVE | STD | AVE | STD | AVE | STD |
| | CCMVO | 7.3026E-01 | 1.0201E-02 | **7.9406E-01** | **2.3928E-02** | **8.3677E-01** | **3.2696E-02** | **8.6590E-01** | 3.0172E-02 | **9.1071E-01** | **2.2779E-02** | **9.3469E-01** | **2.2323E-02** |
| | MVO | **7.3068E-01** | 2.8703E-02 | 7.6932E-01 | 3.8024E-02 | 8.3201E-01 | 4.6173E-02 | 8.5650E-01 | 3.2364E-02 | 8.9196E-01 | 3.5381E-02 | 9.1559E-01 | 2.5602E-02 |
| | WOA | 7.0813E-01 | 4.1388E-02 | 7.3628E-01 | 6.1784E-02 | 8.1369E-01 | 5.4844E-02 | 8.2879E-01 | 4.2840E-02 | 8.8727E-01 | 4.4773E-02 | 9.3193E-01 | 2.8918E-02 |
| | SCA | 7.2180E-01 | 2.2502E-02 | 7.5117E-01 | 5.5833E-02 | 7.7258E-01 | 5.6205E-02 | 7.8857E-01 | 3.6546E-02 | 8.4520E-01 | 4.3082E-02 | 8.7533E-01 | 3.7543E-02 |
| | HHO | 6.9842E-01 | 4.7141E-02 | 7.1713E-01 | 6.6514E-02 | 7.7831E-01 | 7.0183E-02 | 8.1916E-01 | 4.2318E-02 | 8.7835E-01 | 3.2692E-02 | 9.0826E-01 | 3.5459E-02 |
| | BLPSO | 6.8708E-01 | 2.3093E-02 | 7.1915E-01 | 4.0328E-02 | 7.5459E-01 | 3.6549E-02 | 8.1203E-01 | **2.8911E-02** | 8.6228E-01 | 2.7111E-02 | 9.0184E-01 | 2.6099E-02 |
| | IGWO | 7.1989E-01 | **4.1371E-03** | 7.4428E-01 | 2.8432E-02 | 7.7052E-01 | 4.1371E-02 | 8.2304E-01 | 3.8218E-02 | 8.6402E-01 | 2.9136E-02 | 8.8949E-01 | 3.5875E-02 |
| | IWOA | 6.9937E-01 | 2.8769E-02 | 7.2324E-01 | 3.7991E-02 | 7.7283E-01 | 4.0515E-02 | 8.2405E-01 | 4.2646E-02 | 8.6952E-01 | 4.1919E-02 | 9.0378E-01 | 3.4516E-02 |
| | SCADE | 7.1851E-01 | 7.9122E-03 | 7.2909E-01 | 3.1121E-02 | 7.4122E-01 | 3.6489E-02 | 7.9504E-01 | 3.6905E-02 | 8.2948E-01 | 3.8150E-02 | 8.7534E-01 | 3.1390E-02 |
| Image G | Thresholds | 2 | | 4 | | 6 | | 10 | | 15 | | 20 | |
| | Item | AVE | STD | AVE | STD | AVE | STD | AVE | STD | AVE | STD | AVE | STD |
| | CCMVO | 6.9977E-01 | **2.0404E-03** | 7.4061E-01 | **8.4536E-03** | **8.0460E-01** | **1.9890E-02** | **8.5711E-01** | **2.6461E-02** | **9.1764E-01** | **2.1589E-02** | **9.3578E-01** | **2.0219E-02** |
| | MVO | **7.0070E-01** | 2.0423E-03 | **7.4814E-01** | 2.0130E-02 | 7.9621E-01 | 3.3914E-02 | 8.4717E-01 | 4.5849E-02 | 8.9325E-01 | 3.0313E-02 | 9.1241E-01 | 3.3693E-02 |
| | WOA | 6.9591E-01 | 2.6746E-02 | 7.3001E-01 | 4.2244E-02 | 7.8724E-01 | 4.6327E-02 | 8.4080E-01 | 4.1796E-02 | 8.8641E-01 | 3.8994E-02 | 9.2310E-01 | 2.4161E-02 |
| | SCA | 6.9232E-01 | 2.4155E-02 | 7.1871E-01 | 4.9263E-02 | 7.4702E-01 | 5.5965E-02 | 7.9219E-01 | 5.2329E-02 | 8.3998E-01 | 3.5346E-02 | 8.7847E-01 | 3.2943E-02 |
| | HHO | 6.7669E-01 | 3.4563E-02 | 7.2759E-01 | 4.6159E-02 | 7.9104E-01 | 5.8087E-02 | 8.3527E-01 | 4.9184E-02 | 8.7165E-01 | 4.1311E-02 | 9.0972E-01 | 3.1443E-02 |
| | BLPSO | 6.1696E-01 | 2.5742E-02 | 6.8277E-01 | 2.4944E-02 | 7.4267E-01 | 3.7831E-02 | 8.1084E-01 | 3.4976E-02 | 8.7502E-01 | 2.9677E-02 | 8.9786E-01 | 2.6227E-02 |
| | IGWO | 6.4772E-01 | 2.8803E-03 | 7.2679E-01 | 2.0771E-02 | 7.7023E-01 | 3.9633E-02 | 8.1485E-01 | 5.2702E-02 | 8.6636E-01 | 3.4375E-02 | 8.9506E-01 | 2.6002E-02 |
| | IWOA | 6.4254E-01 | 1.7696E-02 | 6.9103E-01 | 4.7130E-02 | 7.5134E-01 | 3.7984E-02 | 8.0757E-01 | 3.2640E-02 | 8.6871E-01 | 3.4591E-02 | 9.1165E-01 | 2.5179E-02 |
| | SCADE | 6.5042E-01 | 9.5335E-03 | 6.9419E-01 | 2.6860E-02 | 7.0451E-01 | 5.2477E-02 | 7.6700E-01 | 4.0250E-02 | 8.3854E-01 | 3.8531E-02 | 8.8090E-01 | 3.0941E-02 |

(*continued on next page*)

**Table A.3** (*continued*)

| Image | Thresholds | 2 | | 4 | | 6 | | 10 | | 15 | | 20 | |
|---|---|---|---|---|---|---|---|---|---|---|---|---|---|
| A | Item | AVE | STD | AVE | STD | AVE | STD | AVE | STD | AVE | STD | AVE | STD |
| Image H | Thresholds | 2 | | 4 | | 6 | | 10 | | 15 | | 20 | |
| | Item | AVE | STD | AVE | STD | AVE | STD | AVE | STD | AVE | STD | AVE | STD |
| | CCMVO | 6.4929E-01 | 2.1282E-03 | 7.3525E-01 | **1.5845E-02** | **7.9573E-01** | **2.1034E-02** | **8.9821E-01** | **1.6337E-02** | **9.3445E-01** | **1.6943E-02** | **9.5576E-01** | **1.5018E-02** |
| | MVO | 6.4016E-01 | 1.5902E-02 | 7.2285E-01 | 2.6769E-02 | 7.7982E-01 | 3.9168E-02 | 8.7228E-01 | 3.3376E-02 | 9.1077E-01 | 3.5306E-02 | 9.3420E-01 | 2.2217E-02 |
| | WOA | 6.3647E-01 | 1.7869E-02 | 6.9413E-01 | 5.2344E-02 | 7.5369E-01 | 4.6916E-02 | 8.5537E-01 | 4.6832E-02 | 9.1518E-01 | 3.1473E-02 | 9.4045E-01 | 2.6496E-02 |
| | SCA | 6.4726E-01 | 9.5807E-03 | 6.6759E-01 | 3.9937E-02 | 7.0217E-01 | 4.6446E-02 | 8.1645E-01 | 5.3926E-02 | 8.6535E-01 | 4.1437E-02 | 8.8676E-01 | 3.9322E-02 |
| | HHO | 6.2348E-01 | 2.7086E-02 | 6.8615E-01 | 3.9512E-02 | 7.3668E-01 | 5.1279E-02 | 8.6204E-01 | 4.5595E-02 | 9.0646E-01 | 3.2394E-02 | 9.1987E-01 | 2.9618E-02 |
| | BLPSO | 6.7369E-01 | 2.4273E-02 | 7.3627E-01 | 2.2842E-02 | 7.7521E-01 | 3.3370E-02 | 8.4639E-01 | 3.1649E-02 | 8.8778E-01 | 2.6097E-02 | 9.1919E-01 | 2.7030E-02 |
| | IGWO | **7.1631E-01** | **1.8553E-03** | **7.7539E-01** | 2.8374E-02 | 7.9341E-01 | 4.4224E-02 | 8.5832E-01 | 3.9998E-02 | 8.9025E-01 | 3.5398E-02 | 9.2201E-01 | 2.5478E-02 |
| | IWOA | 6.9727E-01 | 2.0317E-02 | 7.2687E-01 | 4.9557E-02 | 7.7701E-01 | 4.8185E-02 | 8.4357E-01 | 5.2341E-02 | 8.8774E-01 | 3.9898E-02 | 9.2395E-01 | 2.6932E-02 |
| | SCADE | 7.0921E-01 | 1.3862E-02 | 7.4427E-01 | 4.1542E-02 | 7.5686E-01 | 4.6920E-02 | 8.1171E-01 | 4.6255E-02 | 8.4698E-01 | 3.8962E-02 | 8.9871E-01 | 3.2213E-02 |
| Image I | Thresholds | 2 | | 4 | | 6 | | 10 | | 15 | | 20 | |
| | Item | AVE | STD | AVE | STD | AVE | STD | AVE | STD | AVE | STD | AVE | STD |
| | CCMVO | **7.2467E-01** | 9.7718E-03 | **7.9643E-01** | 2.5451E-02 | **8.3621E-01** | 4.2321E-02 | **8.6103E-01** | **1.7793E-02** | **9.0112E-01** | **1.3569E-02** | **9.2261E-01** | **1.4652E-02** |
| | MVO | 6.8899E-01 | 3.0220E-02 | 7.4311E-01 | 5.1404E-02 | 8.1846E-01 | 3.6947E-02 | 8.2945E-01 | 3.7198E-02 | 8.8995E-01 | 2.7260E-02 | 9.0589E-01 | 2.1975E-02 |
| | WOA | 6.8879E-01 | 4.2654E-02 | 7.0721E-01 | 5.0345E-02 | 7.8379E-01 | 4.6275E-02 | 8.3254E-01 | 3.0522E-02 | 8.8507E-01 | 3.5887E-02 | 9.1766E-01 | 2.3694E-02 |
| | SCA | 7.1373E-01 | 1.3302E-02 | 7.3179E-01 | 4.4424E-02 | 7.6549E-01 | 4.1170E-02 | 7.7419E-01 | 3.2022E-02 | 8.2015E-01 | 3.2541E-02 | 8.6500E-01 | 3.8640E-02 |
| | HHO | 6.6882E-01 | 5.0417E-02 | 7.2533E-01 | 3.9027E-02 | 7.8355E-01 | 5.3598E-02 | 8.1242E-01 | 3.7286E-02 | 8.5851E-01 | 3.2731E-02 | 8.8339E-01 | 3.4108E-02 |
| | BLPSO | 6.6987E-01 | 1.6932E-02 | 7.0360E-01 | 2.2371E-02 | 7.4259E-01 | 2.5496E-02 | 8.0669E-01 | 2.5274E-02 | 8.4615E-01 | 3.1482E-02 | 8.8775E-01 | 2.6372E-02 |
| | IGWO | 6.9389E-01 | **3.0299E-03** | 7.2884E-01 | **1.6208E-02** | 7.6133E-01 | **2.3650E-02** | 8.1739E-01 | 3.1786E-02 | 8.6243E-01 | 2.9999E-02 | 8.8501E-01 | 3.0213E-02 |
| | IWOA | 6.7673E-01 | 2.0342E-02 | 7.1229E-01 | 2.8145E-02 | 7.4788E-01 | 3.6888E-02 | 7.9451E-01 | 2.5570E-02 | 8.5533E-01 | 3.4398E-02 | 8.9205E-01 | 3.2084E-02 |
| | SCADE | 6.9358E-01 | 9.9750E-03 | 7.0621E-01 | 2.7964E-02 | 7.3077E-01 | 3.5809E-02 | 7.6858E-01 | 3.6006E-02 | 8.3183E-01 | 3.6320E-02 | 8.7421E-01 | 2.9051E-02 |
| Image J | Thresholds | 2 | | 4 | | 6 | | 10 | | 15 | | 20 | |
| | Item | AVE | STD | AVE | STD | AVE | STD | AVE | STD | AVE | STD | AVE | STD |
| | CCMVO | 7.1513E-01 | **1.4322E-03** | **7.7855E-01** | **1.9220E-02** | **8.2482E-01** | **2.5106E-02** | **9.2113E-01** | **2.5895E-02** | **9.5459E-01** | **1.3998E-02** | **9.6192E-01** | 1.8704E-02 |
| | MVO | 7.0733E-01 | 1.8954E-02 | 7.7584E-01 | 2.4755E-02 | 8.0203E-01 | 4.4884E-02 | 9.0171E-01 | 3.7976E-02 | 9.2747E-01 | 3.3449E-02 | 9.4803E-01 | 3.1013E-02 |
| | WOA | 7.0581E-01 | 1.6812E-02 | 7.4801E-01 | 4.7503E-02 | 7.8683E-01 | 5.3173E-02 | 8.8258E-01 | 4.9093E-02 | 9.3802E-01 | 2.6450E-02 | 9.6012E-01 | **1.5390E-02** |
| | SCA | 7.0571E-01 | 1.6999E-02 | 7.3692E-01 | 4.2312E-02 | 7.5834E-01 | 5.1489E-02 | 8.3164E-01 | 5.3473E-02 | 8.8343E-01 | 5.1121E-02 | 9.0585E-01 | 4.5147E-02 |
| | HHO | 6.8562E-01 | 2.8271E-02 | 7.3993E-01 | 4.5900E-02 | 7.7570E-01 | 4.4815E-02 | 8.8623E-01 | 5.5641E-02 | 9.2278E-01 | 4.0683E-02 | 9.3348E-01 | 3.5875E-02 |
| | BLPSO | 6.9129E-01 | 2.4195E-02 | 7.4311E-01 | 4.4186E-02 | 7.8052E-01 | 4.6703E-02 | 8.6607E-01 | 3.1017E-02 | 9.0926E-01 | 3.1867E-02 | 9.1931E-01 | 2.6289E-02 |
| | IGWO | **7.3492E-01** | 1.2133E-02 | 7.7307E-01 | 3.7872E-02 | 8.0606E-01 | 5.6915E-02 | 8.6879E-01 | 3.9556E-02 | 9.0891E-01 | 3.6687E-02 | 9.3567E-01 | 2.6343E-02 |
| | IWOA | 7.1087E-01 | 3.2692E-02 | 7.2538E-01 | 6.4207E-02 | 7.9879E-01 | 6.0129E-02 | 8.6513E-01 | 5.2136E-02 | 9.0828E-01 | 5.0318E-02 | 9.1861E-01 | 5.0038E-02 |
| | SCADE | 7.1762E-01 | 2.3350E-02 | 7.3217E-01 | 4.0894E-02 | 7.6350E-01 | 6.8782E-02 | 8.1718E-01 | 4.5472E-02 | 8.7888E-01 | 5.2107E-02 | 9.0534E-01 | 5.1155E-02 |

**Table A.4**
PSNR's evaluation results

| Image | Thresholds | 2 | | 4 | | 6 | | 10 | | 15 | | 20 | |
|---|---|---|---|---|---|---|---|---|---|---|---|---|---|
| A | Item | AVE | STD | AVE | STD | AVE | STD | AVE | STD | AVE | STD | AVE | STD |
| | CCMVO | 1.2192E+01 | **4.9434E-01** | 1.7689E+01 | 2.1025E+00 | **2.2006E+01** | **1.1840E+00** | **2.4694E+01** | 2.5452E+00 | **2.7987E+01** | 2.0970E+00 | **2.9102E+01** | 2.6000E+00 |
| | MVO | 1.1904E+01 | 9.9616E-01 | 1.7462E+01 | 2.3218E+00 | 2.0690E+01 | 1.7042E+00 | 2.3401E+01 | 2.8418E+00 | 2.6544E+01 | 2.6518E+00 | 2.8370E+01 | 2.6949E+00 |
| | WOA | 1.2105E+01 | 8.3169E-01 | 1.6308E+01 | 2.1877E+00 | 1.9433E+01 | 2.5690E+00 | 2.3225E+01 | 3.2773E+00 | 2.6516E+01 | 2.1802E+00 | 2.8837E+01 | 2.4657E+00 |
| | SCA | 1.1084E+01 | 1.3750E+00 | 1.4341E+01 | 2.7441E+00 | 1.7429E+01 | 3.1192E+00 | 2.2156E+01 | 2.7854E+00 | 2.3304E+01 | 3.7809E+00 | 2.6709E+01 | 2.4959E+00 |
| | HHO | 1.2861E+01 | 2.4047E+00 | 1.7075E+01 | 2.6700E+00 | 1.8857E+01 | 2.1490E+00 | 2.2858E+01 | 2.8917E+00 | 2.5584E+01 | **1.8887E+00** | 2.8018E+01 | 3.0043E+00 |
| | BLPSO | 1.4624E+01 | 1.8033E+00 | 1.7464E+01 | **1.8735E+00** | 1.9818E+01 | 2.1239E+00 | 2.2973E+01 | 2.5877E+00 | 2.4999E+01 | 1.9513E+00 | 2.7761E+01 | **2.0647E+00** |
| | IGWO | **1.8149E+01** | 8.7158E-01 | **1.9610E+01** | 2.3819E+00 | 2.0910E+01 | 2.9258E+00 | 2.3888E+01 | 2.4661E+00 | 2.4978E+01 | 1.9733E+00 | 2.7269E+01 | 2.1594E+00 |
| | IWOA | 1.6236E+01 | 2.5835E+00 | 1.8633E+01 | 2.5556E+00 | 1.9420E+01 | 3.0235E+00 | 2.1995E+01 | 2.7411E+00 | 2.5095E+01 | 2.8446E+00 | 2.7798E+01 | 2.2082E+00 |
| | SCADE | 1.7222E+01 | 9.4548E-01 | 1.7976E+01 | 2.0013E+00 | 1.8961E+01 | 2.4735E+00 | 2.1979E+01 | **2.4019E+00** | 2.4197E+01 | 2.0299E+00 | 2.6455E+01 | 2.8726E+00 |
| Image | Thresholds | 2 | | 4 | | 6 | | 10 | | 15 | | 20 | |
| B | Item | AVG | STD | AVG | STD | AVG | STD | AVG | STD | AVG | STD | AVG | STD |
| | CCMVO | 1.3442E+01 | **4.4611E-02** | **1.9054E+01** | **1.5492E+00** | **2.0751E+01** | 2.0230E+00 | **2.4276E+01** | 1.5186E+00 | **2.7301E+01** | **1.7036E+00** | **2.9611E+01** | **1.3404E+00** |
| | MVO | 1.2714E+01 | 1.7539E+00 | 1.7353E+01 | 1.8746E+00 | 2.0724E+01 | 1.8662E+00 | 2.3262E+01 | 2.1197E+00 | 2.6507E+01 | 1.9144E+00 | 2.8394E+01 | 1.9625E+00 |
| | WOA | 1.1930E+01 | 2.6586E+00 | 1.5824E+01 | 2.6129E+00 | 1.9491E+01 | 2.2332E+00 | 2.3991E+01 | 2.0116E+00 | 2.6667E+01 | 1.8357E+00 | 2.9535E+01 | 2.0207E+00 |
| | SCA | 1.2668E+01 | 1.1748E+00 | 1.4966E+01 | 2.9252E+00 | 1.7767E+01 | 2.4739E+00 | 2.1173E+01 | 2.5098E+00 | 2.3742E+01 | 3.3718E+00 | 2.5287E+01 | 2.4470E+00 |
| | HHO | 1.2256E+01 | 2.7306E+00 | 1.5645E+01 | 2.7379E+00 | 1.9245E+01 | 2.2648E+00 | 2.1525E+01 | 2.5901E+00 | 2.4588E+01 | 2.8994E+00 | 2.8441E+01 | 2.8172E+00 |
| | BLPSO | **1.3705E+01** | 1.7082E+00 | 1.6745E+01 | 2.2032E+00 | 1.9375E+01 | 1.7292E+00 | 2.3042E+01 | **1.1152E+00** | 2.5496E+01 | 1.8945E+00 | 2.7143E+01 | 2.1501E+00 |
| | IGWO | 1.2566E+01 | 2.0425E+00 | 1.6235E+01 | 3.1471E+00 | 1.9794E+01 | **1.5079E+00** | 2.2134E+01 | 2.5224E+00 | 2.5243E+01 | 2.1335E+00 | 2.7680E+01 | 1.5850E+00 |
| | IWOA | 1.2291E+01 | 2.5398E+00 | 1.6534E+01 | 2.0236E+00 | 1.9297E+01 | 2.1368E+00 | 2.2439E+01 | 2.7589E+00 | 2.5611E+01 | 2.0149E+00 | 2.7798E+01 | 1.6727E+00 |
| | SCADE | 1.3324E+01 | 1.1299E+00 | 1.6132E+01 | 2.5822E+00 | 1.7818E+01 | 2.7850E+00 | 2.0744E+01 | 1.7445E+00 | 2.3754E+01 | 2.0869E+00 | 2.5805E+01 | 1.9418E+00 |
| Image | Thresholds | 2 | | 4 | | 6 | | 10 | | 15 | | 20 | |
| C | Item | AVG | STD | AVG | STD | AVG | STD | AVG | STD | AVG | STD | AVG | STD |
| | CCMVO | **1.8168E+01** | 3.5928E-01 | **2.0413E+01** | 9.9644E-01 | **2.2504E+01** | **1.7092E+00** | **2.5077E+01** | **1.0449E+00** | **2.8003E+01** | **1.2894E+00** | **3.0168E+01** | **1.1251E+00** |
| | MVO | 1.5991E+01 | 3.7430E+00 | 1.9580E+01 | 2.2489E+00 | 2.1292E+01 | 2.3618E+00 | 2.4243E+01 | 1.7582E+00 | 2.6936E+01 | 1.5366E+00 | 2.8656E+01 | 2.4815E+00 |
| | WOA | 1.5686E+01 | 3.6585E+00 | 1.7684E+01 | 3.5548E+00 | 1.9594E+01 | 2.4224E+00 | 2.4132E+01 | 2.1811E+00 | 2.6958E+01 | 2.2792E+00 | 2.9764E+01 | 1.6666E+00 |
| | SCA | 1.6781E+01 | 1.0449E+00 | 1.7311E+01 | 2.9462E+00 | 1.7274E+01 | 2.5338E+00 | 2.1087E+01 | 2.2872E+00 | 2.3318E+01 | 2.4611E+00 | 2.5510E+01 | 2.5603E+00 |
| | HHO | 1.6199E+01 | 2.3673E+00 | 1.8002E+01 | 3.1152E+00 | 2.0222E+01 | 3.1162E+00 | 2.3300E+01 | 2.4887E+00 | 2.6315E+01 | 2.0381E+00 | 2.7856E+01 | 2.1212E+00 |
| | BLPSO | 1.4729E+01 | 2.1175E+00 | 1.7942E+01 | 1.7718E+00 | 1.9411E+01 | 2.5116E+00 | 2.2909E+01 | 1.4561E+00 | 2.5427E+01 | 1.6582E+00 | 2.7206E+01 | 1.5105E+00 |
| | IGWO | 1.7126E+01 | **5.8481E-02** | 1.9941E+01 | **8.6638E-01** | 2.1249E+01 | 1.9433E+00 | 2.2979E+01 | 1.5558E+00 | 2.5365E+01 | 2.0648E+00 | 2.7698E+01 | 1.5884E+00 |
| | IWOA | 1.6563E+01 | 7.6387E-01 | 1.7923E+01 | 2.0502E+00 | 1.9493E+01 | 2.0872E+00 | 2.2660E+01 | 2.2969E+00 | 2.5894E+01 | 1.8676E+00 | 2.7690E+01 | 2.3069E+00 |
| | SCADE | 1.6522E+01 | 6.0441E-01 | 1.7748E+01 | 2.0449E+00 | 1.8948E+01 | 2.5525E+00 | 2.1518E+01 | 2.5081E+00 | 2.2947E+01 | 2.8197E+00 | 2.5920E+01 | 2.2796E+00 |
| Image | Thresholds | 2 | | 4 | | 6 | | 10 | | 15 | | 20 | |
| D | Item | AVG | STD | AVG | STD | AVG | STD | AVG | STD | AVG | STD | AVG | STD |
| | CCMVO | 1.3299E+01 | **7.1430E-01** | **1.8347E+01** | **1.2183E+00** | **2.1533E+01** | 1.3620E+00 | **2.5566E+01** | **1.1566E+00** | **2.8215E+01** | **1.5148E+00** | **3.0091E+01** | 1.6925E+00 |
| | MVO | 1.2914E+01 | 1.1847E+00 | 1.8158E+01 | 1.3388E+00 | 2.1447E+01 | **1.2819E+00** | 2.4428E+01 | 1.3288E+00 | 2.6913E+01 | 2.2085E+00 | 2.7950E+01 | 2.1308E+00 |
| | WOA | 1.2332E+01 | 1.5896E+00 | 1.7903E+01 | 1.3410E+00 | 1.9500E+01 | 2.2601E+00 | 2.2883E+01 | 2.2663E+00 | 2.6680E+01 | 1.9543E+00 | 2.9043E+01 | **1.5205E+00** |
| | SCA | 1.2467E+01 | 1.3072E+00 | 1.6009E+01 | 1.8275E+00 | 1.7440E+01 | 2.1736E+00 | 2.0449E+01 | 1.8706E+00 | 2.3844E+01 | 2.0659E+00 | 2.5930E+01 | 2.3604E+00 |
| | HHO | 1.2478E+01 | 1.5665E+00 | 1.6581E+01 | 1.5404E+00 | 1.8493E+01 | 2.8634E+00 | 2.1399E+01 | 3.2168E+00 | 2.6200E+01 | 2.0961E+00 | 2.7608E+01 | 2.3088E+00 |
| | BLPSO | **1.3861E+01** | 1.3636E+00 | 1.6405E+01 | 1.9066E+00 | 1.9192E+01 | 1.7304E+00 | 2.2643E+01 | 2.0229E+00 | 2.5018E+01 | 1.5588E+00 | 2.7483E+01 | 1.9061E+00 |
| | IGWO | 1.2691E+01 | 9.4342E-01 | 1.7744E+01 | 1.6058E+00 | 1.9347E+01 | 2.2047E+00 | 2.2699E+01 | 2.0451E+00 | 2.5670E+01 | 1.7791E+00 | 2.7494E+01 | 1.8161E+00 |
| | IWOA | 1.3433E+01 | 1.2757E+00 | 1.6612E+01 | 2.5572E+00 | 1.9825E+01 | 2.3372E+00 | 2.2814E+01 | 1.8024E+00 | 2.4526E+01 | 2.3593E+00 | 2.7345E+01 | 2.6205E+00 |
| | SCADE | 1.2486E+01 | 1.4919E+00 | 1.5650E+01 | 2.6433E+00 | 1.8010E+01 | 2.1587E+00 | 2.1228E+01 | 2.3372E+00 | 2.3338E+01 | 2.9934E+00 | 2.6227E+01 | 1.9057E+00 |

(*continued on next page*)

**Table A.4** (*continued*)

| Image | Thresholds | 2 | | 4 | | 6 | | 10 | | 15 | | 20 | |
|---|---|---|---|---|---|---|---|---|---|---|---|---|---|
| A | Item | AVE | STD | AVE | STD | AVE | STD | AVE | STD | AVE | STD | AVE | STD |
| Image | Thresholds | 2 | | 4 | | 6 | | 10 | | 15 | | 20 | |
| E | Item | AVG | STD | AVG | STD | AVG | STD | AVG | STD | AVG | STD | AVG | STD |
| | CCMVO | 1.3107E+01 | **1.0316E-01** | **1.8326E+01** | **6.6056E-01** | **2.1284E+01** | **9.6751E-01** | **2.4493E+01** | **1.1869E+00** | 2.6822E+01 | 1.5624E+00 | 2.8817E+01 | **1.0614E+00** |
| | MVO | 1.2903E+01 | 5.4319E-01 | 1.7446E+01 | 9.9067E-01 | 2.0512E+01 | 1.0590E+00 | 2.4255E+01 | 2.0168E+00 | 2.5979E+01 | 2.1494E+00 | 2.7789E+01 | 2.4967E+00 |
| | WOA | 1.2961E+01 | 4.7866E-01 | 1.6410E+01 | 1.5059E+00 | 1.8403E+01 | 1.6039E+00 | 2.3632E+01 | 1.6056E+00 | **2.6861E+01** | 1.9092E+00 | **2.9231E+01** | 2.1687E+00 |
| | SCA | 1.2530E+01 | 1.0605E+00 | 1.5332E+01 | 1.8197E+00 | 1.7022E+01 | 1.9181E+00 | 1.9824E+01 | 2.8305E+00 | 2.3078E+01 | 3.0711E+00 | 2.5570E+01 | 1.8247E+00 |
| | HHO | **1.3527E+01** | 9.4762E-01 | 1.5808E+01 | 1.6141E+00 | 1.8154E+01 | 2.3528E+00 | 2.1901E+01 | 2.7306E+00 | 2.5206E+01 | 1.8795E+00 | 2.7781E+01 | 2.1899E+00 |
| | BLPSO | 1.2963E+01 | 2.7409E+00 | 1.6543E+01 | 1.7088E+00 | 1.9715E+01 | 1.8128E+00 | 2.2590E+01 | 1.6979E+00 | 2.5197E+01 | 1.9555E+00 | 2.8156E+01 | 1.4702E+00 |
| | IGWO | 1.1632E+01 | 8.7795E-01 | 1.5798E+01 | 2.2734E+00 | 1.9091E+01 | 2.0582E+00 | 2.2527E+01 | 2.1016E+00 | 2.5253E+01 | **1.4076E+00** | 2.7289E+01 | 1.5676E+00 |
| | IWOA | 1.1860E+01 | 1.6282E+00 | 1.6749E+01 | 2.5342E+00 | 1.9007E+01 | 2.2938E+00 | 2.2928E+01 | 1.9285E+00 | 2.4937E+01 | 1.9673E+00 | 2.7536E+01 | 1.8536E+00 |
| | SCADE | 1.1196E+01 | 1.2353E+00 | 1.4768E+01 | 2.5660E+00 | 1.7302E+01 | 2.6369E+00 | 2.0514E+01 | 2.2129E+00 | 2.3331E+01 | 2.7179E+00 | 2.5031E+01 | 2.6273E+00 |
| Image | Thresholds | 2 | | 4 | | 6 | | 10 | | 15 | | 20 | |
| F | Item | AVG | STD | AVG | STD | AVG | STD | AVG | STD | AVG | STD | AVG | STD |
| | CCMVO | **1.3925E+01** | 1.4083E+00 | **1.9539E+01** | **1.1701E+00** | **2.1776E+01** | **1.1015E+00** | **2.4734E+01** | 1.4636E+00 | **2.7211E+01** | 1.5283E+00 | **2.9224E+01** | **1.3679E+00** |
| | MVO | 1.2607E+01 | **8.2235E-01** | 1.8753E+01 | 1.4907E+00 | 2.1480E+01 | 1.7795E+00 | 2.4480E+01 | 1.4103E+00 | 2.6276E+01 | 2.1231E+00 | 2.7948E+01 | 1.6158E+00 |
| | WOA | 1.3082E+01 | 1.3057E+00 | 1.7142E+01 | 2.6133E+00 | 2.0263E+01 | 2.3819E+00 | 2.2889E+01 | 2.1127E+00 | 2.5907E+01 | 2.4550E+00 | 2.8979E+01 | 1.9164E+00 |
| | SCA | 1.2928E+01 | 1.3749E+00 | 1.6179E+01 | 2.4485E+00 | 1.8012E+01 | 2.7590E+00 | 2.0975E+01 | 1.7164E+00 | 2.3878E+01 | 2.6423E+00 | 2.5620E+01 | 2.1844E+00 |
| | HHO | 1.3457E+01 | 2.1965E+00 | 1.6269E+01 | 2.8338E+00 | 1.9087E+01 | 2.8434E+00 | 2.1800E+01 | 2.6394E+00 | 2.5261E+01 | 2.0483E+00 | 2.7740E+01 | 1.9309E+00 |
| | BLPSO | 1.3375E+01 | 1.8170E+00 | 1.6610E+01 | 1.6759E+00 | 1.8970E+01 | 1.5467E+00 | 2.2611E+01 | **1.3560E+00** | 2.4838E+01 | 1.7844E+00 | 2.7296E+01 | 1.5999E+00 |
| | IGWO | 1.2842E+01 | 9.3926E-01 | 1.7353E+01 | 1.7674E+00 | 1.9597E+01 | 1.9070E+00 | 2.2551E+01 | 1.7826E+00 | 2.4945E+01 | **1.4955E+00** | 2.6920E+01 | 1.9553E+00 |
| | IWOA | 1.2791E+01 | 1.1550E+00 | 1.6997E+01 | 1.6609E+00 | 1.9675E+01 | 2.2371E+00 | 2.3013E+01 | 2.0128E+00 | 2.4949E+01 | 2.4961E+00 | 2.7415E+01 | 1.8999E+00 |
| | SCADE | 1.2424E+01 | 1.0663E+00 | 1.4863E+01 | 2.0477E+00 | 1.6551E+01 | 2.3765E+00 | 2.0814E+01 | 2.4523E+00 | 2.3218E+01 | 1.9158E+00 | 2.5290E+01 | 2.3007E+00 |
| Image | Thresholds | 2 | | 4 | | 6 | | 10 | | 15 | | 20 | |
| G | Item | AVG | STD | AVG | STD | AVG | STD | AVG | STD | AVG | STD | AVG | STD |
| | CCMVO | 1.7127E+01 | 3.7419E-02 | 2.0133E+01 | **4.2424E-01** | **2.2437E+01** | **7.2737E-01** | **2.4588E+01** | **1.3173E+00** | **2.7722E+01** | **1.4742E+00** | **2.9458E+01** | 1.5614E+00 |
| | MVO | **1.7145E+01** | **2.4732E-02** | **2.0168E+01** | 6.5630E-01 | 2.2013E+01 | 1.2182E+00 | 2.3794E+01 | 2.2216E+00 | 2.6426E+01 | 2.1036E+00 | 2.7901E+01 | 2.2644E+00 |
| | WOA | 1.6541E+01 | 1.8838E+00 | 1.8857E+01 | 2.4255E+00 | 2.1054E+01 | 2.2977E+00 | 2.3711E+01 | 2.4165E+00 | 2.5838E+01 | 2.5951E+00 | 2.8501E+01 | 1.4543E+00 |
| | SCA | 1.6499E+01 | 5.4345E-01 | 1.6990E+01 | 2.0605E+00 | 1.8757E+01 | 2.9303E+00 | 2.1784E+01 | 2.2087E+00 | 2.3908E+01 | 2.1261E+00 | 2.6323E+01 | 1.6714E+00 |
| | HHO | 1.5809E+01 | 2.1284E+00 | 1.8097E+01 | 2.5151E+00 | 2.0910E+01 | 2.4172E+00 | 2.3140E+01 | 2.2575E+00 | 2.5208E+01 | 2.5647E+00 | 2.7629E+01 | 2.2615E+00 |
| | BLPSO | 1.4192E+01 | 9.5823E-01 | 1.7185E+01 | 1.4323E+00 | 1.9768E+01 | 1.8167E+00 | 2.2993E+01 | 1.5323E+00 | 2.5958E+01 | 1.5330E+00 | 2.7376E+01 | 1.5880E+00 |
| | IGWO | 1.4646E+01 | 4.1493E-01 | 1.9031E+01 | 1.1712E+00 | 2.0988E+01 | 1.7213E+00 | 2.2611E+01 | 2.2611E+00 | 2.5213E+01 | 1.8315E+00 | 2.7169E+01 | 1.5519E+00 |
| | IWOA | 1.4400E+01 | 9.5120E-01 | 1.7423E+01 | 2.2596E+00 | 1.9999E+01 | 1.9312E+00 | 2.2116E+01 | 1.5867E+00 | 2.5521E+01 | 1.8133E+00 | 2.8022E+01 | **1.3749E+00** |
| | SCADE | 1.4196E+01 | 8.7420E-01 | 1.6112E+01 | 1.8600E+00 | 1.7915E+01 | 2.5695E+00 | 2.0351E+01 | 2.3014E+00 | 2.3838E+01 | 2.0999E+00 | 2.6292E+01 | 2.0417E+00 |
| Image | Thresholds | 2 | | 4 | | 6 | | 10 | | 15 | | 20 | |
| H | Item | AVG | STD | AVG | STD | AVG | STD | AVG | STD | AVG | STD | AVG | STD |
| | CCMVO | 1.4721E+01 | 2.8410E-01 | **1.9507E+01** | **8.9853E-01** | **2.2052E+01** | **9.3056E-01** | **2.5192E+01** | **7.6662E-01** | **2.7740E+01** | **9.5796E-01** | **2.9917E+01** | **1.1051E+00** |
| | MVO | 1.4453E+01 | 1.2439E+00 | 1.8935E+01 | 1.3845E+00 | 2.1371E+01 | 1.8058E+00 | 2.4253E+01 | 1.4117E+00 | 2.6308E+01 | 2.1853E+00 | 2.8375E+01 | 1.4699E+00 |
| | WOA | 1.4320E+01 | 1.4827E+00 | 1.7332E+01 | 2.7170E+00 | 1.9832E+01 | 2.4728E+00 | 2.3212E+01 | 2.1732E+00 | 2.6697E+01 | 1.6605E+00 | 2.8694E+01 | 1.8440E+00 |
| | SCA | 1.4391E+01 | 9.4176E-01 | 1.5842E+01 | 2.2196E+00 | 1.7965E+01 | 2.0429E+00 | 2.1237E+01 | 2.6261E+00 | 2.4213E+01 | 2.0715E+00 | 2.5707E+01 | 1.8035E+00 |

(*continued on next page*)

**Table A.4** (*continued*)

| Image | Thresholds | 2 | | 4 | | 6 | | 10 | | 15 | | 20 | |
|---|---|---|---|---|---|---|---|---|---|---|---|---|---|
| A | Item | AVE | STD | AVE | STD | AVE | STD | AVE | STD | AVE | STD | AVE | STD |
| | HHO | 1.3354E+01 | 1.8333E+00 | 1.6987E+01 | 2.1740E+00 | 1.8520E+01 | 2.9881E+00 | 2.3529E+01 | 2.4632E+00 | 2.6046E+01 | 2.0134E+00 | 2.7454E+01 | 2.1427E+00 |
| | BLPSO | 1.4226E+01 | 9.8649E-01 | 1.7546E+01 | 1.7589E+00 | 1.9790E+01 | 1.2823E+00 | 2.3031E+01 | 1.3903E+00 | 2.5597E+01 | 1.1134E+00 | 2.7504E+01 | 1.5943E+00 |
| | IGWO | **1.4937E+01** | **1.2061E-01** | 1.8913E+01 | 1.1328E+00 | 2.0077E+01 | 2.2455E+00 | 2.3325E+01 | 1.8912E+00 | 2.5272E+01 | 1.7767E+00 | 2.7436E+01 | 1.6844E+00 |
| | IWOA | 1.4871E+01 | 8.4041E-01 | 1.7455E+01 | 2.6167E+00 | 1.9361E+01 | 2.3220E+00 | 2.2882E+01 | 2.2954E+00 | 2.5445E+01 | 2.1332E+00 | 2.7617E+01 | 1.5296E+00 |
| | SCADE | 1.4531E+01 | 7.7053E-01 | 1.6738E+01 | 1.4581E+00 | 1.8359E+01 | 2.1940E+00 | 2.0782E+01 | 1.8157E+00 | 2.3285E+01 | 2.0739E+00 | 2.6024E+01 | 2.0178E+00 |
| Image | Thresholds | 2 | | 4 | | 6 | | 10 | | 15 | | 20 | |
| I | Item | AVG | STD | AVG | STD | AVG | STD | AVG | STD | AVG | STD | AVG | STD |
| | CCMVO | **1.3468E+01** | 1.0567E+00 | **1.9887E+01** | 1.2448E+00 | **2.1874E+01** | 1.5931E+00 | **2.4754E+01** | **1.1726E+00** | **2.7023E+01** | **1.1427E+00** | **2.8945E+01** | **1.0419E+00** |
| | MVO | 1.3220E+01 | 1.3802E+00 | 1.8389E+01 | 1.8558E+00 | 2.1141E+01 | 1.5132E+00 | 2.3683E+01 | 1.8136E+00 | 2.6336E+01 | 1.9338E+00 | 2.7841E+01 | 1.4065E+00 |
| | WOA | 1.2386E+01 | 1.3467E+00 | 1.6016E+01 | 2.4872E+00 | 1.9432E+01 | 1.8579E+00 | 2.3360E+01 | 1.5683E+00 | 2.6161E+01 | 1.8548E+00 | 2.8573E+01 | 1.5808E+00 |
| | SCA | 1.3094E+01 | 1.2857E+00 | 1.5838E+01 | 2.8174E+00 | 1.8228E+01 | 1.8905E+00 | 1.9924E+01 | 2.3769E+00 | 2.2994E+01 | 2.0791E+00 | 2.5557E+01 | 1.9871E+00 |
| | HHO | 1.2308E+01 | 2.4243E+00 | 1.6045E+01 | 2.4349E+00 | 1.9595E+01 | 2.3838E+00 | 2.1765E+01 | 1.9908E+00 | 2.4555E+01 | 1.9877E+00 | 2.6287E+01 | 2.0926E+00 |
| | BLPSO | 1.3333E+01 | 1.4635E+00 | 1.6208E+01 | 1.6006E+00 | 1.9032E+01 | 2.0025E+00 | 2.2331E+01 | 1.6867E+00 | 2.4547E+01 | 1.9805E+00 | 2.7184E+01 | 1.4410E+00 |
| | IGWO | 1.3148E+01 | **1.4906E-01** | 1.7583E+01 | **1.1553E+00** | 1.9207E+01 | **1.5049E+00** | 2.2170E+01 | 1.7646E+00 | 2.5283E+01 | 1.6218E+00 | 2.6758E+01 | 1.7360E+00 |
| | IWOA | 1.2877E+01 | 1.0325E+00 | 1.6863E+01 | 1.4373E+00 | 1.8571E+01 | 1.8170E+00 | 2.1478E+01 | 1.9060E+00 | 2.5107E+01 | 1.6955E+00 | 2.7153E+01 | 2.0259E+00 |
| | SCADE | 1.2766E+01 | 1.0122E+00 | 1.4983E+01 | 2.2159E+00 | 1.6772E+01 | 2.2972E+00 | 1.9861E+01 | 2.3980E+00 | 2.3249E+01 | 2.4115E+00 | 2.5960E+01 | 1.9903E+00 |
| Image | Thresholds | 2 | | 4 | | 6 | | 10 | | 15 | | 20 | |
| J | Item | AVG | STD | AVG | STD | AVG | STD | AVG | STD | AVG | STD | AVG | STD |
| | CCMVO | 1.4999E+01 | **7.5833E-02** | **2.0083E+01** | **9.9730E-01** | **2.1782E+01** | **1.4790E+00** | **2.5250E+01** | **1.1491E+00** | **2.7929E+01** | **1.1825E+00** | **2.9626E+01** | **1.3461E+00** |
| | MVO | 1.4864E+01 | 7.9750E-01 | 1.9504E+01 | 1.0169E+00 | 2.0995E+01 | 1.8679E+00 | 2.4447E+01 | 1.6649E+00 | 2.6512E+01 | 1.7364E+00 | 2.8221E+01 | 1.7612E+00 |
| | WOA | 1.4843E+01 | 7.3868E-01 | 1.7701E+01 | 2.5251E+00 | 1.9908E+01 | 2.4488E+00 | 2.3566E+01 | 2.0758E+00 | 2.7316E+01 | 1.5957E+00 | 2.9142E+01 | 1.4529E+00 |
| | SCA | 1.4350E+01 | 8.3561E-01 | 1.6791E+01 | 1.9803E+00 | 1.7913E+01 | 2.3718E+00 | 2.0935E+01 | 1.9699E+00 | 2.3770E+01 | 2.3365E+00 | 2.5715E+01 | 2.2909E+00 |
| | HHO | 1.4103E+01 | 1.3522E+00 | 1.7049E+01 | 2.4757E+00 | 1.9087E+01 | 2.3865E+00 | 2.3424E+01 | 2.3086E+00 | 2.5842E+01 | 2.1797E+00 | 2.7558E+01 | 2.3463E+00 |
| | BLPSO | **1.5089E+01** | 1.2288E+00 | 1.7770E+01 | 1.4756E+00 | 1.9764E+01 | 1.6882E+00 | 2.3102E+01 | 1.2905E+00 | 2.5659E+01 | 1.3963E+00 | 2.6766E+01 | 1.4350E+00 |
| | IGWO | 1.2760E+01 | 1.0421E+00 | 1.7942E+01 | 1.6157E+00 | 2.0316E+01 | 2.0801E+00 | 2.3088E+01 | 1.8184E+00 | 2.5593E+01 | 1.6042E+00 | 2.7754E+01 | 1.5372E+00 |
| | IWOA | 1.4039E+01 | 1.6550E+00 | 1.6737E+01 | 2.7223E+00 | 1.9698E+01 | 2.1524E+00 | 2.2773E+01 | 2.5089E+00 | 2.5249E+01 | 2.6578E+00 | 2.6652E+01 | 2.3387E+00 |
| | SCADE | 1.2665E+01 | 1.4560E+00 | 1.5528E+01 | 2.6417E+00 | 1.7751E+01 | 2.9599E+00 | 2.0991E+01 | 2.4380E+00 | 2.3674E+01 | 2.3779E+00 | 2.5729E+01 | 2.7383E+00 |

**Table A.5**
SSIM's evaluation results

| Image | Thresholds | 2 | | 4 | | 6 | | 10 | | 15 | | 20 | |
|---|---|---|---|---|---|---|---|---|---|---|---|---|---|
| A | Item | AVE | STD | AVE | STD | AVE | STD | AVE | STD | AVE | STD | AVE | STD |
| | CCMVO | **5.9939E-01** | **1.2753E-02** | **6.7254E-01** | 4.8310E-02 | **6.9277E-01** | **3.0320E-02** | **7.5307E-01** | 6.5061E-02 | **8.3984E-01** | 3.9770E-02 | **8.6037E-01** | **3.8995E-02** |
| | MVO | 5.5139E-01 | 7.1608E-02 | 6.4369E-01 | 7.0279E-02 | 6.7512E-01 | 4.5694E-02 | 7.2637E-01 | 6.5235E-02 | 8.1019E-01 | 5.5224E-02 | 8.4525E-01 | 5.5645E-02 |
| | WOA | 5.8399E-01 | 4.3712E-02 | 5.9245E-01 | 7.5759E-02 | 6.6522E-01 | 7.1396E-02 | 7.2551E-01 | 7.1839E-02 | 8.0686E-01 | 4.2874E-02 | 8.5311E-01 | 4.7490E-02 |
| | SCA | 5.7664E-01 | 2.5464E-02 | 6.3223E-01 | 4.2465E-02 | 6.2760E-01 | 5.7870E-02 | 7.0884E-01 | 5.8211E-02 | 7.4129E-01 | 8.6366E-02 | 8.1992E-01 | 4.3820E-02 |
| | HHO | 5.2065E-01 | 1.1126E-01 | 6.0468E-01 | 7.4929E-02 | 6.3384E-01 | 5.4191E-02 | 7.3044E-01 | 7.3563E-02 | 7.9402E-01 | **3.9231E-02** | 8.3744E-01 | 6.3287E-02 |
| | BLPSO | 5.3733E-01 | 5.1778E-02 | 6.0150E-01 | **3.8968E-02** | 6.4177E-01 | 5.5499E-02 | 7.1434E-01 | 6.2360E-02 | 7.7909E-01 | 4.1525E-02 | 8.2790E-01 | 4.2041E-02 |
| | IGWO | 5.7591E-01 | 1.5783E-02 | 6.3597E-01 | 6.4345E-02 | 6.7282E-01 | 8.0789E-02 | 7.5169E-01 | 5.7163E-02 | 7.7264E-01 | 4.5708E-02 | 8.2186E-01 | 4.7366E-02 |
| | IWOA | 5.3022E-01 | 1.0502E-01 | 6.1229E-01 | 6.3803E-02 | 6.2894E-01 | 8.8352E-02 | 7.0944E-01 | 6.5265E-02 | 7.7841E-01 | 5.4534E-02 | 8.3099E-01 | 4.8349E-02 |
| | SCADE | 5.7576E-01 | 5.1533E-02 | 6.2327E-01 | 5.0918E-02 | 6.3868E-01 | 6.3422E-02 | 7.0565E-01 | **5.6578E-02** | 7.5848E-01 | 4.7653E-02 | 8.0077E-01 | 6.1195E-02 |
| Image B | Thresholds | 2 | | 4 | | 6 | | 10 | | 15 | | 20 | |
| | Item | AVE | STD | AVE | STD | AVE | STD | AVE | STD | AVE | STD | AVE | STD |
| | CCMVO | 5.7362E-01 | **7.5380E-04** | **6.4959E-01** | **4.3420E-02** | 6.6061E-01 | 4.7134E-02 | **7.5560E-01** | 3.3128E-02 | **8.3519E-01** | 3.5050E-02 | **8.7936E-01** | **2.0126E-02** |
| | MVO | 4.8594E-01 | 9.6444E-02 | 6.0303E-01 | 6.0190E-02 | **6.6850E-01** | 4.5755E-02 | 7.3958E-01 | 3.9813E-02 | 8.2065E-01 | **3.3630E-02** | 8.5426E-01 | 3.8022E-02 |
| | WOA | 4.4856E-01 | 1.5043E-01 | 5.4854E-01 | 7.5909E-02 | 6.4722E-01 | 5.2013E-02 | 7.5310E-01 | 4.4086E-02 | 8.1924E-01 | 3.9738E-02 | 8.7627E-01 | 3.3508E-02 |
| | SCA | 5.6995E-01 | 2.0428E-02 | 5.9050E-01 | 7.7839E-02 | 6.1705E-01 | 5.4447E-02 | 6.9192E-01 | 5.7521E-02 | 7.5550E-01 | 6.8665E-02 | 7.9109E-01 | 4.7389E-02 |
| | HHO | 4.3522E-01 | 1.1709E-01 | 5.3659E-01 | 8.1090E-02 | 6.4185E-01 | 4.6490E-02 | 7.1334E-01 | 5.4793E-02 | 7.7881E-01 | 5.7479E-02 | 8.5489E-01 | 4.7284E-02 |
| | BLPSO | 4.9645E-01 | 7.4408E-02 | 5.7798E-01 | 5.8131E-02 | 6.4833E-01 | 4.1318E-02 | 7.3683E-01 | **2.7131E-02** | 7.9075E-01 | 3.7516E-02 | 8.2671E-01 | 4.0947E-02 |
| | IGWO | 5.2991E-01 | 1.2389E-01 | 5.7415E-01 | 8.0683E-02 | 6.5357E-01 | **3.3422E-02** | 7.1305E-01 | 5.4528E-02 | 7.9031E-01 | 3.9789E-02 | 8.3723E-01 | 2.9641E-02 |
| | IWOA | 4.4346E-01 | 1.2448E-01 | 5.7358E-01 | 5.6952E-02 | 6.4110E-01 | 4.6408E-02 | 7.2039E-01 | 6.2566E-02 | 7.9471E-01 | 4.3351E-02 | 8.4376E-01 | 3.2173E-02 |
| | SCADE | **5.7469E-01** | 1.8095E-02 | 5.8448E-01 | 6.3247E-02 | 6.1380E-01 | 6.1578E-02 | 6.9693E-01 | 4.3979E-02 | 7.5902E-01 | 4.3293E-02 | 8.0894E-01 | 3.2262E-02 |
| Image C | Thresholds | 2 | | 4 | | 6 | | 10 | | 15 | | 20 | |
| | Item | AVE | STD | AVE | STD | AVE | STD | AVE | STD | AVE | STD | AVE | STD |
| | CCMVO | 5.7081E-01 | 1.3995E-02 | 6.4512E-01 | 2.4771E-02 | 6.9070E-01 | 4.8094E-02 | **7.7932E-01** | 2.5483E-02 | **8.4225E-01** | **2.2970E-02** | **8.8022E-01** | **1.6039E-02** |
| | MVO | 4.8474E-01 | 1.7165E-01 | 6.3004E-01 | 5.4954E-02 | 6.6520E-01 | 6.7621E-02 | 7.6681E-01 | 3.8872E-02 | 8.2257E-01 | 3.2174E-02 | 8.5473E-01 | 4.2507E-02 |
| | WOA | 4.9081E-01 | 1.6713E-01 | 5.8025E-01 | 1.0349E-01 | 6.3745E-01 | 6.0337E-02 | 7.7157E-01 | 4.6842E-02 | 8.2425E-01 | 4.3642E-02 | 8.7079E-01 | 2.9416E-02 |
| | SCA | 5.6585E-01 | 4.5573E-02 | 5.8490E-01 | 1.3271E-01 | 5.8947E-01 | 9.4202E-02 | 7.3146E-01 | 4.1127E-02 | 7.6988E-01 | 5.0905E-02 | 8.0390E-01 | 5.0158E-02 |
| | HHO | 5.3966E-01 | 7.6802E-02 | 5.8961E-01 | 9.8999E-02 | 6.4775E-01 | 9.1953E-02 | 7.6402E-01 | 5.9270E-02 | 8.2076E-01 | 3.6563E-02 | 8.4977E-01 | 3.6233E-02 |
| | BLPSO | 5.5955E-01 | 1.1334E-01 | 6.5371E-01 | 5.5049E-02 | 6.8325E-01 | 7.0330E-02 | 7.4958E-01 | **2.5460E-02** | 7.9359E-01 | 2.8106E-02 | 8.2882E-01 | 2.5157E-02 |
| | IGWO | 6.4188E-01 | **4.7531E-03** | **6.8996E-01** | **2.0831E-02** | **7.3055E-01** | **3.5516E-02** | 7.6673E-01 | 3.7484E-02 | 8.0786E-01 | 3.6101E-02 | 8.4333E-01 | 2.6033E-02 |
| | IWOA | 6.3038E-01 | 4.0367E-02 | 6.4389E-01 | 5.6730E-02 | 6.8500E-01 | 4.9109E-02 | 7.4708E-01 | 4.6229E-02 | 8.0889E-01 | 3.6416E-02 | 8.4263E-01 | 3.6379E-02 |
| | SCADE | **6.4330E-01** | 3.4384E-02 | 6.7491E-01 | 5.0589E-02 | 6.8635E-01 | 6.1080E-02 | 7.3740E-01 | 3.2734E-02 | 7.7102E-01 | 4.9033E-02 | 8.1951E-01 | 3.5751E-02 |
| Image D | Thresholds | 2 | | 4 | | 6 | | 10 | | 15 | | 20 | |
| | Item | AVE | STD | AVE | STD | AVE | STD | AVE | STD | AVE | STD | AVE | STD |
| | CCMVO | **6.7409E-01** | **3.4348E-03** | **7.1976E-01** | **1.4421E-02** | **7.3598E-01** | 3.3832E-02 | **7.7764E-01** | **2.1168E-02** | **8.4357E-01** | 2.7519E-02 | **8.8011E-01** | 2.8602E-02 |
| | MVO | 6.3073E-01 | 7.4767E-02 | 6.8879E-01 | 5.5229E-02 | 7.1694E-01 | **2.7568E-02** | 7.5211E-01 | 3.2189E-02 | 8.1943E-01 | 3.9067E-02 | 8.4761E-01 | 2.8701E-02 |
| | WOA | 5.9987E-01 | 1.1826E-01 | 6.7813E-01 | 5.6036E-02 | 6.8214E-01 | 6.4955E-02 | 7.2750E-01 | 4.7126E-02 | 8.1586E-01 | 3.4094E-02 | 8.6015E-01 | **2.6541E-02** |
| | SCA | 6.6070E-01 | 1.6421E-02 | 6.8055E-01 | 3.9478E-02 | 6.8898E-01 | 4.7762E-02 | 7.0374E-01 | 4.3210E-02 | 7.6821E-01 | 4.3311E-02 | 8.0424E-01 | 4.3134E-02 |
| | HHO | 5.4369E-01 | 1.0027E-01 | 6.5599E-01 | 7.0444E-02 | 6.7082E-01 | 7.4927E-02 | 7.1306E-01 | 5.6262E-02 | 8.0779E-01 | 3.5595E-02 | 8.4217E-01 | 3.9227E-02 |
| | BLPSO | | | | | | | | | | | | |

(continued on next page)

**Table A.5** (*continued*)

| Image | Thresholds | 2 | | 4 | | 6 | | 10 | | 15 | | 20 | |
|---|---|---|---|---|---|---|---|---|---|---|---|---|---|
| A | Item | AVE | STD | AVE | STD | AVE | STD | AVE | STD | AVE | STD | AVE | STD |
| | | 5.6660E-01 | 6.5203E-02 | 5.9409E-01 | 4.9506E-02 | 6.5638E-01 | 3.4666E-02 | 7.3099E-01 | 4.0402E-02 | 7.7911E-01 | **2.4848E-02** | 8.2873E-01 | 3.3490E-02 |
| | IGWO | 6.0599E-01 | 7.5056E-02 | 6.1952E-01 | 4.1709E-02 | 6.5224E-01 | 3.6126E-02 | 7.2651E-01 | 3.4381E-02 | 7.9439E-01 | 3.3546E-02 | 8.3071E-01 | 3.7734E-02 |
| | IWOA | 5.5054E-01 | 6.7387E-02 | 5.8403E-01 | 6.2049E-02 | 6.6350E-01 | 4.0300E-02 | 7.3061E-01 | 3.2281E-02 | 7.7409E-01 | 4.4776E-02 | 8.3762E-01 | 4.3752E-02 |
| | SCADE | 6.2626E-01 | 2.3470E-02 | 6.3912E-01 | 6.0022E-02 | 6.4050E-01 | 5.2826E-02 | 7.1926E-01 | 4.8573E-02 | 7.5246E-01 | 5.1767E-02 | 8.0970E-01 | 3.0018E-02 |
| Image E | Thresholds | 2 | | 4 | | 6 | | 10 | | 15 | | 20 | |
| | Item | AVE | STD | AVE | STD | AVE | STD | AVE | STD | AVE | STD | AVE | STD |
| | CCMVO | 6.3582E-01 | **2.9384E-03** | **7.3450E-01** | **8.7625E-03** | **7.5907E-01** | **2.2319E-02** | 7.6258E-01 | **2.7809E-02** | **8.2469E-01** | 3.2061E-02 | 8.6302E-01 | **1.9898E-02** |
| | MVO | 5.9915E-01 | 8.0160E-02 | 6.9232E-01 | 6.6090E-02 | 7.3545E-01 | 4.8806E-02 | **7.6300E-01** | 4.1140E-02 | 8.1299E-01 | 4.2895E-02 | 8.4645E-01 | 4.2836E-02 |
| | WOA | 5.9544E-01 | 8.0992E-02 | 6.8917E-01 | 8.1687E-02 | 6.8011E-01 | 7.2040E-02 | 7.5868E-01 | 3.5368E-02 | 8.2296E-01 | 3.9509E-02 | **8.7794E-01** | 2.5970E-02 |
| | SCA | **6.3881E-01** | 2.2467E-02 | 6.8693E-01 | 5.1051E-02 | 7.0216E-01 | 5.3687E-02 | 6.7184E-01 | 5.7940E-02 | 7.5908E-01 | 5.0966E-02 | 7.9613E-01 | 4.0105E-02 |
| | HHO | 5.5900E-01 | 7.6103E-02 | 6.2345E-01 | 1.0243E-01 | 6.9396E-01 | 6.4019E-02 | 7.2677E-01 | 5.8075E-02 | 7.9564E-01 | 4.0946E-02 | 8.4382E-01 | 4.4564E-02 |
| | BLPSO | 5.0232E-01 | 1.1034E-01 | 5.9182E-01 | 5.3092E-02 | 6.6433E-01 | 3.6149E-02 | 7.2562E-01 | 4.0324E-02 | 7.9203E-01 | 3.6783E-02 | 8.4699E-01 | 2.8457E-02 |
| | IGWO | 5.8526E-01 | 4.5185E-02 | 5.7571E-01 | 7.4628E-02 | 6.5064E-01 | 6.0264E-02 | 7.2590E-01 | 5.3624E-02 | 8.0177E-01 | **2.8616E-02** | 8.3573E-01 | 3.4723E-02 |
| | IWOA | 5.4670E-01 | 8.0811E-02 | 6.0254E-01 | 5.7861E-02 | 6.5136E-01 | 4.9190E-02 | 7.3532E-01 | 3.8869E-02 | 7.8614E-01 | 4.2495E-02 | 8.3452E-01 | 3.7679E-02 |
| | SCADE | 5.8348E-01 | 2.1489E-02 | 6.1509E-01 | 6.7450E-02 | 6.3896E-01 | 5.6775E-02 | 7.0180E-01 | 4.6319E-02 | 7.5377E-01 | 5.3424E-02 | 7.8754E-01 | 5.8022E-02 |
| Image F | Thresholds | 2 | | 4 | | 6 | | 10 | | 15 | | 20 | |
| | Item | AVE | STD | AVE | STD | AVE | STD | AVE | STD | AVE | STD | AVE | STD |
| | CCMVO | 6.0732E-01 | 1.0167E-02 | 6.5722E-01 | **2.3748E-02** | 6.6363E-01 | **2.5825E-02** | **7.7880E-01** | 3.0533E-02 | **8.3458E-01** | **2.0980E-02** | **8.7084E-01** | **1.9165E-02** |
| | MVO | 6.0289E-01 | 5.5763E-02 | 6.3558E-01 | 4.7909E-02 | 6.6397E-01 | 4.4758E-02 | 7.7764E-01 | 2.6302E-02 | 8.1868E-01 | 3.2022E-02 | 8.4759E-01 | 2.5996E-02 |
| | WOA | 5.7579E-01 | 7.4390E-02 | 5.8531E-01 | 8.3610E-02 | 6.5930E-01 | 6.0712E-02 | 7.5463E-01 | 3.8106E-02 | 8.0607E-01 | 4.0873E-02 | 8.6354E-01 | 3.0158E-02 |
| | SCA | 6.0305E-01 | 1.9032E-02 | 6.1813E-01 | 6.3075E-02 | 6.4155E-01 | 5.0775E-02 | 7.3753E-01 | 3.5267E-02 | 7.8041E-01 | 4.0619E-02 | 8.1204E-01 | 3.3454E-02 |
| | HHO | 5.4876E-01 | 1.0841E-01 | 5.7853E-01 | 8.3752E-02 | 6.2881E-01 | 7.6933E-02 | 7.5669E-01 | 4.1149E-02 | 8.0684E-01 | 2.9131E-02 | 8.4371E-01 | 3.1295E-02 |
| | BLPSO | 5.7375E-01 | 9.0613E-02 | 6.3982E-01 | 6.3662E-02 | 6.9541E-01 | 3.6046E-02 | 7.4469E-01 | **2.5102E-02** | 7.9817E-01 | 2.5033E-02 | 8.3537E-01 | 2.3268E-02 |
| | IGWO | **6.7305E-01** | **5.9583E-03** | **6.9542E-01** | 5.5099E-02 | **7.1282E-01** | 4.6835E-02 | 7.4896E-01 | 4.1462E-02 | 7.9689E-01 | 2.2234E-02 | 8.2624E-01 | 3.1899E-02 |
| | IWOA | 6.0689E-01 | 8.9659E-02 | 6.5320E-01 | 5.6120E-02 | 7.0119E-01 | 4.9852E-02 | 7.4780E-01 | 4.1893E-02 | 8.0532E-01 | 4.1378E-02 | 8.3939E-01 | 3.0402E-02 |
| | SCADE | 6.6300E-01 | 1.3627E-02 | 6.7738E-01 | 4.6181E-02 | 6.8279E-01 | 6.0645E-02 | 7.4131E-01 | 4.7541E-02 | 7.7328E-01 | 3.3967E-02 | 8.1602E-01 | 3.0081E-02 |
| Image G | Thresholds | 2 | | 4 | | 6 | | 10 | | 15 | | 20 | |
| | Item | AVE | STD | AVE | STD | AVE | STD | AVE | STD | AVE | STD | AVE | STD |
| | CCMVO | 6.4122E-01 | **1.8925E-03** | 6.9168E-01 | **7.5496E-03** | **7.2985E-01** | **1.3282E-02** | **7.7907E-01** | 3.2099E-02 | **8.4855E-01** | 2.2129E-02 | **8.7621E-01** | 2.3080E-02 |
| | MVO | **6.4144E-01** | 2.6829E-03 | **6.9431E-01** | 1.7374E-02 | 7.2422E-01 | 2.4263E-02 | 7.6804E-01 | 3.6387E-02 | 8.2492E-01 | 3.3900E-02 | 8.5398E-01 | **2.1465E-02** |
| | WOA | 6.1623E-01 | 1.0323E-01 | 6.5500E-01 | 1.0068E-01 | 7.1188E-01 | 5.3305E-02 | 7.7008E-01 | 7.3433E-02 | 8.1435E-01 | 5.0908E-02 | 8.6117E-01 | 2.5399E-02 |
| | SCA | 6.3210E-01 | 3.4412E-02 | 6.6455E-01 | 6.6476E-02 | 6.9553E-01 | 6.9562E-02 | 7.4944E-01 | 3.7316E-02 | 7.8527E-01 | 4.0866E-02 | 8.2565E-01 | 2.5918E-02 |
| | HHO | 5.8806E-01 | 1.1697E-01 | 6.6790E-01 | 6.1391E-02 | 7.1682E-01 | 6.9497E-02 | 7.6639E-01 | 4.9482E-02 | 8.0870E-01 | 5.3548E-02 | 8.5196E-01 | 3.4680E-02 |
| | BLPSO | 4.8002E-01 | 6.8149E-02 | 6.0130E-01 | 8.2137E-02 | 6.9292E-01 | 5.8218E-02 | 7.5445E-01 | **2.9742E-02** | 8.1678E-01 | **2.1706E-02** | 8.3804E-01 | 2.2237E-02 |
| | IGWO | 5.9423E-01 | 1.9275E-02 | 6.7427E-01 | 6.5254E-02 | 7.1172E-01 | 5.7896E-02 | 7.5763E-01 | 5.6730E-02 | 8.1292E-01 | 2.7808E-02 | 8.3951E-01 | 2.4862E-02 |
| | IWOA | 5.3161E-01 | 8.5059E-02 | 6.0898E-01 | 1.1140E-01 | 6.8688E-01 | 7.1184E-02 | 7.3767E-01 | 4.2565E-02 | 8.0624E-01 | 3.1636E-02 | 8.5148E-01 | 2.3713E-02 |
| | SCADE | 5.6747E-01 | 5.3417E-02 | 6.7427E-01 | 4.5678E-02 | 6.5486E-01 | 9.5468E-02 | 7.3936E-01 | 4.0677E-02 | 7.8652E-01 | 3.7571E-02 | 8.2046E-01 | 3.9008E-02 |
| Image H | Thresholds | 2 | | 4 | | 6 | | 10 | | 15 | | 20 | |
| | Item | AVE | STD | AVE | STD | AVE | STD | AVE | STD | AVE | STD | AVE | STD |
| | CCMVO | 5.8386E-01 | 1.7520E-02 | 6.8166E-01 | 5.6174E-02 | **7.2793E-01** | **3.4278E-02** | **7.9324E-01** | **1.9644E-02** | **8.4420E-01** | **2.1063E-02** | **8.8052E-01** | **1.5925E-02** |

(continued on next page)

**Table A.5** (*continued*)

| Image | Thresholds | 2 | | 4 | | 6 | | 10 | | 15 | | 20 | |
|---|---|---|---|---|---|---|---|---|---|---|---|---|---|
| A | Item | AVE | STD | AVE | STD | AVE | STD | AVE | STD | AVE | STD | AVE | STD |
| | MVO | 5.4762E-01 | 1.0010E-01 | 6.5300E-01 | 7.9020E-02 | 7.0191E-01 | 7.0638E-02 | 7.7049E-01 | 2.9720E-02 | 8.1949E-01 | 3.6190E-02 | 8.5867E-01 | 2.3362E-02 |
| | WOA | 5.3935E-01 | 1.1209E-01 | 6.0571E-01 | 1.2706E-01 | 6.7911E-01 | 8.7677E-02 | 7.5720E-01 | 4.9947E-02 | 8.2559E-01 | 3.2310E-02 | 8.6510E-01 | 2.7507E-02 |
| | SCA | **5.8531E-01** | 6.1987E-02 | 6.0948E-01 | 9.7943E-02 | 6.6492E-01 | 6.1957E-02 | 7.4211E-01 | 6.5197E-02 | 7.8971E-01 | 3.7752E-02 | 8.1301E-01 | 4.0041E-02 |
| | HHO | 4.4259E-01 | 1.2866E-01 | 5.8243E-01 | 1.1868E-01 | 6.2335E-01 | 1.2345E-01 | 7.6698E-01 | 5.7937E-02 | 8.2606E-01 | 3.0705E-02 | 8.4737E-01 | 3.1576E-02 |
| | BLPSO | 5.1107E-01 | 7.5305E-02 | 6.3836E-01 | 6.7171E-02 | 6.9127E-01 | 4.2553E-02 | 7.5001E-01 | 3.2500E-02 | 8.0336E-01 | 2.4410E-02 | 8.4052E-01 | 2.6295E-02 |
| | IGWO | 5.7792E-01 | **8.3430E-03** | **7.0970E-01** | **3.4228E-02** | 6.8962E-01 | 9.0505E-02 | 7.7009E-01 | 3.9855E-02 | 8.0876E-01 | 3.3778E-02 | 8.4482E-01 | 2.3676E-02 |
| | IWOA | 5.6764E-01 | 6.2693E-02 | 6.1430E-01 | 1.2319E-01 | 6.8560E-01 | 8.1965E-02 | 7.5318E-01 | 5.2539E-02 | 8.0523E-01 | 3.4733E-02 | 8.4897E-01 | 2.2465E-02 |
| | SCADE | 5.7266E-01 | 4.5458E-02 | 6.7243E-01 | 6.5381E-02 | 6.7020E-01 | 7.6154E-02 | 7.3899E-01 | 4.3305E-02 | 7.7614E-01 | 4.5240E-02 | 8.2367E-01 | 3.4647E-02 |
| Image | Thresholds | 2 | | 4 | | 6 | | 10 | | 15 | | 20 | |
| I | Item | AVE | STD | AVE | STD | AVE | STD | AVE | STD | AVE | STD | AVE | STD |
| | CCMVO | **6.4983E-01** | 9.8361E-03 | 6.6862E-01 | **2.3052E-02** | 6.9334E-01 | 3.2955E-02 | **7.9858E-01** | **2.9128E-02** | **8.5025E-01** | **1.4032E-02** | **8.7232E-01** | **1.6465E-02** |
| | MVO | 5.4253E-01 | 7.9829E-02 | 6.2978E-01 | 3.6837E-02 | 6.7561E-01 | **3.0714E-02** | 7.7847E-01 | 3.4675E-02 | 8.3275E-01 | 3.5315E-02 | 8.6197E-01 | 1.7571E-02 |
| | WOA | 5.6116E-01 | 1.1048E-01 | 5.6546E-01 | 5.9785E-02 | 6.5423E-01 | 4.4208E-02 | 7.7527E-01 | 3.5140E-02 | 8.3837E-01 | 2.7513E-02 | 8.6933E-01 | 2.2454E-02 |
| | SCA | 6.3445E-01 | 2.0238E-02 | 6.2897E-01 | 5.5737E-02 | 6.5553E-01 | 5.0960E-02 | 7.5223E-01 | 4.6287E-02 | 7.8900E-01 | 2.6231E-02 | 8.2721E-01 | 3.1182E-02 |
| | HHO | 5.0428E-01 | 1.2810E-01 | 5.7353E-01 | 5.8396E-02 | 6.5929E-01 | 5.1739E-02 | 7.7763E-01 | 3.4788E-02 | 8.1424E-01 | 2.9304E-02 | 8.4193E-01 | 3.1076E-02 |
| | BLPSO | 5.5494E-01 | 8.3497E-02 | 6.5243E-01 | 7.9318E-02 | 7.1394E-01 | 5.1432E-02 | 7.6411E-01 | 3.6692E-02 | 8.0944E-01 | 2.1165E-02 | 8.4392E-01 | 1.9949E-02 |
| | IGWO | 6.3630E-01 | **5.1889E-03** | **7.2433E-01** | 4.4840E-02 | **7.3992E-01** | 5.0281E-02 | 7.7867E-01 | 4.0628E-02 | 8.0984E-01 | 3.3316E-02 | 8.4430E-01 | 2.5076E-02 |
| | IWOA | 5.8518E-01 | 9.0411E-02 | 6.6549E-01 | 7.3639E-02 | 7.0262E-01 | 6.5302E-02 | 7.5637E-01 | 4.2279E-02 | 8.1290E-01 | 2.4424E-02 | 8.4918E-01 | 2.0752E-02 |
| | SCADE | 6.3381E-01 | 2.2452E-02 | 6.8497E-01 | 6.1800E-02 | 7.2082E-01 | 5.8332E-02 | 7.4231E-01 | 5.4626E-02 | 7.9317E-01 | 3.5771E-02 | 8.3356E-01 | 2.9936E-02 |
| Image | Thresholds | 2 | | 4 | | 6 | | 10 | | 15 | | 20 | |
| J | Item | AVE | STD | AVE | STD | AVE | STD | AVE | STD | AVE | STD | AVE | STD |
| | CCMVO | 5.7993E-01 | **6.6419E-03** | **6.9326E-01** | 4.9542E-02 | **7.1376E-01** | 4.9851E-02 | **7.6596E-01** | 3.0539E-02 | **8.3587E-01** | 2.5362E-02 | **8.6834E-01** | **2.4052E-02** |
| | MVO | 5.7392E-01 | 6.2422E-02 | 6.8681E-01 | 4.8467E-02 | 6.9313E-01 | 6.5647E-02 | 7.5062E-01 | 4.0615E-02 | 8.0998E-01 | 3.9112E-02 | 8.4607E-01 | 3.4916E-02 |
| | WOA | 5.7454E-01 | 5.7227E-02 | 6.3946E-01 | 1.0965E-01 | 6.8526E-01 | 7.8548E-02 | 7.4069E-01 | 4.6368E-02 | 8.2234E-01 | 3.1622E-02 | 8.6138E-01 | 2.6582E-02 |
| | SCA | 5.6718E-01 | 6.0427E-02 | 6.7306E-01 | 4.3817E-02 | 6.9763E-01 | 5.8839E-02 | 7.0448E-01 | 5.2258E-02 | 7.6810E-01 | 4.7123E-02 | 7.9542E-01 | 4.3575E-02 |
| | HHO | 5.1771E-01 | 9.3993E-02 | 6.0172E-01 | 1.1991E-01 | 6.7165E-01 | 8.4243E-02 | 7.5411E-01 | 5.3979E-02 | 8.0790E-01 | 4.6262E-02 | 8.3190E-01 | 4.2897E-02 |
| | BLPSO | 5.6912E-01 | 2.9673E-02 | 6.0720E-01 | 4.3537E-02 | 6.3760E-01 | **4.5183E-02** | 7.2178E-01 | **2.5890E-02** | 7.8672E-01 | **2.4181E-02** | 8.0733E-01 | 3.1098E-02 |
| | IGWO | **6.1509E-01** | 7.5537E-03 | 6.5384E-01 | **3.2974E-02** | 6.6251E-01 | 5.6846E-02 | 7.2733E-01 | 3.6385E-02 | 7.8627E-01 | 3.3627E-02 | 8.3268E-01 | 3.2064E-02 |
| | IWOA | 5.7825E-01 | 6.5620E-02 | 5.6181E-01 | 1.0094E-01 | 6.4968E-01 | 6.2974E-02 | 7.3465E-01 | 5.0672E-02 | 7.9236E-01 | 4.9903E-02 | 8.1729E-01 | 4.7200E-02 |
| | SCADE | 6.0083E-01 | 1.8975E-02 | 6.1730E-01 | 3.8908E-02 | 6.3386E-01 | 7.2585E-02 | 6.8099E-01 | 4.3879E-02 | 7.5210E-01 | 4.9963E-02 | 7.9580E-01 | 5.1332E-02 |

**Table A.6**
Fitness values generated during the segmentation process

| Image | Thresholds | CCMVO | MVO | WOA | SCA | HHO | BLPSO | IGWO | IWOA | SCADE |
|---|---|---|---|---|---|---|---|---|---|---|
| A | 2 | **2.5954E+01** | 2.5954E+01 | 2.5954E+01 | 2.5908E+01 | 2.5952E+01 | 2.5493E+01 | 2.5954E+01 | 2.5952E+01 | 2.5921E+01 |
| | 4 | 3.9362E+01 | **3.9369E+01** | 3.9205E+01 | 3.8029E+01 | 3.9159E+01 | 3.7363E+01 | 3.9289E+01 | 3.8957E+01 | 3.7961E+01 |
| | 6 | 5.0165E+01 | **5.0246E+01** | 4.9948E+01 | 4.7016E+01 | 4.9909E+01 | 4.7532E+01 | 4.9957E+01 | 4.9360E+01 | 4.8133E+01 |
| | 10 | **6.8130E+01** | 6.8031E+01 | 6.7400E+01 | 6.2416E+01 | 6.7071E+01 | 6.4826E+01 | 6.6176E+01 | 6.5557E+01 | 6.2806E+01 |
| | 15 | 8.5566E+01 | 8.4947E+01 | **8.5930E+01** | 7.6089E+01 | 8.4009E+01 | 8.1062E+01 | 8.3605E+01 | 8.2043E+01 | 7.6492E+01 |
| | 20 | 1.0053E+02 | 9.8346E+01 | **1.0135E+02** | 8.9437E+01 | 9.7415E+01 | 9.5711E+01 | 9.5683E+01 | 9.5439E+01 | 9.2791E+01 |
| B | 2 | **2.5564E+01** | 2.5564E+01 | 2.5564E+01 | 2.5554E+01 | 2.5460E+01 | 2.5417E+01 | 2.5564E+01 | 2.5545E+01 | 2.5548E+01 |
| | 4 | 3.8872E+01 | 3.8815E+01 | **3.8920E+01** | 3.8019E+01 | 3.8787E+01 | 3.8341E+01 | 3.8554E+01 | 3.8509E+01 | 3.7834E+01 |

(continued on next page)

**Table A.6** (*continued*)

| Image | Thresholds | CCMVO | MVO | WOA | SCA | HHO | BLPSO | IGWO | IWOA | SCADE |
|---|---|---|---|---|---|---|---|---|---|---|
| | 6 | **5.0077E+01** | 4.9590E+01 | 4.9459E+01 | 4.7742E+01 | 4.8948E+01 | 4.7753E+01 | 4.9314E+01 | 4.9693E+01 | 4.6455E+01 |
| | 10 | 6.7613E+01 | 6.7608E+01 | **6.8297E+01** | 6.2857E+01 | 6.6545E+01 | 6.4718E+01 | 6.6447E+01 | 6.7190E+01 | 6.3408E+01 |
| | 15 | 8.5208E+01 | 8.5069E+01 | **8.7288E+01** | 7.7741E+01 | 8.5958E+01 | 8.1386E+01 | 8.3136E+01 | 8.3405E+01 | 7.7277E+01 |
| | 20 | **1.0080E+02** | 9.8876E+01 | 1.0028E+02 | 9.0391E+01 | 9.9741E+01 | 9.3086E+01 | 9.4836E+01 | 9.5493E+01 | 9.3923E+01 |
| C | 2 | **2.5887E+01** | 2.5887E+01 | 2.5887E+01 | 2.5858E+01 | 2.5887E+01 | 2.4887E+01 | 2.5887E+01 | 2.5879E+01 | 2.5855E+01 |
| | 4 | **3.8521E+01** | 3.8521E+01 | 3.8506E+01 | 3.7748E+01 | 3.8287E+01 | 3.6583E+01 | 3.8484E+01 | 3.8430E+01 | 3.7786E+01 |
| | 6 | **4.9436E+01** | 4.9298E+01 | 4.9120E+01 | 4.7402E+01 | 4.8573E+01 | 4.6811E+01 | 4.9163E+01 | 4.8730E+01 | 4.7499E+01 |
| | 10 | 6.7583E+01 | **6.7825E+01** | 6.6785E+01 | 6.2859E+01 | 6.7330E+01 | 6.4057E+01 | 6.6308E+01 | 6.5094E+01 | 6.1938E+01 |
| | 15 | 8.5274E+01 | 8.4693E+01 | **8.6138E+01** | 7.8243E+01 | 8.4882E+01 | 8.1716E+01 | 8.2955E+01 | 8.2385E+01 | 7.8859E+01 |
| | 20 | 9.9852E+01 | 9.9416E+01 | **1.0076E+02** | 9.2595E+01 | 9.9937E+01 | 9.4663E+01 | 9.5311E+01 | 9.7695E+01 | 9.1824E+01 |
| D | 2 | **2.5612E+01** | 2.5612E+01 | 2.5358E+01 | 2.5346E+01 | 2.5572E+01 | 2.5170E+01 | 2.5602E+01 | 2.5509E+01 | 2.5419E+01 |
| | 4 | 3.8692E+01 | **3.8772E+01** | 3.8683E+01 | 3.7063E+01 | 3.7738E+01 | 3.7080E+01 | 3.8430E+01 | 3.7808E+01 | 3.6923E+01 |
| | 6 | **4.9434E+01** | 4.9172E+01 | 4.8394E+01 | 4.7478E+01 | 4.8058E+01 | 4.7424E+01 | 4.8414E+01 | 4.8313E+01 | 4.6104E+01 |
| | 10 | **6.7811E+01** | 6.7747E+01 | 6.6868E+01 | 6.1990E+01 | 6.6179E+01 | 6.4105E+01 | 6.5792E+01 | 6.6220E+01 | 6.0747E+01 |
| | 15 | 8.5660E+01 | 8.5649E+01 | **8.5680E+01** | 7.8756E+01 | 8.3991E+01 | 8.0351E+01 | 8.2870E+01 | 8.2360E+01 | 7.7338E+01 |
| | 20 | **1.0014E+02** | 9.9586E+01 | 1.0006E+02 | 8.9943E+01 | 9.7647E+01 | 9.5923E+01 | 9.8304E+01 | 9.7925E+01 | 8.9059E+01 |
| E | 2 | **2.6052E+01** | 2.6052E+01 | 2.6052E+01 | 2.6026E+01 | 2.6032E+01 | 2.5523E+01 | 2.6052E+01 | 2.6017E+01 | 2.6020E+01 |
| | 4 | **3.8834E+01** | 3.8761E+01 | 3.8026E+01 | 3.7868E+01 | 3.8372E+01 | 3.7316E+01 | 3.8605E+01 | 3.8094E+01 | 3.7601E+01 |
| | 6 | **4.9515E+01** | 4.9352E+01 | 4.8969E+01 | 4.5964E+01 | 4.8223E+01 | 4.7620E+01 | 4.9279E+01 | 4.8279E+01 | 4.6260E+01 |
| | 10 | **6.7470E+01** | 6.7275E+01 | 6.6718E+01 | 6.2548E+01 | 6.5825E+01 | 6.4202E+01 | 6.5607E+01 | 6.5498E+01 | 6.0432E+01 |
| | 15 | **8.5151E+01** | 8.4794E+01 | 8.4720E+01 | 7.7386E+01 | 8.4416E+01 | 8.0527E+01 | 8.2470E+01 | 8.2439E+01 | 7.6445E+01 |
| | 20 | **1.0006E+02** | 1.0005E+02 | 9.9882E+01 | 8.6104E+01 | 9.6654E+01 | 9.3197E+01 | 9.3257E+01 | 9.6247E+01 | 8.6733E+01 |
| F | 2 | **2.5807E+01** | 2.5807E+01 | 2.5807E+01 | 2.5783E+01 | 2.5807E+01 | 2.5231E+01 | 2.5807E+01 | 2.5790E+01 | 2.5759E+01 |
| | 4 | 3.8617E+01 | **3.8617E+01** | 3.8488E+01 | 3.7661E+01 | 3.8163E+01 | 3.6742E+01 | 3.8538E+01 | 3.8189E+01 | 3.7052E+01 |
| | 6 | **4.9598E+01** | 4.9509E+01 | 4.9154E+01 | 4.6726E+01 | 4.8868E+01 | 4.6969E+01 | 4.8715E+01 | 4.8323E+01 | 4.5883E+01 |
| | 10 | 6.7143E+01 | **6.7550E+01** | 6.6372E+01 | 6.1144E+01 | 6.6162E+01 | 6.3340E+01 | 6.6074E+01 | 6.5146E+01 | 6.1687E+01 |
| | 15 | **8.6094E+01** | 8.5260E+01 | 8.5518E+01 | 7.4832E+01 | 8.3521E+01 | 7.8585E+01 | 8.1770E+01 | 8.2074E+01 | 7.5258E+01 |
| | 20 | 1.0043E+02 | 1.0022E+02 | **1.0105E+02** | 9.0254E+01 | 9.8287E+01 | 9.2722E+01 | 9.6013E+01 | 9.8205E+01 | 8.8005E+01 |
| G | 2 | **2.5592E+01** | 2.5592E+01 | 2.5589E+01 | 2.5556E+01 | 2.5589E+01 | 2.4787E+01 | 2.5592E+01 | 2.5587E+01 | 2.5564E+01 |
| | 4 | **3.8714E+01** | 3.8710E+01 | 3.8695E+01 | 3.7731E+01 | 3.8187E+01 | 3.7080E+01 | 3.8666E+01 | 3.8408E+01 | 3.7563E+01 |
| | 6 | **4.9774E+01** | 4.9750E+01 | 4.9513E+01 | 4.6799E+01 | 4.8998E+01 | 4.7191E+01 | 4.9168E+01 | 4.8377E+01 | 4.7252E+01 |
| | 10 | **6.7898E+01** | 6.7775E+01 | 6.7637E+01 | 6.1460E+01 | 6.6429E+01 | 6.4835E+01 | 6.5986E+01 | 6.5598E+01 | 6.1305E+01 |
| | 15 | 8.5459E+01 | 8.5662E+01 | 8.5220E+01 | 7.7388E+01 | **8.5761E+01** | 8.0344E+01 | 8.1731E+01 | 8.3531E+01 | 7.8673E+01 |
| | 20 | **9.9712E+01** | 9.8812E+01 | 9.9232E+01 | 8.9979E+01 | 9.9310E+01 | 9.2345E+01 | 9.5927E+01 | 9.7072E+01 | 8.9264E+01 |
| H | 2 | **2.5736E+01** | 2.5736E+01 | 2.5730E+01 | 2.5707E+01 | 2.5727E+01 | 2.5360E+01 | 2.5736E+01 | 2.5736E+01 | 2.5705E+01 |
| | 4 | **3.8664E+01** | 3.8624E+01 | 3.8553E+01 | 3.7647E+01 | 3.8491E+01 | 3.7098E+01 | 3.8541E+01 | 3.8457E+01 | 3.7399E+01 |
| | 6 | 4.9488E+01 | **4.9577E+01** | 4.9286E+01 | 4.6595E+01 | 4.8538E+01 | 4.7218E+01 | 4.9124E+01 | 4.8209E+01 | 4.7211E+01 |
| | 10 | **6.7625E+01** | 6.7448E+01 | 6.7329E+01 | 6.2073E+01 | 6.6305E+01 | 6.3752E+01 | 6.5965E+01 | 6.4884E+01 | 6.1571E+01 |
| | 15 | 8.4701E+01 | **8.5667E+01** | 8.5538E+01 | 7.8022E+01 | 8.3700E+01 | 8.1040E+01 | 8.2052E+01 | 8.1979E+01 | 7.8140E+01 |
| | 20 | 1.0038E+02 | 9.8728E+01 | **1.0057E+02** | 8.8008E+01 | 9.8083E+01 | 9.4795E+01 | 9.4014E+01 | 9.6799E+01 | 8.8641E+01 |
| I | 2 | **2.5611E+01** | 2.5611E+01 | 2.5611E+01 | 2.5575E+01 | 2.5611E+01 | 2.5068E+01 | 2.5611E+01 | 2.5602E+01 | 2.5599E+01 |
| | 4 | 3.8316E+01 | **3.8323E+01** | 3.8189E+01 | 3.7609E+01 | 3.8271E+01 | 3.6605E+01 | 3.8313E+01 | 3.7820E+01 | 3.7670E+01 |
| | 6 | **4.9439E+01** | 4.9341E+01 | 4.9001E+01 | 4.6216E+01 | 4.8329E+01 | 4.6265E+01 | 4.9192E+01 | 4.8376E+01 | 4.6562E+01 |
| | 10 | **6.7518E+01** | 6.7236E+01 | 6.7480E+01 | 6.2550E+01 | 6.6133E+01 | 6.2071E+01 | 6.5880E+01 | 6.4875E+01 | 5.9994E+01 |
| | 15 | 8.4117E+01 | 8.5200E+01 | **8.6546E+01** | 7.7016E+01 | 8.2932E+01 | 7.8163E+01 | 8.2014E+01 | 8.2179E+01 | 7.6101E+01 |
| | 20 | 9.9331E+01 | 9.9174E+01 | **9.9817E+01** | 8.8442E+01 | 9.6200E+01 | 8.9562E+01 | 9.4781E+01 | 9.4942E+01 | 8.6612E+01 |
| J | 2 | **2.5844E+01** | 2.5844E+01 | 2.5844E+01 | 2.5813E+01 | 2.5844E+01 | 2.4856E+01 | 2.5844E+01 | 2.5832E+01 | 2.5820E+01 |
| | 4 | 3.8749E+01 | **3.8787E+01** | 3.8696E+01 | 3.7801E+01 | 3.7984E+01 | 3.7480E+01 | 3.8632E+01 | 3.8244E+01 | 3.7821E+01 |
| | 6 | 4.9456E+01 | **4.9609E+01** | 4.9304E+01 | 4.7556E+01 | 4.9156E+01 | 4.7382E+01 | 4.8954E+01 | 4.7989E+01 | 4.6299E+01 |
| | 10 | **6.8042E+01** | 6.7696E+01 | 6.7536E+01 | 6.1768E+01 | 6.6599E+01 | 6.4099E+01 | 6.5673E+01 | 6.6515E+01 | 6.2010E+01 |
| | 15 | **8.6413E+01** | 8.5103E+01 | 8.5217E+01 | 7.6779E+01 | 8.3811E+01 | 8.0759E+01 | 8.1800E+01 | 8.2842E+01 | 7.7473E+01 |
| | 20 | 9.9799E+01 | 9.9872E+01 | **1.0022E+02** | 8.9684E+01 | 9.7728E+01 | 9.3363E+01 | 9.5132E+01 | 9.5317E+01 | 8.7495E+01 |

## Appendix B

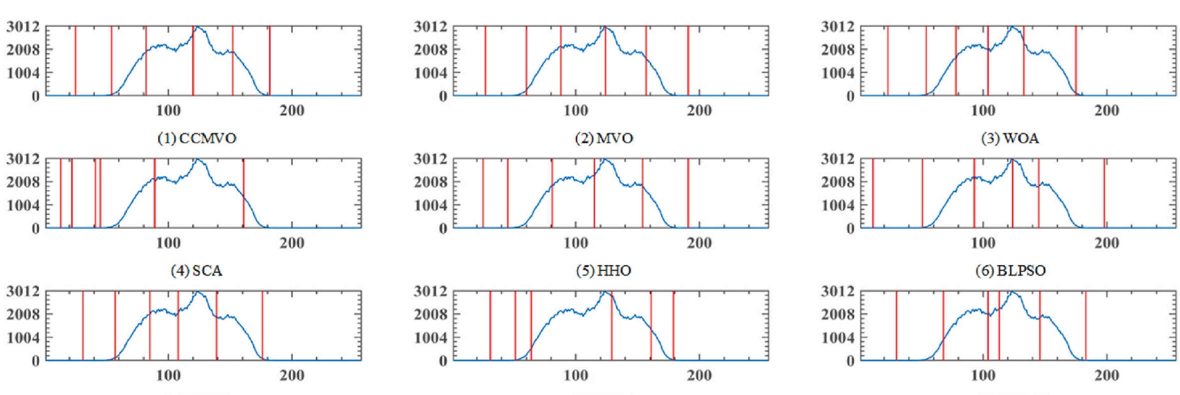


**Fig. B.1.** The segmentation result of image A at threshold level 6.

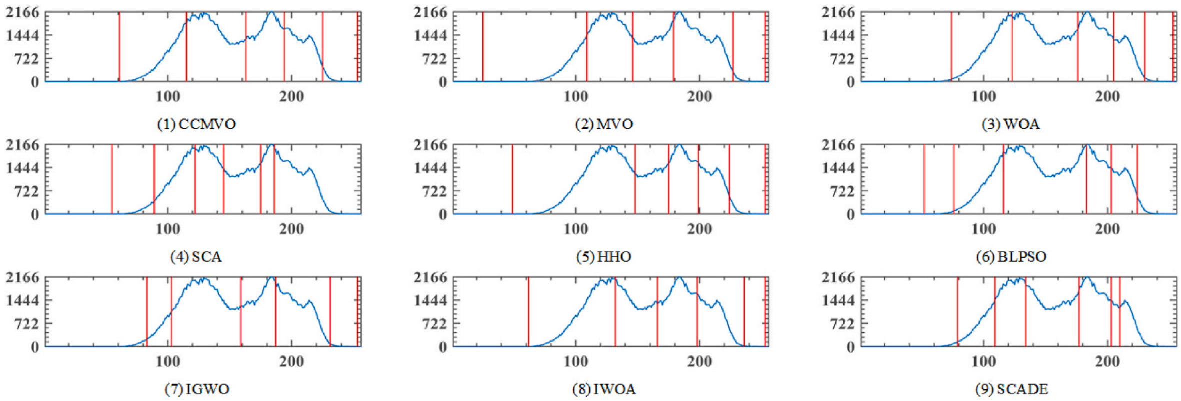


**Fig. B.2.** The segmentation result of image B at threshold level 6.

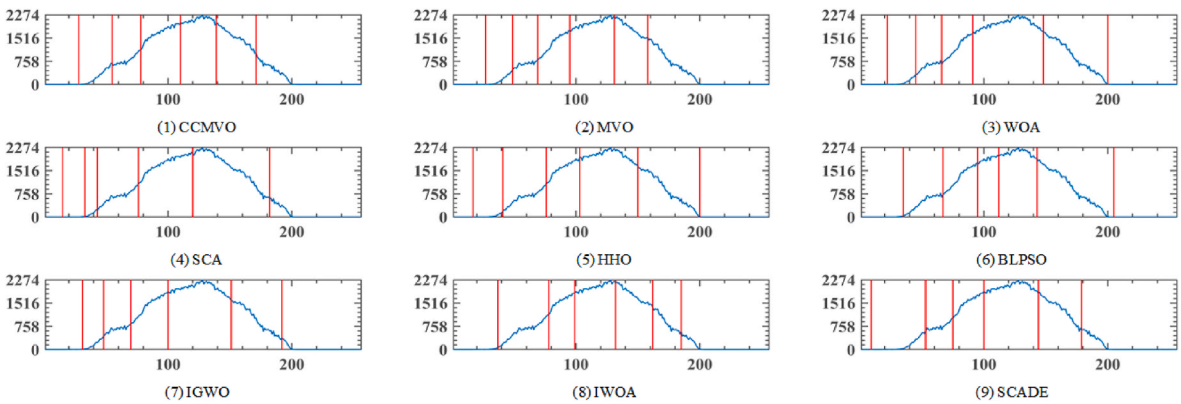


**Fig. B.3.** The segmentation result of image C at threshold level 6.

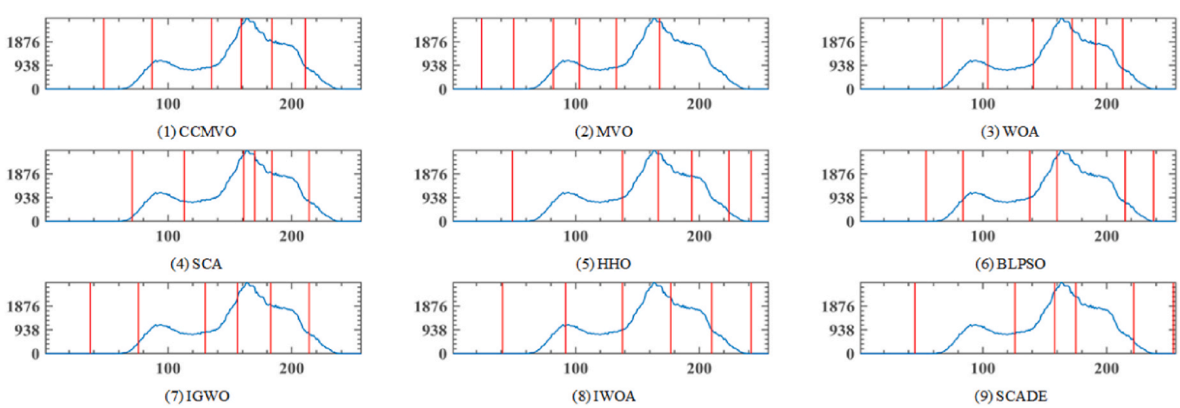


**Fig. B.4.** The segmentation result of image D at threshold level 6.

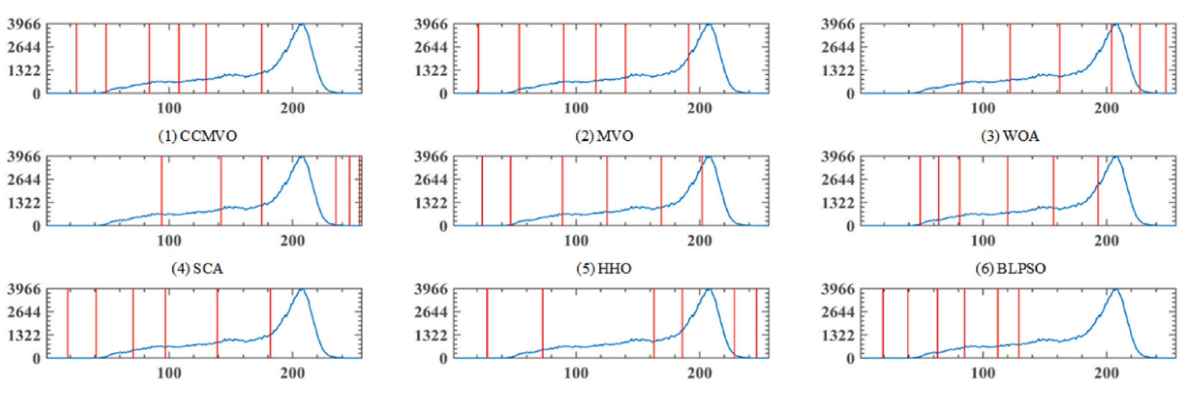


**Fig. B.5.** The segmentation result of image E at threshold level 6.

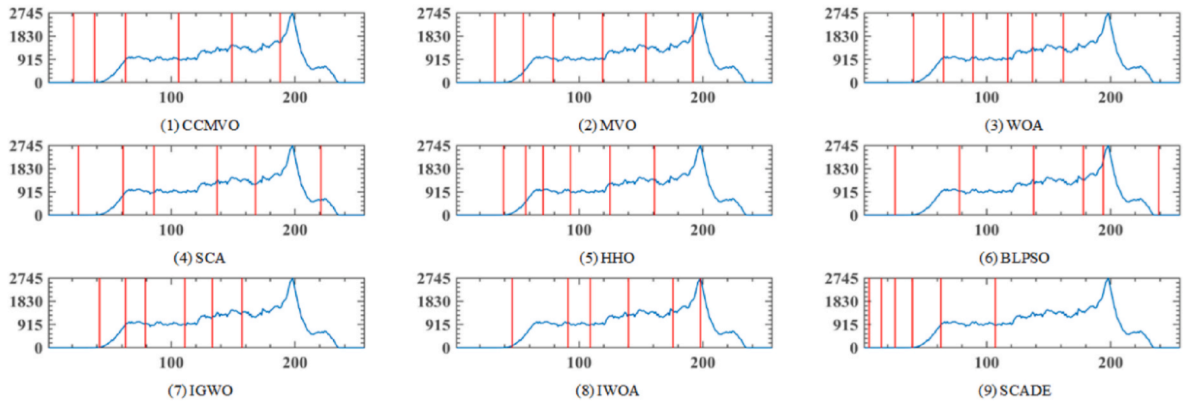


**Fig. B.6.** Segmentation result of image F at threshold level 6.

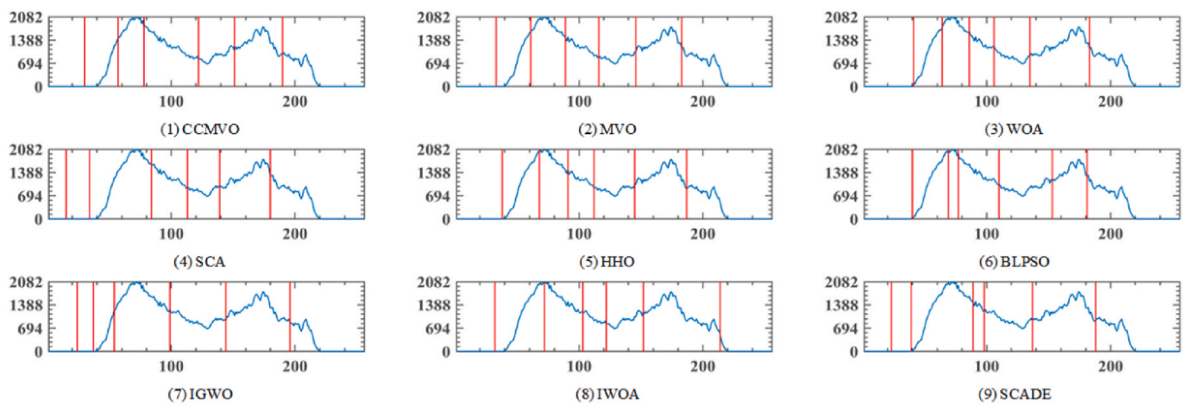


**Fig. B.7.** The segmentation result of image G at threshold level 6.

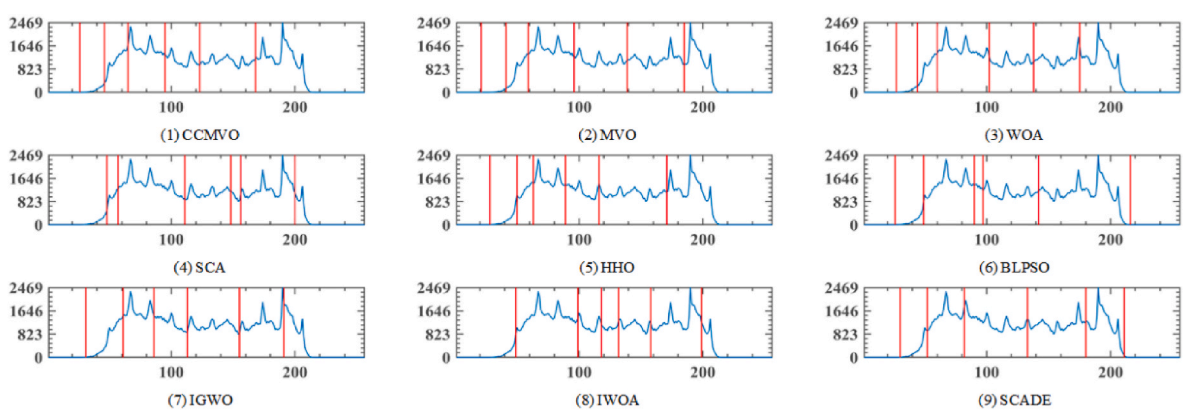


**Fig. B.8.** The segmentation result of image H at threshold level 6.

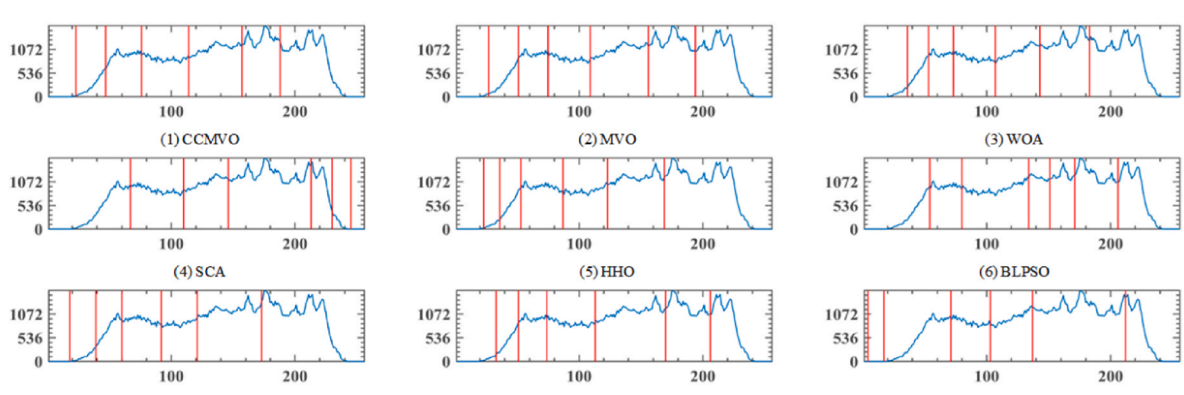


**Fig. B.9.** The segmentation result of image I at threshold level 6.

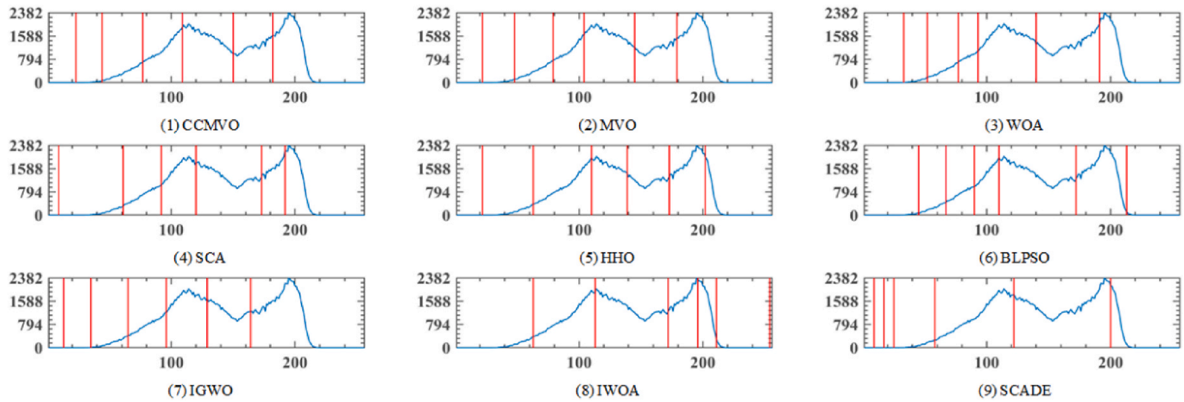


**Fig. B.10.** The segmentation result of image J at threshold level 6.

## References

[1] R. Murugan, T. Goel, E-DiCoNet: Extreme learning machine based classifier for diagnosis of COVID-19 using deep convolutional network, J. Ambient Intell. Hum. Comput. 12 (2021) 8887–8898.
[2] T. Alafif, A.M. Tehame, S. Bajaba, A. Barnawi, S. Zia, Machine and deep learning towards COVID-19 diagnosis and treatment: survey, challenges, and future directions, Int. J. Environ. Res. Publ. Health 18 (2021).
[3] I. Ozsahin, B. Sekeroglu, M.S. Musa, M.T. Mustapha, D.U. Ozsahin, Review on diagnosis of COVID-19 from chest CT images using artificial intelligence, Comput. Math. Methods Med. (2020), https://doi.org/10.1155/2020/9756518, 2020.
[4] C. Hani, N.H. Trieu, I. Saab, S. Dangeard, S. Bennani, G. Chassagnon, M.P. Revel, COVID-19 pneumonia: a review of typical CT findings and differential diagnosis, Diagn. Interventional Imag. 101 (2020) 263–268.
[5] N.S. Gezer, B. Ergan, M.M. Baris, O. Appak, A.A. Sayiner, P. Balci, Z. Kuruuzum, S.A. Cavus, O. Kilinc, COVID-19 S: A new proposal for diagnosis and structured reporting of COVID-19 on computed tomography imaging, Diagn. Interventional Radiol. 26 (2020) 315–322.
[6] E.R.G.R. Aguiar, J. Navas, L.G.C. Pacheco, The COVID-19 diagnostic technology landscape: efficient data sharing drives diagnostic development, Front. Public Health 8 (2020).
[7] Q. Guan, Y. Chen, Z. Wei, A.A. Heidari, H. Hu, X.-H. Yang, J. Zheng, Q. Zhou, H. Chen, F. Chen, Medical image augmentation for lesion detection using a texture-constrained multichannel progressive GAN, Comput. Biol. Med. 145 (2022), 105444.
[8] Y. Chen, X.-H. Yang, Z. Wei, A.A. Heidari, N. Zheng, Z. Li, H. Chen, H. Hu, Q. Zhou, Q. Guan, Generative adversarial networks in medical image augmentation: a review, Comput. Biol. Med. 144 (2022), 105382.
[9] W. Zhou, Q. Guo, J. Lei, L. Yu, J.-N. Hwang, IRFR-Net: interactive recursive feature-reshaping network for detecting salient objects in RGB-D images, IEEE Transact. Neural Networks Learn. Syst. (2021), https://doi.org/10.1109/tnnls.2021.3105484.
[10] D. Zhao, L. Liu, F. Yu, A.A. Heidari, M. Wang, G. Liang, K. Muhammad, H. Chen, Chaotic random spare ant colony optimization for multi-threshold image segmentation of 2D Kapur entropy, Knowl. Base Syst. 216 (2021), 106510.
[11] S. Zhao, P. Wang, A.A. Heidari, H. Chen, W. He, S. Xu, Performance optimization of salp swarm algorithm for multi-threshold image segmentation: comprehensive study of breast cancer microscopy, Comput. Biol. Med. 139 (2021), 105015.
[12] H. Yu, J. Song, C. Chen, A.A. Heidari, J. Liu, H. Chen, A. Zaguia, M. Mafarja, Image segmentation of Leaf Spot Diseases on Maize using multi-stage Cauchy-enabled grey wolf algorithm, Eng. Appl. Artif. Intell. 109 (2022), 104653.
[13] M. Abd Elaziz, D. Oliva, A.A. Ewees, S.W. Xiong, Multi-level thresholding-based grey scale image segmentation using multi-objective multi-verse optimizer, Expert Syst. Appl. 125 (2019) 112–129.
[14] M. Yu, M. Han, X. Li, X. Wei, H. Jiang, H. Chen, R. Yu, Adaptive soft erasure with edge self-attention for weakly supervised semantic segmentation: thyroid ultrasound image case study, Comput. Biol. Med. 144 (2022), 105347.
[15] L. Huang, B.X. Yao, P.D. Chen, A.P. Ren, Y. Xia, Superpixel segmentation method of high resolution remote sensing images based on hierarchical clustering, J. Infrared Millim. Waves 39 (2020) 263–272.
[16] J.Q. Gao, B.B. Wang, Z.Y. Wang, Y.F. Wang, F.Z. Kong, A wavelet transform-based image segmentation method, Optik (2020) 208.
[17] X.F. Yue, H.B. Zhang, A multi-level image thresholding approach using Otsu based on the improved invasive weed optimization algorithm, Signal Image Video Process. 14 (2020) 575–582.
[18] B. Wu, J.X. Zhou, X.Y. Ji, Y.J. Yin, X. Shen, An ameliorated teaching-learning-based optimization algorithm based study of image segmentation for multilevel thresholding using Kapur's entropy and Otsu's between class variance, Inf. Sci. 533 (2020) 72–107.
[19] M. Sun, H. Wei, An improved cuckoo search algorithm for multi-level gray-scale image thresholding, Multimed. Tool. Appl. 79 (2020) 34993–35016.
[20] A.A. Ewees, M. Abd Elaziz, M.A.A. Al-Qaness, H.A. Khalil, S. Kim, Improved artificial bee colony using sine-cosine algorithm for multi-level thresholding image segmentation, IEEE Access 8 (2020) 26304–26315.
[21] H.S.N. Alwerfali, M.A.A. Al-qaness, M. Abd Elaziz, A.A. Ewees, D. Oliva, S.F. Lu, Multi-level image thresholding based on modified spherical search optimizer and fuzzy entropy, Entropy 22 (2020).
[22] X.F. Yue, H.B. Zhang, Improved hybrid bat algorithm with invasive weed and its application in image segmentation, Arabian J. Sci. Eng. 44 (2019) 9221–9234.
[23] O. Tarkhaneh, H.F. Shen, An adaptive differential evolution algorithm to optimal multi-level thresholding for MRI brain image segmentation, Expert Syst. Appl. (2019) 138.
[24] A.M. Hemeida, R. Mansour, M.E. Hussein, Multilevel thresholding for image segmentation using an improved electromagnetism optimization algorithm, Int. J. Interact. Multimed. Artif. Intell. 5 (2019) 102–112.
[25] K.G. Dhal, S. Ray, A. Das, J. Gálvez, S. Das, Fuzzy multi-level color satellite image segmentation using nature-inspired optimizers: a comparative study, J. Indian Soc. Remote Sens. 47 (2019) 1391–1415.
[26] S. Borjigin, P.K. Sahoo, Color image segmentation based on multi-level Tsallis-Havrda-Charvat entropy and 2D histogram using PSO algorithms, Pattern Recogn. 92 (2019) 107–118.
[27] H.S.N. Alwerfali, M. Abd Elaziz, M.A.A. Al-Qaness, A.A. Abbasi, S.F. Lu, F. Liu, L. Li, A multilevel image thresholding based on hybrid salp swarm algorithm and fuzzy entropy, IEEE Access 7 (2019) 181405–181422.
[28] L. Shen, C.Y. Fan, X.T. Huang, Multi-level image thresholding using modified flower pollination algorithm, IEEE Access 6 (2018) 30508–30519.
[29] S.C. Satapathy, N.S.M. Raja, V. Rajinikanth, A.S. Ashour, N. Dey, Multi-level image thresholding using Otsu and chaotic bat algorithm, Neural Comput. Appl. 29 (2018) 1285–1307.
[30] H. Mittal, M. Saraswat, An optimum multi-level image thresholding segmentation using non-local means 2D histogram and exponential Kbest gravitational search algorithm, Eng. Appl. Artif. Intell. 71 (2018) 226–235.
[31] H. Gao, Z. Fu, C.M. Pun, H.D. Hu, R.S. Lan, A multi-level thresholding image segmentation based on an improved artificial bee colony algorithm, Comput. Electr. Eng. 70 (2018) 931–938.
[32] S.-H. Wu, Z.-H. Zhan, J. Zhang, SAFE: scale-adaptive fitness evaluation method for expensive optimization problems, IEEE Trans. Evol. Comput. 25 (2021) 478–491.
[33] J.-Y. Li, Z.-H. Zhan, C. Wang, H. Jin, J. Zhang, Boosting data-driven evolutionary algorithm with localized data generation, IEEE Trans. Evol. Comput. 24 (2020) 923–937.
[34] J. Xia, Z. Wang, D. Yang, R. Li, G. Liang, H. Chen, A.A. Heidari, H. Turabieh, M. Mafarja, Z. Pan, Performance optimization of support vector machine with oppositional grasshopper optimization for acute appendicitis diagnosis, Comput. Biol. Med. (2022), 105206.
[35] J. Xia, D. Yang, H. Zhou, Y. Chen, H. Zhang, T. Liu, A.A. Heidari, H. Chen, Z. Pan, Evolving kernel extreme learning machine for medical diagnosis via a disperse foraging sine cosine algorithm, Comput. Biol. Med. 141 (2022), 105137.
[36] J. Hu, z. Han, A.A. Heidari, Y. Shou, H. Ye, L. Wang, X. Huang, H. Chen, Y. Chen, P. Wu, Detection of COVID-19 severity using blood gas analysis parameters and Harris hawks optimized extreme learning machine, Comput. Biol. Med. 142 (2022), 105166.
[37] J. Hu, Y. Liu, A.A. Heidari, Y. Bano, A. Ibrohimov, G. Liang, H. Chen, X. Chen, A. Zaguia, H. Turabieh, An effective model for predicting serum albumin level in hemodialysis patients, Comput. Biol. Med. 140 (2022), 105054.
[38] G.-Q. Zeng, K.-D. Lu, Y.-X. Dai, Z.-J. Zhang, M.-R. Chen, C.-W. Zheng, D. Wu, W.-W.J.N. Peng, Binary-coded extremal optimization for the design of PID controllers, Neurocomputing 138 (2014) 180–188.

[39] G.-Q. Zeng, J. Chen, Y.-X. Dai, L.-M. Li, C.-W. Zheng, M.-R.J.N. Chen, Design of fractional order PID controller for automatic regulator voltage system based on multi-objective extremal optimization, Neurocomputing 160 (2015) 173–184.

[40] G.-Q. Zeng, X.-Q. Xie, M.-R. Chen, J. Weng, Adaptive population extremal optimization-based PID neural network for multivariable nonlinear control systems, Swarm Evol. Comput. 44 (2019) 320–334.

[41] H. Yu, X. Cheng, C. Chen, A.A. Heidari, J. Liu, Z. Cai, H. Chen, Apple Leaf Disease Recognition Method with Improved Residual Network, Multimedia Tools and Applications, 2022.

[42] J. Hu, H. Chen, A.A. Heidari, M. Wang, X. Zhang, Y. Chen, Z. Pan, Orthogonal learning covariance matrix for defects of grey wolf optimizer: insights, balance, diversity, and feature selection, Knowl. Base Syst. 213 (2021), 106684.

[43] J. Hu, W. Gui, A.A. Heidari, Z. Cai, G. Liang, H. Chen, Z. Pan, Dispersed foraging slime mould algorithm: continuous and binary variants for global optimization and wrapper-based feature selection, Knowl. Base Syst. 237 (2022), 107761.

[44] J. Too, G. Liang, H. Chen, Memory-based Harris Hawk Optimization with Learning Agents: a Feature Selection Approach, Engineering with Computers, 2021.

[45] J. Chen, L. Du, Y. Guo, Label constrained convolutional factor analysis for classification with limited training samples, Inf. Sci. 544 (2021) 372–394.

[46] K. Hu, J. Ye, E. Fan, S. Shen, L. Huang, J. Pi, A novel object tracking algorithm by fusing color and depth information based on single valued neutrosophic cross-entropy, J. Intell. Fuzzy Syst. 32 (2017) 1775–1786.

[47] K. Hu, W. He, J. Ye, L. Zhao, H. Peng, J. Pi, Online visual tracking of weighted multiple instance learning via neutrosophic similarity-based objectness estimation, Symmetry 11 (2019) 832.

[48] R. Dong, H. Chen, A.A. Heidari, H. Turabieh, M. Mafarja, S. Wang, Boosted kernel search: framework, analysis and case studies on the economic emission dispatch problem, Knowl. Base Syst. 233 (2021), 107529.

[49] H. Zhang, T. Liu, X. Ye, A.A. Heidari, G. Liang, H. Chen, Z. Pan, Differential Evolution-Assisted Salp Swarm Algorithm with Chaotic Structure for Real-World Problems, Eng. Comput., 2022.

[50] W. Shan, Z. Qiao, A.A. Heidari, H. Chen, H. Turabieh, Y. Teng, Double adaptive weights for stabilization of moth flame optimizer: balance analysis, engineering cases, and medical diagnosis, Knowl. Base Syst. 214 (2021), 106728.

[51] J. Tu, H. Chen, J. Liu, A.A. Heidari, X. Zhang, M. Wang, R. Ruby, Q.-V. Pham, Evolutionary biogeography-based whale optimization methods with communication structure: towards measuring the balance, Knowl. Base Syst. 212 (2021), 106642.

[52] B. Shi, H. Ye, L. Zheng, J. Lyu, C. Chen, A.A. Heidari, Z. Hu, H. Chen, P. Wu, Evolutionary warning system for COVID-19 severity: colony predation algorithm enhanced extreme learning machine, Comput. Biol. Med. 136 (2021), 104698.

[53] S. Wu, P. Mao, R. Li, Z. Cai, A.A. Heidari, J. Xia, H. Chen, M. Mafarja, H. Turabieh, X. Chen, Evolving fuzzy k-nearest neighbors using an enhanced sine cosine algorithm: case study of lupus nephritis, Comput. Biol. Med. 135 (2021), 104582.

[54] Y. Sun, B. Xue, M. Zhang, G.G. Yen, Evolving deep convolutional neural networks for image classification, IEEE Trans. Evol. Comput. 24 (2019) 394–407.

[55] K. Qiao, J. Liang, K. Yu, M. Yuan, B. Qu, C. Yue, Self-adaptive resources allocation-based differential evolution for constrained evolutionary optimization, Knowl. Base Syst. 235 (2022), 107653.

[56] J. Liang, X. Ban, K. Yu, B. Qu, K. Qiao, Differential evolution with rankings-based fitness function for constrained optimization problems, Appl. Soft Comput. 113 (2021), 108016.

[57] F. Zhao, S. Di, J. Cao, J. Tang, A novel cooperative multi-stage hyper-heuristic for combination optimization problems, Complex Syst. Model. Simul. 1 (2021) 91–108.

[58] X. Lai, Y. Zhou, Analysis of multiobjective evolutionary algorithms on the biobjective traveling salesman problem (1, 2, Multimed. Tool. Appl. 79 (2020) 30839–30860.

[59] Y. Hua, Q. Liu, K. Hao, Y. Jin, A survey of evolutionary algorithms for multi-objective optimization problems with irregular pareto fronts, IEEE/CAA J. Autom. Sin. 8 (2021) 303–318.

[60] X.-F. Liu, Z.-H. Zhan, Y. Gao, J. Zhang, S. Kwong, J. Zhang, Coevolutionary particle swarm optimization with bottleneck objective learning strategy for many-objective optimization, IEEE Trans. Evol. Comput. 23 (2018) 587–602.

[61] W. Deng, X. Zhang, Y. Zhou, Y. Liu, X. Zhou, H. Chen, H. Zhao, An enhanced fast non-dominated solution sorting genetic algorithm for multi-objective problems, Inf. Sci. 585 (2022) 441–453.

[62] X. Han, Y. Han, Q. Chen, J. Li, H. Sang, Y. Liu, Q. Pan, Y. Nojima, Distributed flow shop scheduling with sequence-dependent setup times using an improved iterated greedy algorithm, Complex Syst. Model. Simul. 1 (2021) 198–217.

[63] D. Gao, G.-G. Wang, W. Pedrycz, Solving fuzzy job-shop scheduling problem using DE algorithm improved by a selection mechanism, IEEE Trans. Fuzzy Syst. 28 (2020) 3265–3275.

[64] G.-G. Wang, D. Gao, W. Pedrycz, Solving multi-objective fuzzy job-shop scheduling problem by a hybrid adaptive differential evolution algorithm, IEEE Trans. Ind. Inf. (2022), https://doi.org/10.1109/tii.2022.3165636.

[65] R. Storn, K. Price, Differential evolution – a simple and efficient heuristic for global Optimization over Continuous Spaces, 11, 1997, pp. 341–359.

[66] G.-G. Wang, Moth search algorithm: a bio-inspired metaheuristic algorithm for global optimization problems, Memetic Comput. 10 (2018) 151–164.

[67] Y. Feng, S. Deb, G.-G. Wang, A.H. Alavi, Monarch butterfly optimization: a comprehensive review, Expert Syst. Appl. 168 (2021), 114418.

[68] A.A. Heidari, S. Mirjalili, H. Faris, I. Aljarah, M. Mafarja, H. Chen, Harris hawks optimization: algorithm and applications, Future Gen. Comput. Syst. Int. J. Esci. 97 (2019) 849–872.

[69] S. Li, H. Chen, M. Wang, A.A. Heidari, S. Mirjalili, Slime mould algorithm: a new method for stochastic optimization, Future Generat. Comput. Syst. 111 (2020) 300–323.

[70] S. Mirjalili, A. Lewis, The whale optimization algorithm, Adv. Eng. Software 95 (2016) 51–67.

[71] Y. Yang, H. Chen, A. Asghar Heidari, A.H. Gandomi, Hunger games search: visions, conception, implementation, deep analysis, perspectives, and towards performance shifts, Expert Syst. Appl. (2021), 114864, https://doi.org/10.1016/j.eswa.2021.114864.

[72] S. Mirjalili, Moth-flame optimization algorithm: a novel nature-inspired heuristic paradigm, Knowl. Base Syst. 89 (2015) 228–249.

[73] J. Kennedy, R. Eberhart, Particle swarm optimization, in: Proceedings of ICNN'95 - International Conference on Neural Networks, vol. 1944, 1995, pp. 1942–1948.

[74] A.A. Heidari, S. Mirjalili, H. Faris, I. Aljarah, M. Mafarja, H. Chen, Harris hawks optimization: algorithm and applications, Future Generat. Comput. Syst. 97 (2019) 849–872.

[75] S. Mirjalili, SCA: a Sine Cosine Algorithm for solving optimization problems, Knowl. Base Syst. 96 (2016) 120–133.

[76] B.R. Adarsh, T. Raghunathan, T. Jayabarathi, X.-S. Yang, Economic dispatch using chaotic bat algorithm, Energy 96 (2016) 666–675.

[77] J.J. Liang, A.K. Qin, P.N. Suganthan, S. Baskar, Comprehensive learning particle swarm optimizer for global optimization of multimodal functions, IEEE Trans. Evol. Comput. 10 (2006) 281–295.

[78] H. Nenavath, R.K. Jatoth, Hybridizing sine cosine algorithm with differential evolution for global optimization and object tracking, Appl. Soft Comput. 62 (2018) 1019–1043.

[79] M. Tubishat, M.A.M. Abushariah, N. Idris, I. Aljarah, Improved whale optimization algorithm for feature selection in Arabic sentiment analysis, Appl. Intell. 49 (2019) 1688–1707.

[80] M.A. Elhosseini, A.Y. Haikal, M. Badawy, N. Khashan, Biped robot stability based on an A–C parametric Whale Optimization Algorithm, J. Comput. Sci. 31 (2019) 17–32.

[81] X. Chen, H. Tianfield, C. Mei, W. Du, G. Liu, Biogeography-based learning particle swarm optimization, Soft Comput. 21 (2017) 7519–7541.

[82] Z. Cai, J. Gu, J. Luo, Q. Zhang, H. Chen, Z. Pan, Y. Li, C. Li, Evolving an optimal kernel extreme learning machine by using an enhanced grey wolf optimization strategy, Expert Syst. Appl. 138 (2019), 112814.

[83] S. Mirjalili, S.M. Mirjalili, A. Hatamlou, Multi-Verse Optimizer: a nature-inspired algorithm for global optimization, Neural Comput. Appl. 27 (2016) 495–513.

[84] S.E. Shukri, R. Al-Sayyed, A. Hudaib, S. Mirjalili, Enhanced multi-verse optimizer for task scheduling in cloud computing environments, Expert Syst. Appl. (2021) 168.

[85] H. Rezk, M.A. Mohamed, A.A.Z. Diab, N. Kanagaraj, Load frequency control of multi-interconnected renewable energy plants using multi-verse optimizer, Comput. Syst. Sci. Eng. 37 (2021) 219–231.

[86] B. Mohammadi, F. Ahmadi, S. Mehdizadeh, Y.Q. Guan, Q.B. Pham, N.T.T. Linh, D. Q. Tri, Developing novel robust models to improve the accuracy of daily streamflow modeling, Water Resour. Manag. 34 (2020) 3387–3409.

[87] H.H. Ali, A.M. Kassem, M. Al-Dhaifallah, A. Fathy, Multi-Verse optimizer for model predictive load frequency control of hybrid multi-interconnected plants comprising renewable energy, IEEE Access 8 (2020) 114623–114642.

[88] M. Abdel-Basset, L.A. Shawky, K. Eldrandaly, Grid quorum-based spatial coverage for IoT smart agriculture monitoring using enhanced multi-verse optimizer, Neural Comput. Appl. 32 (2020) 607–624.

[89] A.K. Abasi, A.T. Khader, M.A. Al-Betar, S. Naim, S.N. Makhadmeh, Z.A. A. Alyasseri, Link-based multi-verse optimizer for text documents clustering, Appl. Soft Comput. 87 (2020).

[90] W.H. Lai, M.R. Zhou, F. Hu, K. Bian, Q. Song, A new DBSCAN parameters determination method based on improved MVO, IEEE Access 7 (2019) 104085–104095.

[91] P. Kandhway, A.K. Bhandari, Spatial context cross entropy function based multilevel image segmentation using multi-verse optimizer, Multimed. Tool. Appl. 78 (2019) 22613–22641.

[92] K.F. Geng, C.M. Ye, L. Cao, L. Liu, Multi-objective reentrant hybrid flowshop scheduling with machines turning on and off control strategy using improved multi-verse optimizer algorithm, Math. Probl Eng. (2019) 2019.

[93] A.A. Ewees, M. Abd El Aziz, A.E. Hassanien, Chaotic multi-verse optimizer-based feature selection, Neural Comput. Appl. 31 (2019) 991–1006.

[94] M.A.A. Al-qaness, M. Abd Elaziz, A.A. Ewees, X.H. Cui, A modified adaptive neuro-fuzzy inference system using multi-verse optimizer algorithm for oil consumption forecasting, Electronics 8 (2019).

[95] H.R. Zhao, X.Y. Han, S. Guo, DGM (1,1) model optimized by MVO (multi-verse optimizer) for annual peak load forecasting, Neural Comput. Appl. 30 (2018) 1811–1825.

[96] X.Y. Wang, D.K. Luo, X. Zhao, Z. Sun, Estimates of energy consumption in China using a self-adaptive multi-verse optimizer-based support vector machine with rolling cross-validation, Energy 152 (2018) 539–548.

[97] A. Fathy, H. Rezk, Multi-verse optimizer for identifying the optimal parameters of PEMFC model, Energy 143 (2018) 634–644.

[98] H. Faris, M.A. Hassonah, A.M. Al-Zoubi, S. Mirjalili, I. Aljarah, A multi-verse optimizer approach for feature selection and optimizing SVM parameters based on a robust system architecture, Neural Comput. Appl. 30 (2018) 2355–2369.

[99] T. Peng, J.Z. Zhou, C. Zhang, W.L. Fu, Streamflow forecasting using empirical wavelet transform and artificial neural networks, Water (2017) 9.
[100] P. Jangir, S.A. Parmar, I.N. Trivedi, R.H. Bhesdadiya, A novel hybrid Particle Swarm Optimizer with multi verse optimizer for global numerical optimization and Optimal Reactive Power Dispatch problem, Eng. Sci. Technol. Int. J. Jestech 20 (2017) 570–586.
[101] E.E. Ali, M.A. El-Hameed, A.A. El-Fergany, M.M. El-Arini, Parameter extraction of photovoltaic generating units using multi-verse optimizer, Sustain. Energy Technol. Assessments 17 (2016) 68–76.
[102] S. García, A. Fernández, J. Luengo, F. Herrera, Advanced nonparametric tests for multiple comparisons in the design of experiments in computational intelligence and data mining: experimental analysis of power, Inf. Sci. 180 (2010) 2044–2064.
[103] J. Derrac, S. García, D. Molina, F. Herrera, A practical tutorial on the use of nonparametric statistical tests as a methodology for comparing evolutionary and swarm intelligence algorithms, Swarm Evol. Comput. 1 (2011) 3–18.
[104] L. Zhang, L. Zhang, X. Mou, D. Zhang, FSIM: a feature similarity Index for image quality assessment, IEEE Trans. Image Process. 20 (2011) 2378–2386.
[105] Q. Huynh-Thu, M. Ghanbari, Scope of Validity of PSNR in Image/video Quality Assessment, Electronics Letters, Institution of Engineering and Technology, 2008, pp. 800–801.
[106] A.S. Abutaleb, Automatic thresholding of gray-level pictures using two-dimensional entropy, Comput. Vis. Graph Image Process 47 (1989) 22–32.
[107] A. Buades, B. Coll, J. Morel, A non-local algorithm for image denoising, in: 2005 IEEE Computer Society Conference on Computer Vision and Pattern Recognition (CVPR'05), vol. 62, 2005, pp. 60–65.
[108] J.P. Cohen, P. Morrison, L. Dao, K. Roth, T.Q. Duong, M.J.a.p.a. Ghassemi, Covid-19 Image Data Collection: Prospective Predictions Are the Future, 2020 [Online]. Available: https://github.com/ieee8023/covid-chestxray-dataset.
[109] I. Ahmadianfar, A. Asghar Heidari, A.H. Gandomi, X. Chu, H. Chen, RUN beyond the metaphor: an efficient optimization algorithm based on Runge Kutta method, Expert Syst. Appl. (2021), 115079.
[110] J. Tu, H. Chen, M. Wang, A.H. Gandomi, The colony predation algorithm, JBE 18 (2021) 674–710.
[111] I. Ahmadianfar, A. Asghar Heidari, S. Noshadian, H. Chen, A.H. Gandomi, INFO: an efficient optimization algorithm based on weighted mean of vectors, Expert Syst. Appl. (2022), 116516.
[112] Y. Yang, H. Chen, A.A. Heidari, A.H. Gandomi, Hunger games search: visions, conception, implementation, deep analysis, perspectives, and towards performance shifts, Expert Syst. Appl. 177 (2021), 114864.
[113] Y. Wei, H. Lv, M. Chen, M. Wang, A.A. Heidari, H. Chen, C. Li, Predicting entrepreneurial intention of students: an extreme learning machine with Gaussian barebone Harris hawks optimizer, IEEE Access 8 (2020) 76841–76855.
[114] S. Jiao, G. Chong, C. Huang, H. Hu, M. Wang, A.A. Heidari, H. Chen, X. Zhao, Orthogonally adapted Harris hawks optimization for parameter estimation of photovoltaic models, Energy 203 (2020), 117804.
[115] H. Zhang, A.A. Heidari, M. Wang, L. Zhang, H. Chen, C. Li, Orthogonal Nelder-Mead moth flame method for parameters identification of photovoltaic modules, Energy Convers. Manag. 211 (2020), 112764.
[116] S. Song, P. Wang, A.A. Heidari, M. Wang, X. Zhao, H. Chen, W. He, S. Xu, Dimension decided Harris hawks optimization with Gaussian mutation: balance analysis and diversity patterns, Knowl. Base Syst. 215 (2021), 106425.
[117] J. Fu, Y. Zhang, Y. Wang, H. Zhang, J. Liu, J. Tang, Q. Yang, H. Sun, W. Qiu, Y. Ma, Z. Li, M. Zheng, F. Zhu, Optimization of metabolomic data processing using NOREVA, Nat. Protoc. 17 (2022) 129–151.
[118] B. Li, J. Tang, Q. Yang, S. Li, X. Cui, Y. Li, Y. Chen, W. Xue, X. Li, F. Zhu, NOREVA: normalization and evaluation of MS-based metabolomics data, Nucleic Acids Res. 45 (2017) W162–W170.
[119] Q. Yang, Y. Wang, Y. Zhang, F. Li, W. Xia, Y. Zhou, Y. Qiu, H. Li, F. Zhu, NOREVA: enhanced normalization and evaluation of time-course and multi-class metabolomic data, Nucleic Acids Res. 48 (2020) W436–W448.
[120] C. Yu, M. Chen, K. Cheng, X. Zhao, C. Ma, F. Kuang, H. Chen, SGOA: annealing-behaved grasshopper optimizer for global tasks, Eng. Comput., 1-28.
[121] Y. Zhang, R. Liu, A.A. Heidari, X. Wang, Y. Chen, M. Wang, H. Chen, Towards augmented kernel extreme learning models for bankruptcy prediction: algorithmic behavior and comprehensive analysis, Neurocomputing 430 (2021) 185–212.
[122] A.B. Meng, Y.C. Chen, H. Yin, S.Z. Chen, Crisscross optimization algorithm and its application, Knowl. Base Syst. 67 (2014) 218–229.
[123] D. Zhao, L. Liu, F. Yu, A.A. Heidari, H. Chen, Ant colony optimization with horizontal and vertical crossover search: fundamental visions for multi-threshold image segmentation, Expert Syst. Appl. 167 (2020), 114122.
[124] C. Zuo, J. Qian, S. Feng, W. Yin, Y. Li, P. Fan, J. Han, K. Qian, Q. Chen, Deep learning in optical metrology: a review, Light Sci. Appl. 11 (2022) 1–54.
[125] K. Jin, Y. Yan, M. Chen, J. Wang, X. Pan, X. Liu, M. Liu, L. Lou, Y. Wang, J. Ye, Multimodal deep learning with feature level fusion for identification of choroidal neovascularization activity in age-related macular degeneration, Acta Ophthalmol. 100 (2022) e512–e520.
[126] Z. Liu, L. Fang, D. Jiang, R. Qu, A machine-learning based fault diagnosis method with adaptive secondary sampling for multiphase drive systems, IEEE Trans. Power Electron. (2022).
[127] Q. Xu, Y. Zeng, W. Tang, W. Peng, T. Xia, Z. Li, F. Teng, W. Li, J. Guo, Multi-task joint learning model for segmenting and classifying tongue images using a deep neural network, IEEE J. Biomed. Health Inf. 24 (2020) 2481–2489.
[128] H. Liu, J. Liu, S. Hou, T. Tao, J. Han, Perception consistency ultrasound image super-resolution via self-supervised CycleGAN, Neural Comput. Appl. (2021) 1–11.
[129] J. Li, K. Xu, S. Chaudhuri, E. Yumer, H. Zhang, L. Guibas, Grass: generative recursive autoencoders for shape structures, ACM Trans. Graph. 36 (2017) 1–14.
[130] C. Qin, G. Shi, J. Tao, H. Yu, Y. Jin, D. Xiao, Z. Zhang, C. Liu, An adaptive hierarchical decomposition-based method for multi-step cutterhead torque forecast of shield machine, Mech. Syst. Signal Process. 175 (2022), 109148.
[131] M. Issa, A. Hassanien, D. Oliva, A. Helmi, I. Ziedan, A. Alzohairy, ASCA-PSO: adaptive sine cosine optimization algorithm integrated with particle swarm for pairwise local sequence alignment, Expert Syst. Appl. 99 (2018) 56–70.
[132] Y. Su, C. Liu, Y. Niu, F. Cheng, X. Zhang, A community structure enhancement-based community detection algorithm for complex networks, IEEE Trans. Syst. Man Cybern.: Systems 51 (2019) 2833–2846.
[133] Y. Tian, X. Su, Y. Su, X. Zhang, EMODMI: a multi-objective optimization based method to identify disease modules, IEEE Trans. Emerg. Topics Comput. Intell. 5 (2020) 570–582.
[134] L. Cai, C. Lu, J. Xu, Y. Meng, P. Wang, X. Fu, X. Zeng, Y. Su, Drug repositioning based on the heterogeneous information fusion graph convolutional network, Briefings Bioinf. 22 (2021), bbab319.
[135] Y. Li, X. Li, J. Hong, Y. Wang, J. Fu, H. Yang, C. Yu, F. Li, J. Hu, W. Xue, Y. Jiang, Y. Chen, F. Zhu, Clinical trials, progression-speed differentiating features and swiftness rule of the innovative targets of first-in-class drugs, Briefings Bioinf. 21 (2020) 649–662.
[136] F. Zhu, X. Li, S. Yang, Y. Chen, Clinical success of drug targets prospectively predicted by in silico study, Trends Pharmacol. Sci. 39 (2018) 229–231.
[137] J. Yin, W. Sun, F. Li, J. Hong, X. Li, Y. Zhou, Y. Lu, M. Liu, X. Zhang, N. Chen, X. Jin, J. Xue, S. Zeng, L. Yu, F. Zhu, VARIDT 1.0: variability of drug transporter database, Nucleic Acids Res. 48 (2020) D1042–D1050.
[138] F. Zhu, Z. Shi, C. Qin, L. Tao, X. Liu, F. Xu, L. Zhang, Y. Song, X. Liu, J. Zhang, B. Han, P. Zhang, Y. Chen, Therapeutic target database update 2012: a resource for facilitating target-oriented drug discovery, Nucleic Acids Res. 40 (2012) D1128–D1136.
[139] Z. Wu, R. Li, J. Xie, Z. Zhou, J. Guo, X. Xu, A user sensitive subject protection approach for book search service, J. Assoc. Inf. Sci. Technol. 71 (2020) 183–195.
[140] Z. Wu, S. Shen, X. Lian, X. Su, E. Chen, A dummy-based user privacy protection approach for text information retrieval, Knowl. Base Syst. 195 (2020), 105679.
[141] Z. Wu, S. Shen, H. Zhou, H. Li, C. Lu, D. Zou, An effective approach for the protection of user commodity viewing privacy in e-commerce website, Knowl. Base Syst. 220 (2021), 106952.
[142] R. Guan, H. Zhang, Y. Liang, F. Giunchiglia, L. Huang, X. Feng, Deep feature-based text clustering and its explanation, IEEE Trans. Knowl. Data Eng. (2020), https://doi.org/10.1109/tkde.2020.3028943.
[143] D. Wang, Y. Liang, D. Xu, X. Feng, R.J.K.-B.S. Guan, A content-based recommender system for computer science publications, Knowl. Base Syst. 157 (2018) 1–9.
[144] J. Li, X.-L. Zheng, S.-T. Chen, W.-W. Song, D.-r. Chen, An efficient and reliable approach for quality-of-service-aware service composition, Inf. Sci. 269 (2014) 238–254.
[145] S. Liu, B. Yang, Y. Wang, J. Tian, L. Yin, W. Zheng, 2D/3D multimode medical image registration based on normalized cross-correlation, Appl. Sci. 12 (2022) 2828.
[146] G. Zhou, X. Bao, S. Ye, H. Wang, H. Yan, Selection of optimal building facade texture images from UAV-based multiple oblique image flows, IEEE Trans. Geosci. Rem. Sens. 59 (2020) 1534–1552.
[147] Z. Cao, Y. Wang, W. Zheng, L. Yin, Y. Tang, W. Miao, S. Liu, B. Yang, The algorithm of stereo vision and shape from shading based on endoscope imaging, Biomed. Signal Process Control 76 (2022), 103658.
[148] M. Zhang, Y. Chen, J. Lin, A privacy-preserving optimization of neighborhood-based recommendation for medical-aided diagnosis and treatment, IEEE Internet Things J. 8 (2021) 10830–10842.
[149] M. Zhang, Y. Chen, W. Susilo, PPO-CPQ: a privacy-preserving optimization of clinical pathway query for e-healthcare systems, IEEE Internet Things J. 7 (2020) 10660–10672.
[150] H. Pei, B. Yang, J. Liu, K. Chang, Active Surveillance via Group Sparse Bayesian Learning, IEEE Transactions on Pattern Analysis and Machine Intelligence, 2020, https://doi.org/10.1109/TPAMI.2020.3023092.
[151] G. Liang, B.-W. On, D. Jeong, A.A. Heidari, H.-C. Kim, G.S. Choi, Y. Shi, Q. Chen, H. Chen, A text GAN framework for creative essay recommendation, Knowl. Base Syst. 232 (2021), 107501.

[152] Z. Wu, G. Li, S. Shen, Z. Cui, X. Lian, G. Xu, Constructing dummy query sequences to protect location privacy and query privacy in location-based services, World Wide Web 24 (2021) 25–49.
[153] Z. Wu, R. Wang, Q. Li, X. Lian, G. Xu, A location privacy-preserving system based on query range cover-up for location-based services, IEEE Trans. Veh. Technol. (2020) 69.
[154] D.-C. Wang, H.-Y. Yu, L. Jiang, D. Qi, X. Zhang, L. Chen, W. Lv, W. Xu, K.C. Tam, Flexible, anti-damage, and non-contact sensing electronic skin implanted with MWCNT to block public pathogens contact infection, Nano Res. 15 (2022) 2616–2625.
[155] Z. Ouyang, S. Cui, H. Yu, D. Xu, C. Wang, D. Tang, K.C. Tam, Versatile sensing devices for self-driven designated therapy based on robust breathable composite films, Nano Res. 15 (2022) 1027–1038.
[156] C. Huang, H. Yu, S.Y.H. Abdalkarim, Y. Li, X. Chen, X. Yang, Y. Zhou, L. Zhang, A comprehensive investigation on cellulose nanocrystals with different crystal structures from cotton via an efficient route, Carbohydr. Polym. 276 (2022) 118766.
[157] S. Qiu, Z. Hao, Z. Wang, L. Liu, J. Liu, H. Zhao, G. Fortino, Sensor Combination Selection Strategy for Kayak Cycle Phase Segmentation Based on Body Sensor Networks, IEEE Internet of Things Journal, 2021, https://doi.org/10.1109/JIOT.2021.3102856.
[158] S. Qiu, H. Zhao, N. Jiang, D. Wu, G. Song, H. Zhao, Z. Wang, Sensor network oriented human motion capture via wearable intelligent system, Int. J. Intell. Syst. 37 (2021) 1646–1673, https://doi.org/10.1002/int.22689.
[159] H. Yu, J. Liu, C. Chen, A.A. Heidari, Q. Zhang, H. Chen, Optimized deep residual network system for diagnosing tomato pests, Comput. Electron. Agric. 195 (2022), 106805.
[160] T. Wang, X. Zhang, R. Jiang, L. Zhao, H. Chen, W. Luo, Video deblurring via spatiotemporal pyramid network and adversarial gradient prior, Comput. Vis. Image Understand. 203 (2021), 103135.